Sliding Evaluation and Results

Non-proprietary Version

January 2013

Revision History

Revision	Page	Description
0	All	Initial Issue
1	All	Includes revised methodology and inclusion of analysis results. This is an extensive revision, so no revision bars are shown in the margins.

Mitsubishi Heavy Industries, Ltd.

16-5, Konan 2-chome, Minato-ku

Tokyo 108-8215 Japan

ABSTRACT

The purpose of this Technical Report (TeR) is to present the methodology and results of nonlinear sliding analyses due to seismic events for the United States-Advanced Pressurized Water Reactor (US-APWR) Standard Plant.

This revision of the TeR describes:

- Objectives and scope of the nonlinear sliding time history analyses.
- Development of five time histories developed to be compatible to the Certified Seismic Design Response Spectra (CSDRS) in accordance with Standard Review Plan (SRP) 3.7.1 Acceptance Criteria.
- General analysis method, including: Assumptions, Seismic Loads, Material Properties, and Contact Modeling.
- Specific aspects, including special features of the Finite Element (FE) models, and methodology for building, calibrating, and validating a computationally effective numerical model for nonlinear sliding analyses.
- The results of nonlinear sliding analysis for the Reactor Building (R/B) complex and for the Turbine Building (T/B) subjected time histories developed to be compatible to the CSDRS, and results of sensitivity studies supporting the selected parameters and calculation method.
- Sliding analysis result processing and selection of values for plant design.

The maximum expected seismic induced sliding to be used for plant design is:

[ ]

TABLE OF CONTENTS

LIST OF FIGURES

LIST OF TABLES

LIST OF ACRONYMS AND ABBREVIATIONS

The following list defines the acronyms used in this document.

A/B	Auxiliary Building
AI	Arias Intensity
ANSYS	Computer Program "ANSYS"
ARPSB	Group of Structures Consisting of the R/B, A/B and East & West PS/Bs
ASCE	American Society of Civil Engineers
ATH	Acceleration Time History
CIS	Containment Internal Structure
CoV	Coefficient of Variation
CM	Center of Mass
CSDRS	Certified Seismic Design Response Spectra
DC	Design Certification
DOF	Degree of Freedom
E/R	Electrical Room
EPRI	Electric Power Research Institute
EW	East-West
FE	Finite Element
FoS	Factor of Safety
GWL	Groundwater Level
LMS	Lumped Mass Stick
LMSM	Lumped Mass Stick Model
MHI	Mitsubishi Heavy Industries, Inc.
NRC	U.S. Nuclear Regulatory Commission
NS	North-South
NUREG	U.S. Nuclear Regulatory Commission Regulation
PCCV	Pre-stressed Concrete Containment Vessel
PEER	Pacific Earthquake Engineering Research
PGA	Peak Ground Acceleration
PS/B	Power Source Building
PSD	Power Spectral Density
R/B	Reactor Building
RG	Regulatory Guide
SASSI	Computer Program "ACS SASSI"
SP	Subgrade Profile
SRP	Standard Review Plan
SSI	Soil-Structure Interaction
T/B	Turbine Building
TeR	Technical Report
TR	Transmissibility
US-APWR	United States Advanced Pressurized Water Reactor

1.0 INTRODUCTION

U.S. Nuclear Regulatory Commission (NRC) Standard Review Plan (SRP) 3.8.5 (Reference 1) requires that Seismic Category I structures have a margin of safety for sliding expressed as a Factor of Safety (FoS) against sliding greater than 1.1. These FoS are typically calculated as the ratio of the minimum seismic resistance to the maximum seismic demand. Both resistance and demand are conservatively derived based on pseudo-static analyses and use conservative parameters that envelop a variety of site situations.

As stated in PVP2011-57600 (Reference 2), it has been difficult to demonstrate seismic stability using simple calculations in Design Certification (DC) applications. This is due to the nature of the DC applications, where the design parameters for both seismic demand and seismic resistance are not based on actual site investigations, but in general are conservatively specified representing envelopes of the site-specific characteristics to be expected at the potential sites (Reference 2).

This issue is resolved by performing the seismic sliding evaluation for the Reactor Building (R/B) complex and Turbine Building (T/B) structures using nonlinear time history analysis that is more realistic than the pseudo-static approach. This type of analysis can indicate, in some cases, that small amounts of sliding occur for short time intervals during the seismic event. Maximum expected upper bounds for sliding are conservatively estimated using a statistical evaluation of the analytical results.

In addition to specifying a series of conservative assumptions and conservatively assessed parameters, a safety margin for seismic induced sliding is secured by amplifying all components of the input seismic motion by a factor of 1.1. This is equivalent to a FoS of two applied to the calculated sliding results (see Section 6.3 and Appendix B).

2.0 PURPOSE AND SCOPE

The purpose of this Technical Report (TeR) is to present the methodology and results of nonlinear sliding analyses due to Certified Seismic Design Response Spectra (CSDRS) compatible time histories.

The purpose is also to develop five sets of Acceleration Time Histories (ATH), as described in Sections 4.1 and 5.1, that are used in conjunction with Soil-Structure Interaction (SSI) analyses of the R/B complex and T/B to produce input to the nonlinear sliding analyses.

The seismic sliding analysis is performed for the following Standard Plant structures:

1. R/B complex, which consists of the R/B and Fuel Handling Area, Pre-stressed Concrete Containment Vessel (PCCV), the Containment Internal Structure (CIS) including the Reactor Coolant Loop, the East Power Source Building (East PS/B), the West Power Source Building (West PS/B), the Auxiliary Building (A/B), and the Essential Service Water Pipe Chase, all on a common foundation basemat.
2. T/B, which consists of the T/B structure and the Electrical Room (E/R), placed on a common basemat, not including the Turbine Pedestal.

For the R/B complex sliding analyses, both cracked and uncracked concrete properties are considered. Based on sensitivity study results presented in Appenidx B, only uncracked concrete properties are considered for the T/B analyses.

Seismic induced sliding is calculated using the five sets of ATH and six sets of Subgrade Profiles (SP). The results are processed in terms of maximum expected sliding with an exceedance probability of 2.5%. There is no FoS applied to the analysis results. However, the use of conservative inputs in the analyses can be considered equivalent to a FoS of at least two, applied to this maximum expected sliding (see discussion in Appendix B and Section 6.3).

3.0 OBJECTIVES

The objective of this TeR is to estimate conservative upper bounds for seismic sliding displacements for the R/B complex and the T/B subjected to CSDRS compatible ATHs. The upper bounds for sliding values calculated here are used to satisfy the requirements of SRP 3.8.5 (Reference 1) and are applied in the detailed design of the Standard Plant.

4.0 METHODOLOGY

The methodology presented in the following subsections includes:

- The methodology to develop time histories compatible with the CSDRS for nonlinear sliding.
- The methodology of the development of the Finite Element (FE) model of the R/B complex and T/B.
- The methodology of the development of the Lumped Mass Stick Models (LMSM) of the R/B complex. This model is exclusively used for screening the governing cases to be analyzed with the FE model.
- Development of the SPs used in the nonlinear sliding analyses.
- The methodology of the nonlinear sliding analyses and the post-processing of results.

4.1 Time Histories for Nonlinear Sliding

A set of five earthquakes, three components each, compatible with the requirements of SRP 3.7.1, Acceptance Criteria II.1.B, Option 2 (Reference 3) for multiple sets of time histories, are developed from seeds for the nonlinear sliding analyses. Specifically, for each direction, the average response spectra and Power Spectral Densities (PSD) of the five sets of time histories envelope the CSDRS (Reference 4) and the target PSDs (Section 01.5.1.1, Reference 5) in accordance with the requirements of SRP 3.7.1, Option 1, Approach 1. The time histories also comply with the duration requirements, statistical independence, and V/A and AD/V^2 (A, V, and D are Peak Ground Acceleration (PGA), peak ground velocity, and peak ground displacement, respectively) requirements in SRP 3.7.1 Acceptance Criteria II.1.B.

In order to achieve the CSDRS match, the Fourier amplitudes of the seed time histories are modified to generate three new time histories. This Fourier amplitude modification process is iterated until the average response spectra calculated from the modified time histories envelopes the target response spectra at 5% damping. Once the response spectra of the time histories envelope the CSDRS, the smoothed PSDs of the time histories are computed over a frequency bandwidth of ±20%, centered at each frequency. The smoothed PSDs of the components of the five time histories are averaged and compared to 80% of the target PSDs. If the average PSD for a particular direction does not envelope the 80% of target PSD, the components of the five time histories in that direction are scaled. Then a baseline correction is applied to the time histories. Next, the resulting time histories are verified again for their compliance with the SRP 3.7.1, Option 1, Approach 1 and Option 2 Acceptance Criteria. The baseline corrected time histories are scaled to comply with the enveloping criteria for the spectra at 5% damping, and the envelope requirements for the target PSD functions. Finally, the modified time histories are checked for the requirements of strong motion duration, correlation coefficients, and V/A and AD/V^2 ratios. The final modified time histories, presented in Section 5.1, are then used in conjunction with SSI analysis results (refer to Reference 5) to produce the input ATHs for the nonlinear sliding analyses.

4.1.1 Development of Time Histories in Accordance with SRP 3.7.1 Option 1, Approach 1 and Option 2

The requirements defined for the development of the artificial earthquakes are defined in SRP 3.7.1 Acceptance Criteria II.1.B Option 2. The PSD requirements from Acceptance Criteria

II.1.B Option 1, Approach 1 are applied to the development of the time histories as well as certain requirements from Option 1, Approach 2. The requirements are as follows:

- The total duration of each component should be at least 20 seconds (Option 1, Approach 2);
- The time step of each component should be at most 0.005 seconds (Option 1, Approach 2);
- The average (Option 2) of the response spectra of the components in one direction must envelope the target CSDRS at 5% damping. The enveloping criteria is defined as not having more than 5 spectral values below the target and by no more than 10% below using the frequency list in Table 3.7.1-1 of Reference 3 (Option 1, Approach 1);
- The average of the smoothed (±20%) PSD of the components in one direction must envelope 80% of the target PSD over the frequency range of interest. The frequency range of interest was initially targeted to be 50 Hz, to be the same as the frequency range of interest for the design basis time history in Reference 5. During the course of the time history development it was determined that maintaining this frequency range would result in non-compliant time histories. Studies of the sliding analyses have shown very little effect on the sliding response for Fourier components above approximately 20 to 25 Hz as shown in Sections 5.2.2.2 and 5.3.2.2. Also, higher frequencies do not affect the sliding response as shown in Section 5.2.2.2. Thus, the upper limit of the frequency range of interest for nonlinear sliding is set at 45 Hz. The lower limit of the frequency range of interest is 0.3 Hz;
- Each pair of time history components for each earthquake must demonstrate statistical independence with a computed absolute value of correlation coefficient not exceeding 0.16;
- The strong motion duration of each component, defined as the time required for the Arias Intensity (AI) to rise from 5% to 75% should be at least 6 seconds (Reference 6) and consistent with the duration criteria for earthquake magnitude and distance bins listed in NUREG/CR-6728 (Reference 7);
- For each component, the ratios V/A and AD/V^2 should be consistent with the values listed in Table 3-6 of Reference 7.

4.1.2 Target Response Spectra – The CSDRS

The CSDRS for the United States-Advanced Pressurized Water Reactor (US-APWR) are provided in Section 01.4.1.1 of Reference 5, which contains the target response spectra for 2%, 3%, 5%, 7%, and 10% damping values. The 5% damped CSDRS is used to develop the time histories for nonlinear sliding analyses. Table 4.1.2-1 provides the control points for the 5% damped CSDRS. The CSDRS are extended from 50 Hz to 100 Hz maintaining a constant acceleration of 0.3g. The accelerations between 0.25 Hz and 0.10 Hz are computed to maintain constant displacement for the E control point similar to the acceleration of the D control point of Regulatory Guide (RG) 1.60 (Reference 8). There are two target response spectrum components: one for horizontal components and one for the vertical component of ground motions. Figure 4.1.2-1 and Figure 4.1.2-2 show the horizontal and vertical CSDRS at 5% damping, respectively.

4.1.3 Development of the US-APWR Target PSD

The target PSDs are developed to be compatible with the CSDRS. Sections 01.4.1.2.1 and 01.5.1.1 Reference 5 provides the methodology and the development of the US-APWR target PSDs.

The horizontal target PSD anchored to 1.0g is as follows:

$$S_{0H}(f) = \begin{cases} 650(f/2.5)^{0.2} & \text{for } f < 2.5\text{Hz} \\ 650(2.5/f)^{1.6} & \text{for } 2.5\text{Hz} \le f < 12\text{Hz} \\ 52.9(12.0/f)^{3} & \text{for } 12\text{Hz} \le f < 18\text{Hz} \\ 15.7(18/f)^{7} & \text{for } 18\text{Hz} \le f \end{cases} \quad (\text{in}^2/\text{sec}^3) \qquad \text{Equation 4.1.3-1}$$

The vertical target PSD anchored to 1.0g is as follows:

$$S_{0V}(f) = \begin{cases} 380(f/3.5)^{0.2} & \text{for } f < 3.5\text{Hz} \\ 380(3.5/f)^{1.6} & \text{for } 3.5\text{Hz} \le f < 12\text{Hz} \\ 52.9(12.0/f)^{3} & \text{for } 12\text{Hz} \le f < 18\text{Hz} \\ 15.7(18/f)^{7} & \text{for } 18\text{Hz} \le f \end{cases} \quad (\text{in}^2/\text{sec}^3) \qquad \text{Equation 4.1.3-2}$$

Figure 4.1.3-1 shows the horizontal and vertical target PSD functions anchored to a PGA of 1.0g.

4.1.4 Earthquake Seeds

Segments of five recorded earthquakes are used to develop the time histories whose response spectra envelope the CSDRS. The segments containing the strong portion of these earthquakes are selected as seeds for the development of the artificial time histories. The Northridge earthquake seed is also selected for the purpose of nonlinear sliding analyses presented herein but is otherwise separate from the the time history development presented in Reference 5.

Table 4.1.4-1 lists the five earthquakes and the segments used as seeds. The Table also shows the time steps at which the earthquakes are reported in the earthquake database. Table 4.1.4-2 provides the correlation coefficients of these segments. Except for the absolute correlation coefficient between components “090” and “Vertical” of the Northridge seed, all the initial seeds satisfy the SRP 3.7.1 requirements to be less than 0.16. The final modified time histories fully satisfy the SRP 3.7.1 requirements (see Section 5.1). The development of the time histories is presented in Section 5.1 and shows that the response spectra of the five time histories envelope the CSDRS and that the SRP 3.7.1 acceptance criteria are met.

The following provides a brief description of each of the selected seed earthquakes:

Chi Chi Earthquake

The Chi Chi, Taiwan earthquake recorded at Station ILA067 on September 21, 1999. This earthquake has a magnitude of 7.6. The Station distance to the earthquake epicenter is listed as 38.8 km. The site of the recording instrument is defined as stiff soil. The records were obtained from the “The Pacific Earthquake Engineering Research (PEER) Center, University of California at Berkeley” strong motion database (Reference 9). The time step is equal to 0.005 seconds.

Darfield Earthquake

The Darfield, New Zealand earthquake recorded at Station DFHS on September 4, 2010. This earthquake has a magnitude of 7.1. The Station distance to the earthquake epicenter is listed as 9 km. The records were obtained from the "GeoNet New Zealand Seismograph Network, GNS Science" strong motion database (Reference 10). The time step is equal to 0.02 seconds.

Hector Mine Earthquake

The Hector Mine, California earthquake recorded at Station Amboy on October 16, 1999. This earthquake has a magnitude of 7.1. The Station distance to the earthquake hypocenter is listed as 48.4 km. The site of the recording instrument is defined as shallow alluvium (approximately 3 meters) over basalt. The records were obtained from Reference 9. The time step is equal to 0.02 seconds.

Nahanni Earthquake

The Nahanni, Canada earthquake recorded at Site 3 on December 23, 1985. This earthquake has a magnitude of 6.76. The depth of the earthquake is listed at 8 km and the epicentral distance to Site 3 at 22.36 km. The recording instrument is located at ground level. The records were obtained from Reference 9. The time step is equal to 0.005 seconds.

Northridge Earthquake

The Northridge earthquake recorded at Mt. Baldy Elementary School Station on January 17, 1994. This earthquake has a magnitude of 6.7. The distance from the station to the closest fault rupture is listed at 71.5 km. The records were obtained from Reference 9. The time step is equal to 0.01 seconds.

The final time histories for nonlinear sliding are presented in Section 5.1.

4.2 Development of Finite Element Models for R/B Complex and T/B

4.2.1 General

There are two FE models for the R/B complex, a Detailed FE model which is used to validate the dynamic model; and one Dynamic FE model, which is used for dynamic analyses in ANSYS (Reference 11) and ACS SASSI (Reference 12). For the Dynamic FE model, there are two types of concrete sections (i.e., cracked and uncracked) in order to capture variations of the material properties of the structural members due to concrete cracking. Correlation between these two models is documented in Reference 5. The Dynamic FE model is the basis for nonlinear sliding analysis and for correlation with the LMSM. Contact (or sliding) elements and a rigid basemat are added to the Dynamic FE model for nonlinear sliding analyses. The Dynamic FE model customized for sliding analyses is referred to herein as the "Finite Element" model (abbreviated as FE model as shown earlier).

Since the T/B is a smaller and relatively simpler structure than the R/B complex, there is only one FE model for each type of concrete section. The differences between the cracked FE model and the uncracked FE model for the T/B are only in the concrete basemat, as the super-structures (T/B and E/R) are steel structures.

4.2.2 Structural Properties

The input parameters used for the FE models of the R/B complex are the same as those used in the SSI analyses, and are discussed in detail in MUAP-10006 (Reference 5). The FE models of the T/B are provided in Reference 13. One parameter that could not be replicated

from the frequency domain analyses performed with ACS SASSI (Reference 12) to the transient analyses performed here with ANSYS (Reference 11) is the damping ratio. ACS SASSI uses a complex damping formulation, while in transient analyses performed with ANSYS, the damping ratio is described via Rayleigh damping, using the *α* and *β* coefficients that multiply the mass matrix and the stiffness matrix, respectively. The viscous damping matrix is given by:

$$[C] = \alpha[M] + \beta[K] \qquad \text{Equation 4.2.2-1}$$

where *M* and *K* are the mass and stiffness matrices, respectively, and *α* and *β* are the Rayleigh damping coefficients.

Rayleigh damping models have a damping ratio that is frequency dependent:

$$\zeta(F) = \frac{\alpha}{4\pi F} + \beta\pi F \qquad \text{Equation 4.2.2-2}$$

The usual approach is to bound the range of structural frequencies of interest for sliding analysis (herein: from *F1*, the lowest fundamental frequency in any direction, to *F2*, the highest frequency that contributes to sliding), and determine the values of *α* and *β* such that the desired modal damping ratio, or target ratio ζ_0, is matched to the frequencies *F1* and *F2* bounding this range, as illustrated in Figure 4.2.2-1 for one of the structures discussed in this TeR. In this manner, the damping ratios used in the sliding analysis, and corresponding to the frequency range relevant for sliding (*F1* to *F2*) will be less or equal to the target modal damping ratio, ζ_0. The selection of the relevant frequency ranges (*F1* to *F2*) considered for each structure analyzed in this TeR, as well as the justification of these ranges based on sensitivity studies, are discussed in Sections 5.2.2.2 and 5.3.2.2.

Since the input ATHs used in the nonlinear sliding analysis have been developed based on 5% damping response spectra, the same value is used as the target for structural damping.

4.2.3 Contact Formulation

The manner in which the dynamic FE model is developed into a nonlinear sliding analysis model is illustrated in Figure 4.2.3-1 based on the R/B complex FE model. Friction contact with no tensile resistance is considered between the basemat and the subgrade. Note that the “basemat” refered to in this TeR includes the entire basement of each structure (R/B complex or T/B) - see Figure A.2.1-1 in Appendix A. A rigid surface is developed and connected to the bottom of the basemat. Another rigid surface is developed and is coincident with the first rigid surface. The two rigid surfaces are connected to each other using contact element pairs located throughout the area of the bottom of the basemat. The “upper” surface is attached to all the nodes at the bottom of the basemat. The “lower” surface is then subjected to ATHs taken from the SSI analysis. The final layout of the FE model prepared for sliding is shown in Figure 4.2.3-2.

The contact elements model Coulomb friction. They are also compression-only elements that are deactivated at locations and time instants where uplift occurs, therefore the uplift effects on sliding are captured by the numerical model. The contact elements used for both the FE model and the LMSM in the ANSYS analyses are CONTA173 elements (Reference 11). The only material property prescribed for these elements is the coefficient of friction, μ = 0.5 (the kinetic friction coefficient). The stiffness of the contact elements is controlled through the real constant FKN, and is calculated for each structure from the condition to avoid spurious rigid body vibrations, as described in the next paragraph. The contact elements are placed at the bottom of the structure basemat. There is a target surface representing the subgrade, where the ATH input motion is prescribed via a pilot node. TARGE170 elements are used in the ANSYS analyses for the target surface. The TARGE170 elements do not require any material properties or real constants.

The stiffness of the contact elements is selected so that spurious vibrations in both horizontal and vertical directions do not occur. These vibrations would be induced by rigid body modes of the entire structure (as a mass) placed on the contact elements (as springs characterized by their stiffness). The minimum stiffness of the contact elements is determined from the requirement that the amplitude of accelerations transmitted to the basemat is within 1% of the ground acceleration amplitudes, i.e., Transmissibility (TR) is less than or equal to 1.01. TR refers to structures on elastic support subjected to harmonic oscillations and it is the ratio between the acceleration transmitted to the structure and the acceleration at the base of the elastic support. The expression for harmonic input motion of circular frequency ω is (Reference 14):

$$TR = \sqrt{\frac{1 + [2\zeta(\omega / \omega_n)]^2}{[1 - (\omega / \omega_n)^2]^2 + [2\zeta(\omega / \omega_n)]^2}} \qquad \text{Equation 4.2.3-1}$$

Where ζ is the damping ratio of the structure and ω_n is the natural frequency of vibration of the single Degree of Freedom (DOF) system represented by the entire mass of the structure placed on the elastic support,

$$\omega_n = \sqrt{\frac{k}{m}} \qquad \text{Equation 4.2.3-2}$$

with k = stiffness of the support (sum of stiffness from all contact elements) and m = mass of the entire structure, e.g., R/B complex.

4.3 Development of Lumped Mass Stick Models

4.3.1 General Considerations

LMSMs that accurately reproduce the lower modes of the detailed structures are developed for the R/B complex with cracked and uncracked concrete sections, validated based on the corresponding FE models, and used (1) to identify governing cases for full FE model analysis by screening all the combinations of soil profiles, time histories, and structure types (see Section 5.2.5), and (2) to perform a series of sensitivity studies (Appendix B).

The calibration and validation method for the LMSM used in nonlinear sliding analyses of the R/B complex are presented in Appendix A and Section 4.3.2, respectively. The purpose of the calibration and validation (Figure 4.3.1-1) is to design a LMSM that is able to accurately reproduce the amount of sliding calculated using the FE model. The LMSM developed for sliding consists of a basemat that supports a number of stick models representing the super-structure. The stick models have concentrated masses at the levels of the main floors of the FE model, and beam elements in between that reproduce the story stiffness of the FE model levels. As for each main floor, all the structural and equipment masses are lumped into one single concentrated mass. A fraction of the floor mass is modeled separately to capture low frequency vibration of floors, as explained in Appendix A, Section A.1.4. The LMSM is validated only for sliding analysis, and is not appropriate for inferring any structural response other than seismic induced sliding.

The calibration method discussed in Appendix A and the validation method discussed in the following Section refer to the R/B complex LMSMs.

4.3.2 Fine Tuning and Validation of the LMSM

4.3.2.1 Screening for Representative Cases

The LMSM, calibrated as described in Appendix A, reproduces the mass and stiffness, and approximately matches the lower vibration modes of the FE model. However, the LMSM has a very limited number of concentrated masses and therefore is not able to reproduce the actual distribution of the modal mass in the FE model. To ensure accurate results in terms of the amount of sliding for the range of input ATHs and SPs considered in the nonlinear sliding analysis, the LMSM is first verified against the FE model in terms of the calculated maximum total sliding (defined in Equation 4.5.5-1) based on a number of representative cases. This verification is done for both LMSMs (with cracked and with uncracked concrete section).

First, the LMSM calibrated as described in Appendix A is used to perform nonlinear sliding analyses for all six SPs and all five ATHs. Five cases are then selected (screened) out of the 30 cases analyzed, based on the following criteria:

4.3.2.2 Fine Tuning of the LMSM

4.3.2.3 Validation Criterion

4.4 Subgrade Properties

Six SPs, described in Reference 5, are considered for the nonlinear sliding analyses. Subgrade properties, including soil layering, as well as stiffness and damping for each layer, are input parameters for the SSI analyses that provide the ground accelerations at the basemat-subgrade level, accounting for the effect of the soil profiles on seismic accelerations, as outlined in Section 4.5.2.

The most important subgrade parameter in sliding analysis is the coefficient of friction at the basemat-subgrade interface. This friction coefficient has different values for the case when the structure has not started sliding (static friction coefficient, μ_s) and for the case when the structure is already sliding (kinetic friction coefficient, μ_k). Values of these coefficients that are appropriate for the Standard Plant design are discussed below.

The kinetic friction coefficient, μ_k = 0.50, is conservatively used throughout the nonlinear sliding analyses.

Relative sliding, due to exceedance of contact friction forces, may occur either (1) between the mud mat (mass concrete placed directly on subgrade) and soil or rock, or (2) between the bottom of the foundation (concrete mat) and the mud mat. These interfaces are discussed below for various types of subgrade. It is also mentioned that no waterproofing membrane will be used below the basemats of the structures, and required concrete waterproofing will be ensured by using appropriate concrete admixtures.

Static friction coefficient, μ_s between the bottom of foundation and mud mat

The cold joint at the mud mat to bottom of foundation contact is a mechanical interface since the mud mat will not be smooth. It will be “raked” to a very rough surface (minimum amplitude greater than ¼ inch - as recommended in ACI 349-06, Reference 15, paragraph 11.7.9) to maintain a minimum friction coefficient of 1.0 for both dry and wet surfaces. Based on laboratory test results from over 150 specimens, the Electric Power Research Institute (EPRI) (Reference 16) indicates a lower bound of 57 degrees for the peak friction angle at the concrete-to-concrete contact for cold joints.

Static friction coefficient, μ_s (rock subgrades):

The static friction coefficient characterizes the shear strength of the interface before sliding occurs. Based on Reference 17, μ_s between mass concrete and various subgrade materials corresponds to an angle of friction (Φ) of 35° for rock and is equal to the friction angle at failure for soils. An angle of friction of 35° is equivalent to a static friction coefficient μ_s = 0.7.

Static friction coefficient, μ_s (granular soil subgrades):

Based on correlations in the literature (see Reference 17), granular soils with properties corresponding to the requirements in Reference 5, namely with shear wave velocities V_S > 270 m/s, have effective friction angles, Φ, of approximately 40°. The governing friction occurs between the mud mat and the underlying granular soil where a thin soil layer exists that is interlocked with the bottom of the mud mat. Upon impending sliding conditions, this layer is constrained to move together with the mud mat. Therefore, sliding of mass concrete placed directly on granular soil is a shear failure phenomenon and the "friction coefficient" is an expression of the shear strength of the soil. A conservative value of Φ = 35°, corresponding to a friction coefficient μ_s = 0.7, is considered for this type of soil. In order to provide a suitable subgrade material, the soil should not include a significant amount of fines and be compacted to an adequate relative density (at least 65%, corresponding to dense sand) before the placement of the mud mat.

Static friction coefficient, μ_s (clay subgrades):

Any in-situ fine grained soil immediately below the basemat will be replaced by engineered fill. The engineered fill will be specified to be approximately 4 to 6 inches thick. This fill will be topped with a mud mat. Engineered fill is specified as a well drained granular backfill with a minimum friction angle of Φ = 35°. Potential sliding between engineered fill and natural clay is not likely due to penetration of granular soil particles into the natural soil during compaction.

Based on the above considerations, a conservative value for the friction angle of natural soil materials and engineered fill below the basemat for all profiles is selected to be Φ = 35°, corresponding to a static friction coefficient μ_s = 0.7.

Kinetic friction coefficient, μ_k (all subgrades):

The kinetic friction coefficient characterizes the shear strength of the interface during sliding. This shear strength is also termed as "residual strength". Based on results of a large number of laboratory and full scale tests (a comprehensive review is presented in Reference 18), the residual strength friction angle at concrete-to-concrete and concrete-to-rock interfaces exceeds 30°, corresponding to kinetic friction coefficients, μ_k > 0.57, for both dry and wet surfaces.

The residual friction angle for granular soils is also known as the constant volume friction angle or the steady state friction angle (e.g., Reference 19). Been and Jefferies (Reference 20) report values of the residual friction angle based on a large number of laboratory soil tests with samples from seven different types of sand. Most values range between 30° and 32°, with extreme values of 27° and 35°, all yielding kinetic friction coefficients, μ_k > 0.5. The soils and soil property conditions considered in this TeR for assessing the residual friction angles, and therefore the friction coefficients, include granular soils with shear wave velocities equal to or larger than 270 m/s, i.e., dense granular soils, either natural soils or engineered fills. The soil samples used in the laboratory soil tests described in Reference 20 include various types of granular soils with friction angles between 28° and 48°, which envelop the range of friction angles for dense granular soils (either natural, or engineered fill) considered for the US-APWR standard design.

Effect of Groundwater:

The friction coefficient between two surfaces in contact is in general affected by the presence of water, as the lubricating effect of water will usually reduce friction. However, the friction coefficient below the mud mat discussed here, representing friction between mass concrete and granular soil, is the result of shear failure in soil rather than of sliding between two surfaces. As discussed previously, this is because the cement penetrates in soil pores during

mat placement and forces the failure surface to occur through soil rather than at the interface, and therefore the friction coefficient is an expression of the shear strength of soil. It has been verified experimentally that the results in terms of effective stresses and the shear strength of granular soils were not affected by the presence of water in the soil sample (e.g., Reference 21). Therefore, it is considered in this analysis that presence of water does not affect the friction coefficient between mud mat and subgrade.

Regarding the concrete-to-concrete and rock-to-concrete interfaces, all experimentally based values of the friction coefficient (References 16 and 18) discussed previously were obtained for both dry and wet interfaces.

4.5 Sliding Analysis Method and Result Processing

There are 60 analytical cases to evaluate for the R/B complex and 30 cases for the T/B. For the R/B complex, they consist of five ATHs for six SPs for both cracked and uncracked structures, thus: 5 x 6 x 2 = 60 cases. Only the uncracked section is analyzed for the T/B, as discussed in Section 5.3.2.3, hence 30 analysis cases. The lower modes of a structure control the sliding potential (see Reference 22). Therefore, the use of a complex FE model to compute sliding for all of these cases is not computationally efficient. Consequently, a LMSM approach using models that accurately reproduce the lower modes of the detailed structures is developed, validated based on the FE model, and used (1) to identify the governing cases for full FE model analysis by screening all the combinations of soil profiles, time histories, and structure types (see Section 5.2.5), and (2) to perform a series of sensitivity studies (Appendix B). As the FE model of the T/B is smaller than that of the R/B complex and there are fewer analysis cases, the full FE model is used for the nonlinear sliding analysis of the T/B.

The LMSMs of the R/B complex for both cracked and uncracked sections are developed using properties derived from the FE models, referred to herein as the Dynamic FE models (see Section 4.2 for more detail). These Dynamic FE models are the ANSYS (Reference 11) models which are translated into ACS SASSI (Reference 12) models which are then used to compute the SSI effects. These Dynamic FE models are modified herein for the purpose of computing sliding. The LMSMs are then refined using correlations to results obtained from Dynamic FE model analyses. Once the LMSMs are developed to be suitable for sliding analysis, they are used to compute sliding displacements for the R/B complex for all the cases described above.

4.5.1 Assumptions

The following assumptions are made and justified in the computation of sliding:

None of the above assumptions require further verification, other than noted.

4.5.2 Input Seismic Accelerations

The loads acting on the structures considered in the sliding analyses are as follows:

- Dead Loads and Live Loads - included through the mass of the model defined at the material property level in the FE analyses. The amount of Live Loads considered in the analysis is discussed in detail in Section 5.2.1.2 and Appendix B.
- Buoyancy forces corresponding to the Groundwater Level (GWL) at one foot below plant grade and applied as upward uniform pressure acting at the bottom of the basemat.
- Seismic ground accelerations compatible with the CSDRS, applied to the subgrade as translational and rotational ATHs, as explained later on in this section.

Other forces, including static and dynamic lateral soil and groundwater pressures are neglected, based on the fact that each structure is embedded on four sides and therefore these pressures cancel each other. As demonstrated in Sections 4.5.3, 5.2.1.3 and 5.3.1.3, neglecting these lateral pressures is conservative with respect to the sliding analysis.

The load acting on the structure and possibly inducing sliding is the ground acceleration. The input to the sliding analyses consists of net translation ATHs extracted from the SSI analyses (Reference 5 and Section 5.3.1.1 of this TeR for the R/B complex and the T/B, respectively) and applied to the subgrade below the basemat in all three directions. Rotations about the two horizontal axes due to rocking are also determined based on the SSI analysis results. Five sets of ATHs are used in the nonlinear sliding analyses for each of the six SPs, and for two types of structural models, i.e., cracked and uncracked.

The subgrade is modeled as a rigid surface, defined by its dimensions in the horizontal plane and by a “pilot” node (see Reference 11) where the input ground motion is applied, and is located at the elevation of the bottom of the basemat. The effect of variability of ground motion between the different points of the basemat is neglected (Section 4.5.1, Assumption 2). To properly account for the effect of soil profile on ground accelerations arriving at the basemat level, the ATHs at the basemat level are calculated in the SSI analysis. The ACS SASSI (Reference 12) computer program is used to perform the SSI analyses of both the R/B complex and T/B FE models. The SSI analyses are performed for the six generic soil profiles (as described in Reference 5). The five time histories discussed and developed in Sections 4.1 and 5.1 are then processed with the SSI analyses according to the methodology outlined in Reference 5. The CSDRS compatible time histories are applied for each orthogonal direction individually. The ATH responses obtained from these analyses are used as input for the nonlinear sliding analyses presented herein. All components of the seismic input accelerations (including rotations) are amplified by a factor of 1.1, as explained in Section 1.0. To obtain values that are representative for the entire basemat area and to avoid any effects of local flexibility of the basemat, the horizontal and vertical accelerations computed in ACS SASSI and used as translational accelerations in the sliding analyses are taken from a location below a major wall of the structure (R/B complex or T/B) and close to the geometric center of the plan of the basemat.

It is concluded based on results of sensitivity studies (see Section 5.2.1.1) that input rocking motions with respect to the two horizontal axes may be important for the results of nonlinear sliding analyses. Therefore, rocking input, applied to the subgrade as rotational accelerations, is included. As the subgrade is modeled as a rigid surface in the sliding analyses, vertical motion at any three non-collinear points on this surface can define the basemat rotations about the two horizontal axes (rocking). This vertical motion is obtained from the SSI analyses (Reference 5 and Section 5.3.1.1 of this TeR) in terms of vertical ATHs at three non-collinear

points on the basemat. If the basemat were modeled as perfectly rigid in the SSI analyses, selection of the three locations would be arbitrary. However, due to basemat flexibility accounted for in the SSI analyses, different sets of three points may result in slightly different input rocking motions for the sliding analysis.

To ensure conservative results in terms of rocking, the locations of points defining rocking are first restricted to the basemat perimeter, where larger basemat flexibility may lead to larger differences between the vertical deflections at the selected locations and therefore to larger rocking motion. As the basemat is in general more flexible at the corners, a reasonable selection for the three locations is considered to consist of two corners of the basemat plus the center of the opposite side. There are four such sets of locations, as illustrated in Figure 4.5.2-1 for the R/B complex, denoted by R1 through R4. One set of locations, namely R1 in Figure 4.5.2-1, was identified based on sensitivity studies to provide, on average, more conservative results (i.e., larger sliding) than the other three sets and was selected as basis for defining rocking input.

The input rotational accelerations are calculated based on the equation of a plane through three non-collinear points, $P_1(x_1, y_1, z_1)$, $P_2(x_2, y_2, z_2)$ and $P_3(x_3, y_3, z_3)$ - Figure 4.5.2-2:

$$a \cdot x + b \cdot y + c \cdot z + d = 0 \qquad \text{Equation 4.5.2-1}$$

where the expressions for the coefficients *a, b, c* and *d* are:

$$a = \begin{vmatrix} 1 & y_1 & z_1 \\ 1 & y_2 & z_2 \\ 1 & y_3 & z_3 \end{vmatrix} \quad b = \begin{vmatrix} x_1 & 1 & z_1 \\ x_2 & 1 & z_2 \\ x_3 & 1 & z_3 \end{vmatrix} \quad c = \begin{vmatrix} x_1 & y_1 & 1 \\ x_2 & y_2 & 1 \\ x_3 & y_3 & 1 \end{vmatrix} \quad d = -\begin{vmatrix} x_1 & y_1 & z_1 \\ x_2 & y_2 & z_2 \\ x_3 & y_3 & z_3 \end{vmatrix}$$

The normal to the plane is the vector $\overline{N}$ (*a, b, c*) - see Figure 4.5.2-2. The angles defining the plane rotation with respect to the two horizontal axes, x and y, are defined as:

$$\theta_x \cong \tan\theta_x = -\frac{b}{c} \rightarrow \text{plane rotation about x-x axis} \qquad \text{Equation 4.5.2-2}$$

and

$$\theta_y \cong \tan\theta_y = \frac{a}{c} \rightarrow \text{plane rotation about y-y axis} \qquad \text{Equation 4.5.2-3}$$

where, for very small angles, the angle measure in radians is numerically equal to its tangent.

Given the plane coordinates (x_i and y_i, i = 1,…,3) of the three points, P1, P2 and P3, and the vertical displacement time histories at these three points, $z_1(t)$, $z_2(t)$, and $z_3(t)$, one can calculate the time histories of the plane rotations about the two horizontal axes by replacing z_i by $z_i(t)$ in Equation 4.5.2-1. Note that when z_i, i = 1,…,3, are functions of time, a and b in Equations 4.5.2-1 through 4.5.2-3 as well as θ_x and θ_y in Equations 4.5.2-2 and 4.5.2-3, become also functions of time, namely $\theta_x(t)$ and $\theta_y(t)$.

In the same manner used to obtain the rotation time histories from the vertical displacement time histories at three points, one can obtain rotational ATHs, $\ddot{\theta}_x(t)$ and $\ddot{\theta}_y(t)$ (units: radians/sec^2) if $z_1(t)$, $z_2(t)$, and $z_3(t)$ are replaced by vertical ATHs. The following procedure is used to input seismic accelerations in nonlinear sliding analyses accounting for rocking:

1. Select a location below a major wall of the structure (R/B complex or T/B) and close to the geometric center of the plan of the basemat - point A in Figure 4.5.2-1.
2. Obtain from the SSI analysis (Reference 5 and Section 5.3.1.1 of this TeR for the R/B complex and the T/B, respectively): (1) the net translation ATHs at the basemat level at location A - in x, y and z directions - these are denoted in the following by $a_{xc}(t)$, $a_{yc}(t)$ and $a_{zc}(t)$, and (2) the vertical ATHs at the basemat level at locations P_1, P_2 and P_3 corresponding to set R1 in Figure 4.5.2-1, and denoted here by $a_{z1}(t)$, $a_{z2}(t)$ and $a_{z3}(t)$, respectively.
3. Replace z_i, i = 1,…,3, in Equation 4.5.2-1 by the vertical ATHs recorded on the perimeter, $a_{z1}(t)$, $a_{z2}(t)$ and $a_{z3}(t)$, and obtain $a(t)$, $b(t)$ and c. Plug the last three quantities in Equations 4.5.2-2 and 4.5.2-3 and obtain the rotational accelerations about the *x-x* and *y-y* axes, $\ddot{\theta}_x(t)$ and $\ddot{\theta}_y(t)$, respectively.
4. Apply the set of five time histories (three translational accelerations, $a_{xc}(t)$, $a_{yc}(t)$ and $a_{zc}(t)$, and two rotational accelerations, $\ddot{\theta}_x(t)$ and $\ddot{\theta}_y(t)$) to the pilot node of the rigid target surface representing the subgrade. The pilot node coordinates are the same as the coordinates of point A in Figure 4.5.2-1.

As explained in Reference 11, the DOFs of the pilot node represent the motion of the entire rigid surface that models the subgrade in the nonlinear sliding analyses, therefore the translational and rotational accelerations are actually applied to the subgrade below the basemat in the transient nonlinear sliding analyses.

This methodology, therefore, develops analyses that are fully coupled, i.e., the SSI effects are explicitly included, and the only additional assumption is that a small amount of sliding would not modify the ground motion in the vicinity of the basemat (Section 4.5.1, Assumption 1).

4.5.3 Backfill Pressures

4.5.4 Sliding of the R/B Complex and the T/B

Seismic induced sliding of the R/B complex and the T/B is calculated using fully coupled nonlinear time history FE analyses performed with ANSYS (Reference 11). The base input ground motion includes three translational accelerations and two rotational accelerations (the latter simulate rocking). The input ATHs prescribed at the basemat level are calculated in SSI analyses performed with ACS SASSI (Reference 12). They include the effects of subgrade as well as the effect of the structure on the seismic accelerations. All components of the seismic

ground motion (three translations and two rotations) are amplified by a factor of 1.1, as discussed in Section 1.0. The kinetic friction coefficient, μ_k = 0.50, is conservatively used throughout the nonlinear sliding analyses for both sliding and non-sliding phases.

The sliding analyses are performed for six SPs (Reference 5). For each SP, sliding is calculated using five different sets of input ATHs, developed as described in Section 4.1, so there are a total of 30 nonlinear sliding analyses for each structure considered here. These structures are:

- The R/B complex with cracked concrete section properties;
- The R/B complex with uncracked concrete section properties;
- The T/B with uncracked concrete section properties.

Based on the results of sensitivity studies discussed in Section 5.3.2.3, it is concluded that the T/B model with uncracked concrete section properties consistently provided more conservative results (i.e., larger sliding) than the model with cracked section.

The nonlinear sliding analyses are performed using the FE models derived from the ANSYS Dynamic FE models that are subsequently prepared for sliding analysis as described in Section 4.2. For the R/B complex, the nonlinear sliding analyses using the FE model proved to be very demanding computationally. The FE model analyses are limited to a number of representative cases and all 60 analyses are performed using a simplified LMSM. The LMSM is calibrated and validated for sliding based on the FE model, as described in Section 4.3. The representative cases where the sliding analyses are performed using the FE model are selected as follows:

- Five cases for each concrete section (cracked and uncracked) screened for validating the two LMSMs as described in Section 4.3.2.1;
- The governing case for each SP (i.e., the case yielding the maximum total sliding for a certain SP, based on the LMSM analyses).

The results of sliding analyses are evaluated in Section 5.4.1 to decide if any more cases need to be analyzed using the FE model.

The decisions regarding several aspects of the nonlinear sliding analyses presented here, including structural properties, loads, and input ground motion, are made based on the results of sensitivity studies, as follows:

1. Verification of frequency ranges used to calculate the Rayleigh damping coefficients - presented in Sections 5.2.2.2 and 5.3.2.2.
2. Effect of concrete section cracking on sliding analysis results - presented in Sections 5.2.2.5 and 5.3.2.3.
3. Effect of rocking - discussed in Section 4.5.2.
4. Effect of variations of the Live Loads on the sliding analysis results - discussed in Appendix B, Section B.1.1.
5. Effect of variations of the GWL on the sliding analysis results - discussed in Appendix B, Section B.1.2.
6. Effect of variations of the friction coefficient assumed at the basemat - subgrade interface - discussed in Appendix B, Section B.1.3.
7. Effect of the factor applied to the input ground motion - discussed in Appendix B, Section B.1.4.

The last two studies (6 and 7) are used to assess the magnitude of the conservatism included in the nonlinear sliding analyses presented here (see Section 6.3).

4.5.5 Statistical Processing of Sliding Analysis Results

The results of sliding analyses are obtained in terms of time histories of relative sliding between the basemat and the subgrade, in two orthogonal directions: $\delta_x(t)$ and $\delta_y(t)$. The main result, used in this TeR for assessing structural safety to sliding and for the design of the Standard Plant, is the maximum total sliding, defined as:

$$\delta_{\max} = \max_t \left(\sqrt{\delta_x^2(t) + \delta_y^2(t)} \right) \qquad \text{Equation 4.5.5-1}$$

The maximum total sliding represents the maximum vector displacement of the structure from its initial location, occurring during the seismic event.

The result of interest for Standard Plant design is the maximum expected value of the maximum total sliding, considering the variability of subgrade properties, loads and structural characteristics, and the uncertainties induced by the ground input motion variability and modeling approximations.

These uncertainties are addressed as follows:

1. Soil property variability - addressed by considering the six design basis generic SPs described in Reference 5.
2. Load variability – the amount of Live Loads considered in the analysis does not significantly affect the resulting sliding (see Appendix B, Section B.1.1) - consider 25% Live Loads in the analysis.
3. Structural characteristics:
   - For T/B - use uncracked section that is proven to govern sliding.
   - For R/B complex - envelope results from cracked and uncracked section.
4. Ground motion: use five ATHs.
5. Modeling approximations:
   - For T/B - use the FE model - the modeling approximations are minimal.
   - For R/B complex - use the LMSM calibrated and validated based on FE model to identify the governing cases (resulting in maximum sliding) for full FE model analysis by screening all the combinations of SPs, ATHs, and structure types; perform FE model analyses for selected cases and use the results for assessing sliding magnitude.

The sliding analysis results are grouped to obtain a significant sample size and calculate the maximum expected sliding with probability of exceedance of 2.5% (for a Normal distribution, this is equivalent to the sample mean plus 2 times the sample standard deviation). Grouping can be done by:

- soil profiles and rock profiles;
- ATHs that consistently result in significantly larger sliding across soil and/or rock profiles for certain structures.

The maximum expected value for sliding (used for design) is selected as the maximum value obtained from all groups considered.

Table 4.1.2-1 Target Control Points for the US-APWR CSDRS

Horizontal Control Points		Vertical Control Points	
Frequency (Hz)	Acceleration (g)	Frequency (Hz)	Acceleration (g)
5% Damping		5% Damping	
A (50)	0.3	A (50)	0.3
B (12)	0.78	B (12)	0.78
C (2.5)	0.94	C (3.5)	0.89
D (0.25)	0.140	D (0.25)	0.094
E (0.1)	0.0226	E (0.1)	0.015

Notes:
1. 0.3 g PGA
2. Based on RG 1.60, Revision 1 amplification factors
3. For Control Point D & E, acceleration is computed as follows:
   Acceleration = $(\varpi^2 D / 386.4\ \text{in/sec}^2)(F_A)(0.3)$
   ϖ = 2π(frequency) [rad/sec]
   D = Displacement [in]
   F_A = Amplification Factor from RG 1.60

Table 4.1.4-1 Selected Earthquakes

Earthquake	Station	Assumed Direction		Selected Segment (sec)	Δt (sec)
		H1 (NS)	H2 (EW)		
Chi Chi	ILA067	N	E	26 - 50	0.005
Darfield	DFHS	S17E	S73W	17 - 42	0.020
Hector Mine	Amboy	90	360	5 - 28	0.020
Nahanni	Site 3	270	360	0 - 19.095(1)	0.005
Northridge	Mt. Baldy	180	90	11 - 33.08	0.010

Notes:
1. Total duration of record. Zero padding will be applied to the Nahanni seed to exceed 20 seconds in duration during the development of the time history.

Table 4.1.4-2 Correlation Coefficients for Seed Components

Earthquake	Components		
Chi Chi	N-E	N-V	E-V
	0.1069	-0.1348	-0.0774
Darfield	S17E-S73W	S17E-V	S73W-V
	0.0795	-0.0930	0.0548
Hector Mine	090-360	090-V	360-V
	0.1098	0.0708	0.0125
Nahanni	270-360	270-V	360-V
	-0.0522	-0.1555	0.1401
Northridge	180-090	180-V	090-V
	-0.0763	0.0246	-0.1848

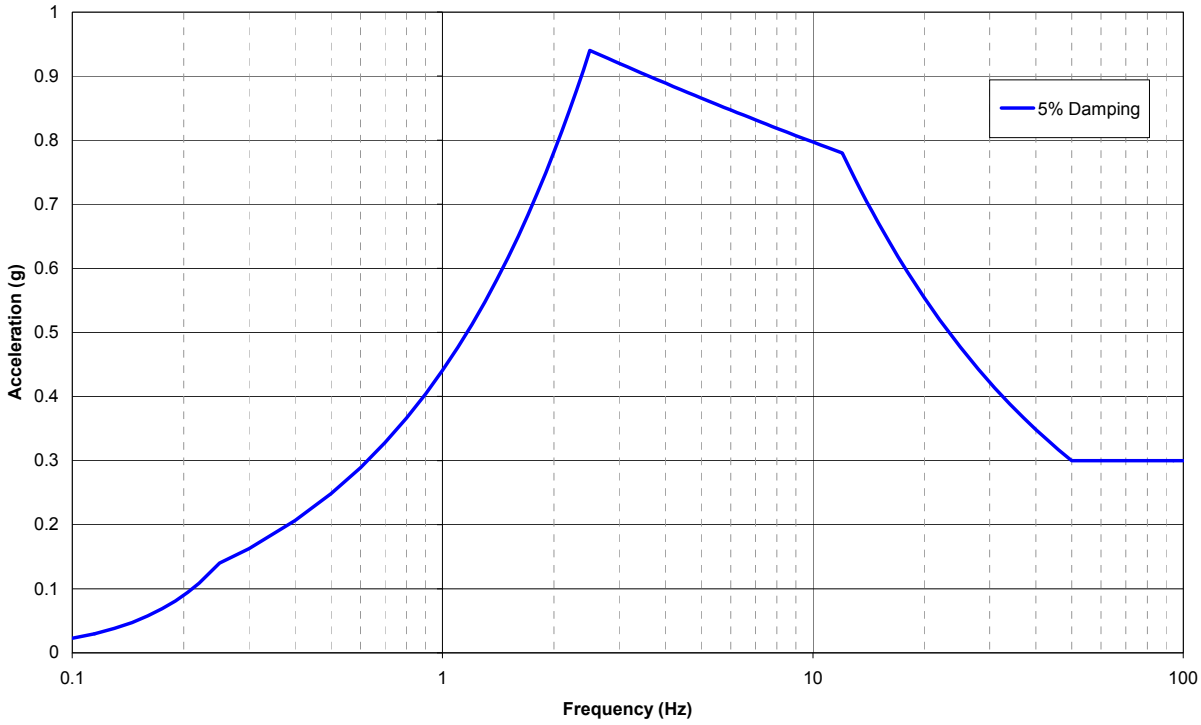

Figure 4.1.2-1 US-APWR Horizontal CSDRS

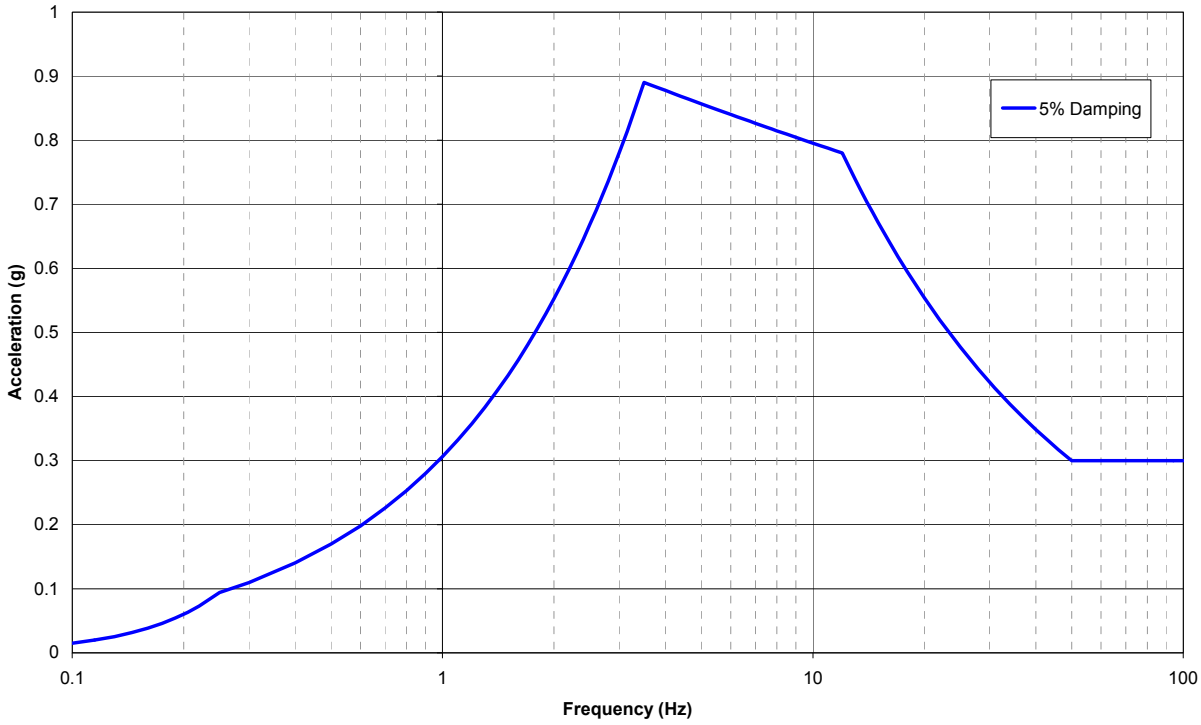

Figure 4.1.2-2 US-APWR Vertical CSDRS

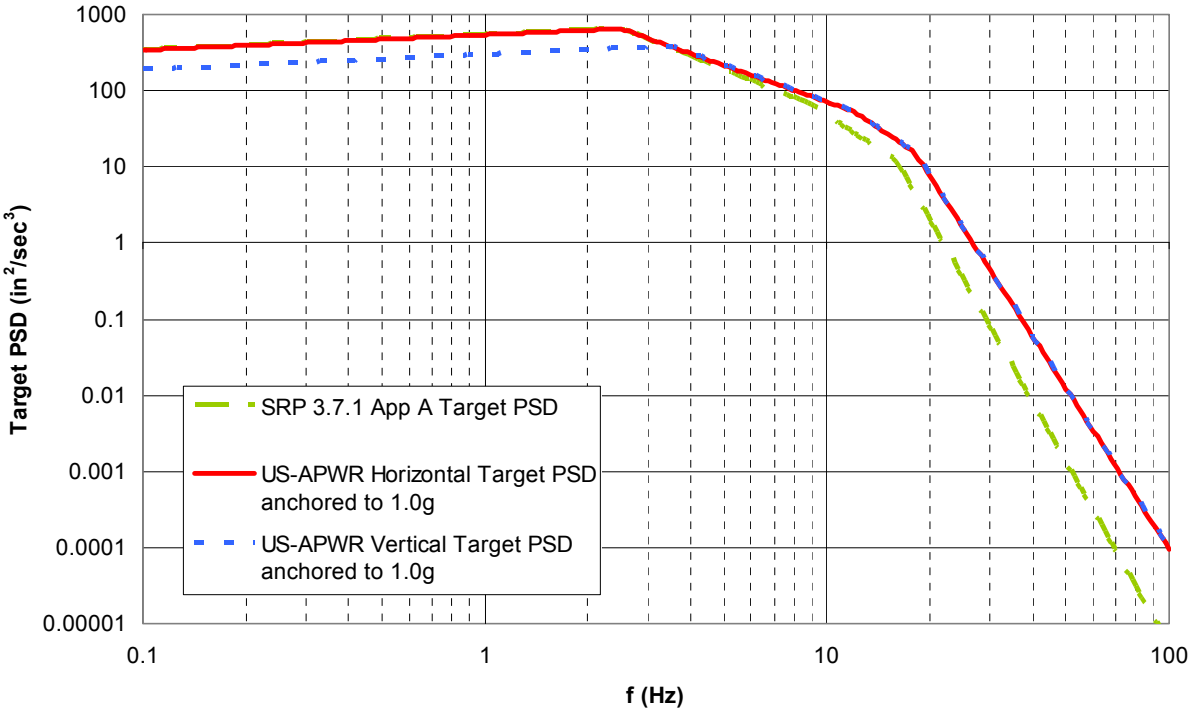

Figure 4.1.3-1 Target Horizontal and Vertical PSD

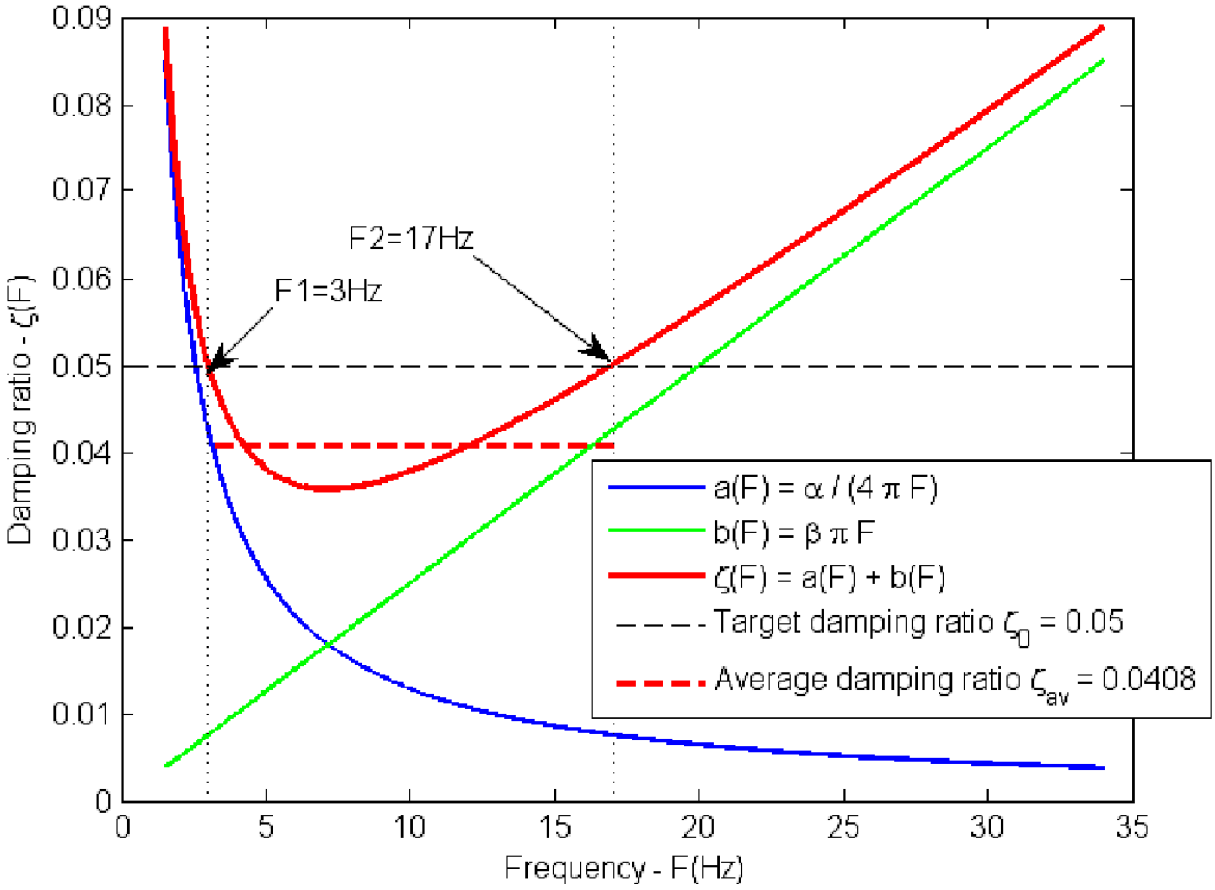

Figure 4.2.2-1 Variation of Rayleigh Damping Ratio with Modal Frequency (FE Model of the R/B Complex with Cracked Concrete Section)

Figure 4.2.3-1 Preparation of the R/B Complex for Sliding Analysis

Figure 4.2.3-2 FE Model of the R/B Complex Prepared for Sliding Analysis

Figure 4.3.1-1 LMSM Calibration Methodology

Figure 4.5.2-1 Locations of nodes for Calculating Base Input Motion for Sliding Analysis of the R/B Complex

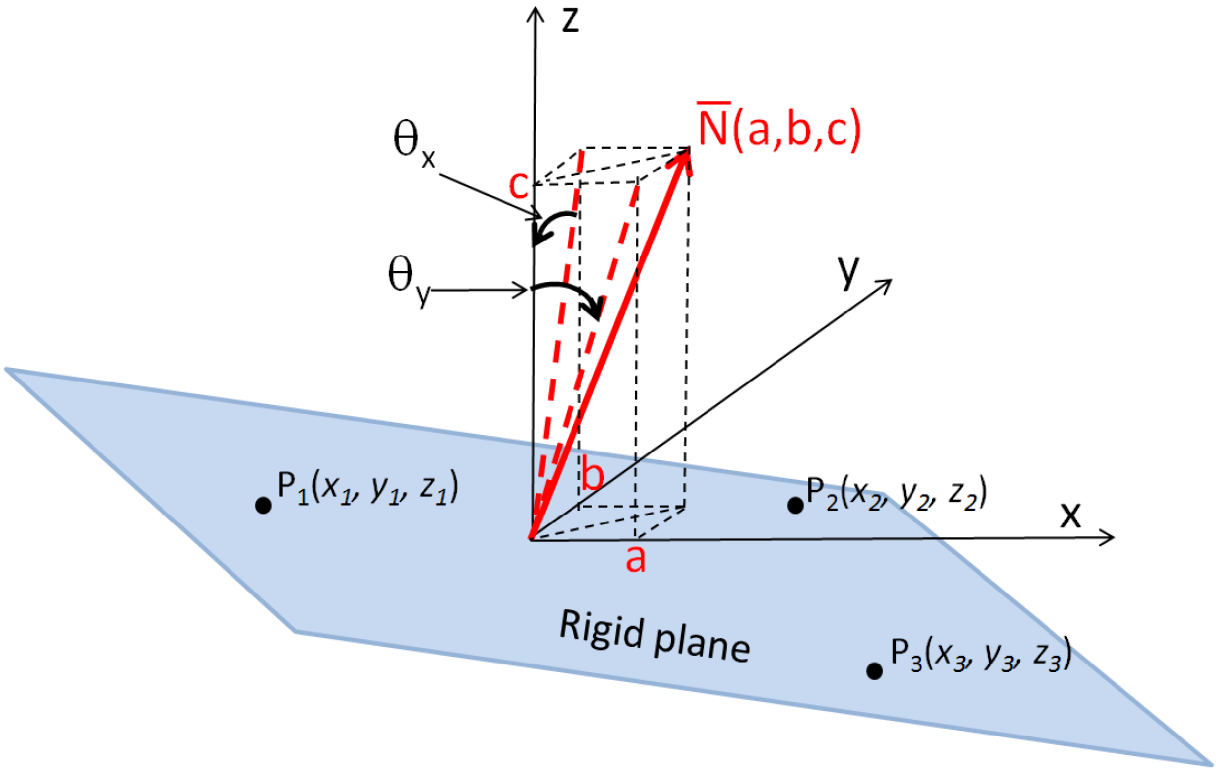

Figure 4.5.2-2 Rotations of a Plane

5.0 CALCULATIONS AND RESULTS

5.1 Time Histories for Nonlinear Sliding

The time histories (shown in Figure 5.1-1 through Figure 5.1-15) are developed by modifying the seed time histories (three components each) as described in Section 4.1. The corresponding velocity and displacement time histories have also been computed and are plotted in the same set of Figures. Each of these component time histories meets the criteria of SRP 3.7.1 Option 1, Approach 1 and Option 2 as described in Section 4.1.1. Compliance to these criteria is summarized in the following paragraphs.

Figure 5.1-16 through Figure 5.1-18 graphically demonstrate that the response spectra derived from the time histories are developed in accordance with SRP 3.7.1 Option 1, Approach 1 and Option 2 (Reference 3), for time history components H1 North-South (NS), H2 East-West (EW), and Vertical (UP), respectively. The average response spectra of all components envelopes the CSDRS at 5% damping in accordance with the criteria described in Section 4.1.1.

Figure 5.1-19 through Figure 5.1-21 show that the average PSDs of the time histories are greater than 80% of the horizontal and 80% of the vertical target PSDs presented in Equations 4.1.3-1 and 4.1.3-2 over the range of 0.3 to 45 Hz. This is in accordance with the requirements described in Section 4.1.1.

Table 5.1-1 provides statistical independence values of the three components for each of the time histories, which satisfies the criterion that the absolute value of correlation coefficients between the components must be less than 0.16.

As demonstrated in Table 5.1-2, the total durations of the design basis time histories meet the SRP guidance criteria that the durations exceed 20 seconds. Table 5.1-3 shows the rise time, strong motion duration, and decay time of each component. These values are computed based on the definition of strong motion duration in SRP 3.7.1, using the normalized AI. Figure 5.1-22 through Figure 5.1-26 shows the normalized AI plots of cumulative energy for each component of the five time histories, respectively. The time history components show an initial time interval of gradual energy buildup, followed by a ramp of rapid energy accumulation, and then followed by a gradual tapering of energy accumulation. The strong motion duration should be at least six seconds, according to SRP 3.7.1, and in compliance with duration criteria for earthquake magnitude and distance bins listed in Table 5.1-4. The strong motion durations of the design basis time history satisfy both duration criteria.

Table 5.1-5 also shows the V/A and AD/V^2 values for mean ratios ± one standard deviation for the earthquakes of magnitude bins of **M**6.5+ with distance bins from 10 to 100 km, using data provided in Table 3-6 of NUREG/CR-6728 (Reference 7). The V/A and AD/V^2 ratios of the design basis time histories are within the limits as shown in Table 5.1-6.

Adequate representation of the Fourier components at low frequency is achieved by ensuring that the artificial time history matches the CSDRS at 5% damping and meets the PSD targets. As demonstrated above, the time histories developed from the five seeds satisfy all the requirements described in the Option 1, Approach 1 and Option 2 of SRP 3.7.1 as outlined in Section 4.1.1.

5.2 R/B Complex

The following abbreviations are used in the figure legends equations and in the tables with the summary of the results:

1. For the five ATH results corresponding to the time histories developed for nonlinear sliding analysis:
   - CC = Chi-Chi time history
   - DR = Darfield time history
   - HM = Hector Mine time history
   - NH = Nahanni time history
   - NR = Northridge time history
2. For the six SP:
   - 22 = Profile 270-200
   - 25 = Profile 270-500
   - 55 = Profile 560-500
   - 92 = Profile 900-200
   - 91 = Profile 900-100
   - 21 = Profile 2032-100
3. For concrete section:
   - CR = Cracked concrete section properties
   - UC = Uncracked concrete section properties
4. Sets of locations for rocking input:
   - R0 = no rocking
   - R1 through R4 - rocking input calculated from the set of locations marked by R1 to R4, respectively, in Figure 4.5.2-1.

For example: 'DR21CR' indicates the results of an analysis for the SP 2032-100, with the Darfield input ATH, and using the cracked concrete section properties.

5.2.1 Loads

5.2.1.1 Seismic Loads

The input to the sliding analysis consists of net translation ATHs extracted from the SSI analyses (Reference 5) and applied to the subgrade below the basemat in all three directions. As briefly discussed in Section 4.5.2, a series of sensitivity analyses were performed using the LMSM: (1) to investigate if rocking (rotations about two horizontal axes) is also important for sliding and has to be included as input in the nonlinear sliding analyses, and (2) to select a set of points at the basemat-subgrade interface for calculating basemat rotations that yield more conservative results in terms of calculated sliding. The results of these studies are presented later on in this section.

The translational and rotational ground ATHs used as input for the sliding analyses are derived based on nodal ATHs calculated in the SSI analyses of the R/B complex at selected locations at the basemat to subgrade interface. The ATHs from the SSI analyses are obtained from the following steps:

1. Select the active structural nodes in the R/B complex model, as marked in Figure 5.2.1.1-1.
2. Post-process the ATHs for the structural nodes from step 1 with the five sets of input ground motion time histories using ACS SASSI (Reference 12).
3. Repeat step 2 for each SP and each concrete section (cracked and uncracked).

The results consist of 60 sets of ATHs (for six SPs times five time histories times two types of concrete sections) at each of the nine nodes shown in Figure 5.2.1.1-1. Each set contains nine time histories, $\hat{a}_{mn}(t)$, where $m = x$, y or z represents the direction of the input motion applied in the SSI analysis and $n = x$, y or z represents the direction of the response acceleration, and the notation *"â"* (a-hat) refers to accelerations calculated in the SSI analyses. The translation accelerations in three orthogonal directions to be used as input in the nonlinear sliding analyses, $a_x(t)$, $a_y(t)$, $a_z(t)$, are calculated by superposition, as:

$$a_x(t) = \sum_{m=x,y,z} \hat{a}_{mx}; \quad a_y(t) = \sum_{m=x,y,z} \hat{a}_{my}; \quad a_z(t) = \sum_{m=x,y,z} \hat{a}_{mz}; \qquad \text{Equation 5.2.1.1-1}$$

All three ATHs, namely $a_x(t)$, $a_y(t)$, $a_z(t)$, are calculated for the central node (node A in Figure 4.5.2-1), based on the ATHs $\hat{a}_{mn}(t)$ calculated in the SSI analyses at node 1937 (Figure 5.2.1.1-1). These are the translational ATHs prescribed to the subgrade in the nonlinear sliding analyses. Only the vertical components of input accelerations are calculated for the perimeter nodes indicated by markers in Figure 4.5.2-1, using the SSI results in vertical direction, $\hat{a}_{mz}(t)$, from the corresponding nodes shown in Figure 5.2.1.1-1. The vertical accelerations at the perimeter nodes, $a_z(t)$, are used to calculate input rocking motions, prescribed to the subgrade as rotational accelerations, as described in Section 4.5.2.

Effect of Rocking:

The first set of sensitivity analyses for investigating the effect of rocking were performed with the LMSM for cracked concrete section calibrated based on the FE model, as discussed in Section 5.2.3 and Appendix A, but not yet validated for sliding (Section 5.2.4), as a decision on the seismic input was needed before validation of the LMSM. Four cases, or combinations of ATH and SP, were selected to perform sensitivity analyses. As no screening information (see Section 5.2.2.3) was available at the time of this preliminary analysis, the selection of the four cases was done based on the results of a limited set of runs performed without considering rocking. The following cases were selected for the preliminary analysis:

1. Profile 2032-100, Darfield ATH (DR21CR)
2. Profile 2032-100, Hector Mine ATH (HM21CR)
3. Profile 900-200, Chi-Chi ATH (CC92CR)
4. Profile 560-500, Hector Mine ATH (HM55CR)

Two more sets of sensitivity analyses were performed using the validated LMSMs for cracked and uncracked sections, to verify the results of the preliminary study:

1. For the cracked concrete section, using all five cases selected in Section 5.2.2.3 for validation of the LMSM. The results are presented in Table 5.2.1.1-2 in terms of maximum total sliding, and in Figure 5.2.1.1-2 through Figure 5.2.1.1-6 in terms of calculated maximum sliding as a function of time.
2. For the uncracked concrete section, using two cases selected from the five cases screened in Section 5.2.2.3 that provided the maximum values of total sliding in the runs with the validated LMSM for uncracked section. The results are presented in Table 5.2.1.1-3, in terms of maximum total sliding, and in Figure 5.2.1.1-7 and Figure 5.2.1.1-8, in terms of total sliding as a function of time.

5.2.1.2 Live Loads

The Live Loads considered for the nonlinear dynamic sliding analyses include, in accordance with SRP 3.7.2 (Reference 24) “25% of the floor design live load and 75% of the roof design snow load”. As the Live Loads may act, under specific circumstances, as stabilizing loads, the effect of considering the Live Loads in the sliding analyses was investigated in a sensitivity study, by comparing the amount of sliding calculated assuming presence of Live Loads as specified by SRP 3.7.2 with the amount of sliding calculated assuming no Live Loads. The sensitivity study, presented in Appendix B, Section B.1.1, was performed for the R/B complex with cracked section using the validated LMSM.

The conclusion of the study was that accounting for or not for the presence of Live Loads in the sliding analysis does not have a significant effect on the results in terms of maximum total sliding (out of 30 cases analyzed, the average difference between results in terms of maximum total sliding, δ_{max}, was zero, and the maximum difference was 0.02in, which represents about 3% of the maximum value of δ_{max}). Therefore, only sliding analyses including presence of Live Loads (as specified in SRP 3.7.2 for dynamic analyses) are considered in this TeR.

5.2.1.3 Lateral Earth Pressures

As stated by Assumptions 3 and 4 (Section 4.5.1), no lateral earth pressures from backfill, acting on the vertical walls of the basement, are considered in the nonlinear sliding analyses presented in this TeR. As explained in Section 4.5.3, neglecting the active earth pressures and passive soil reactions acting on moving basemat walls during sliding (Assumption 3) is conservative. Assumption 4, related to dynamic soil pressures acting on fixed (non-moving) walls when the structure does not slide, is discussed in this section based on a quantitative assessment.

As discussed in Section 4.4, a conservative value of the static friction coefficient at the basemat-subgrade interface for all natural soil and rock subgrades, and for engineered fill

placed below the basemat, is μ_s = 0.7. A conservative value of the kinetic friction coefficient, valid for the case when the structure slides with respect to the subgrade, was established in Section 4.4 as μ_k = 0.5. As discussed in Section 4.4, this reduced friction value is used in the sliding analyses for both sliding and non-sliding (static) phases. Assumption 4 in Section 4.5.1 states that dynamic soil pressures, acting when the structure is not moving with respect to the subgrade, and which are not considered in the analysis, are compensated by the difference between the static friction force and the dynamic friction force that is not accounted for in the analysis.

5.2.2 Development of the FE Model and Analysis

5.2.2.1 Contact Formulation

The modeling of the contact between basemat and subgrade by means of compression only contact elements with Coulomb friction is described in detail in Section 4.2.3. The minimum stiffness of the contact elements necessary to avoid spurious vibrations induced by rigid body motion of the entire structure is determined as described in Section 4.2.3. The R/B complex has a total mass of 37,797 kilo-slugs and rests on the basemat with area of 124,955 ft^2. Using Equations 4.2.3-1 and 4.2.3-2 and assuming 5% structural damping ratio, the minimum contact stiffness per unit area of the basemat needed to avoid rigid body vibrations for frequencies of the input motion of at least 50Hz is approximately 3.0×10^6 kips/ft/ft^2.

5.2.2.2 Damping Formulation and Verification

Selection of the Frequency Range

For both R/B complex models with cracked and uncracked concrete section, modal analyses are performed using the FE model, as follows: (1) one analysis using the entire model of the R/B complex, and (2) one analysis for the superstructure, consisting of the CIS, the PCCV, and the Group of Structures Consisting of the R/B, A/B and East & West PS/Bs (termed here

as ARPSB). The components of the superstructure are fixed at the top of the basemat in this second modal analysis. This second modal analysis (with superstructure only) is performed only for the purpose of establishing criteria to select the frequency range that is relevant for sliding.

The end frequencies *F1* and *F2* of the frequency range described in Section 4.2.2 are computed as follows: First, the lower bound *F1*, of the frequency range, is determined as the lowest modal frequency below which the cumulative modal mass participation ratio of the entire structure in any direction is less than 1%. Next, the upper bound, *F2*, of the frequency range, is selected as the frequency below which the cumulative modal mass ratio of the entire structure (including the basemat) in the vertical direction is at least 70%, and below which the cumulative modal mass ratio of the superstructure in any horizontal direction is at least 80%. The selected values of *F1* and *F2* are verified using sensitivity analysis results, as discussed in the verification part of this Section. The selected values of *F1* and *F2* for the two R/B complex models are summarized in Table 5.2.2.2-1.

R/B Complex - Cracked concrete section:

The lower bound is selected as *F1* = 3 Hz. This corresponds to allowing 100% of the total modal mass in any direction (i.e., all modal frequencies are larger than 3 Hz) - Figure 5.2.2.2-1. The upper bound is selected as *F2* = 17 Hz. This corresponds to 72% of the modal mass of the entire structure in the vertical direction - Figure 5.2.2.2-1, and over 85% of the modal mass of the superstructure in any horizontal direction - Figure 5.2.2.2-2. The frequency range selected for calculating the Rayleigh damping coefficients and the damping ratio $\zeta(F)$ are presented in Figure 5.2.2.2-3.

R/B Complex - Uncracked concrete section:

The lower bound is selected as *F1* = 4.1 Hz. This corresponds to allowing 100% of the total modal mass in any direction (i.e., all modal frequencies are larger than 4.1 Hz) - Figure 5.2.2.2-4.The upper bound is selected as *F2* = 23.4 Hz. This corresponds to 70% of the modal mass of the entire structure in the vertical direction - Figure 5.2.2.2-4, and over 85% of the modal mass of the superstructure in any horizontal direction - Figure 5.2.2.2-5. The frequency range selected for calculating the Rayleigh damping coefficients and the damping ratio $\zeta(F)$ are presented in Figure 5.2.2.2-6.

Verification of the Frequency Ranges

The range of frequencies selected for calculating the Rayleigh damping coefficients may affect the results of nonlinear sliding analyses as follows:

1. If the selected range is too narrow, some vibration modes of the structure that are significant for sliding may be left outside this range. Examining the mathematical expression of the modal damping ratio (Equation 4.2.2-2 and Figure 4.2.2-1), a rapid increase in modal damping ratio can be observed outside the range of frequencies selected to calculate the damping coefficients. Therefore, the modes corresponding to frequencies outside the range *F1* to *F2* are assigned damping ratios larger than the target value. If these modes are important for sliding, the results of the sliding analysis may not be conservative.
2. If the selected range is too wide, the damping ratio assigned to the vibration modes that are important for sliding will be lower than the target damping ratio. This is illustrated in Figure 5.2.2.2-3, which is based on two frequency ranges considered here for the R/B complex with cracked concrete section and a target damping ratio ζ_0 = 5%. As shown in Figure 5.2.2.2-3, an increase of the upper bound of relevant frequencies from *F2* = 17 Hz

to *F2'* = 30 Hz results in a reduction of the average damping ratio over the relevant frequency range from 4.08% to 3.66%.

In order to ensure conservative numerical results in the sliding analysis, all vibration modes that are important for sliding must be assigned damping ratios that are less than or equal to the target. Therefore, it is necessary to appropriately compute the range *F1* to *F2*.

The lower bound, *F1*, is established to allow the inclusion of all of the modal mass in any direction (see Figure 5.2.2.2-1 and Figure 5.2.2.2-4); therefore validation of the lower bound of the frequency range is not necessary.

The validation of the upper bound, *F2*, is accomplished by comparing the results of two sliding analyses in terms of maximum total sliding, as follows:

- One analysis is performed with Rayleigh damping coefficients calculated based on the original frequency range, *F1* to *F2*.
- A second analysis is performed with Rayleigh damping coefficients calculated based on the extended frequency range, from *F1* to *F2'* (with *F2'* about 1.5 to 2 times *F2*).

If the selected original range (*F1* to *F2*) is too narrow, the first analysis would yield maximum sliding values that are significantly different (differences in excess of 5%) from those given in the second analysis, as some modes important for sliding have been over-damped in the first analysis. In this case the original range is extended (i.e., *F2* is increased) and the process is repeated. If the selected original range (*F1* to *F2*) includes all vibration modes significant for sliding then both analyses are expected to produce results in a close range (considered here to be within 5% of each other), the selected upper bound, *F2*, is considered validated, and the selected original range becomes the relevant frequency interval used for calculating the Rayleigh damping coefficients. The allowance of 5% between the results is justified by the fact that the second analysis is conducted with an average damping ratio (applied to relevant vibration modes) that is lower than the average damping ratio in the first analysis (see Figure 5.2.2.2-3).

The extended frequency ranges for the R/B complex with cracked and with uncracked concrete section are listed in Table 5.2.2.2-2. The results of sensitivity analyses using the FE model in terms of maximum total sliding are listed in Table 5.2.2.2-3, and the time histories of total sliding for case HM21UC, with the largest percent difference, are plotted in Figure 5.2.2.2-7. It can be noted that the analysis for extended frequency range (red line in Figure 5.2.2.2-7) was stopped before the end of the ATH. This is because some of the sliding analyses not used to derive final sliding analysis results have been conducted for a smaller number of time steps than the total number included in the ATHs. These runs were stopped at a time instant beyond which the ground input motions become sufficiently small that no additional sliding would be expected.

The percent differences listed in Table 5.2.2.2-3 are calculated as:

$$\Delta(\%) = \frac{\left|\delta_{\max}^{\text{Extended Range}} - \delta_{\max}^{\text{Original Range}}\right|}{\delta_{\max}^{\text{Original Range}}} \times 100 \qquad \text{Equation 5.2.2.2-1}$$

As illustrated in Table 5.2.2.2-3, the maximum percent difference of all the studied cases is less than 5%. The selected frequency range listed in Table 5.2.2.2-1 is thus verified for the sliding analyses of the R/B complex and it is demonstrated that the method for selecting the upper bound, *F2*, is reasonable.

5.2.2.3 Representative Cases

The screening for representative cases of the R/B complex with cracked concrete section was performed based on the sliding analysis results in terms of maximum total sliding obtained using the non-validated LMSM. The results for all 30 cases analyzed are presented in Table 5.2.2.3-1.

The principles used for screening are listed in Section 4.3.2.1. Based on the first principle and using the sliding analysis results listed in Table 5.2.2.3-1, it was concluded that:

1. SPs 270-500 and 270-200 resulted in insignificant values of sliding (0.105 inches or less), and therefore these profiles were excluded from the screening.
2. The Chi-Chi ATH resulted in relatively smaller sliding (less than 0.2 inches) compared to the other four ATHs.

The cases selected for validation of the LMSM of the R/B complex with cracked concrete section are shown in boldface in Table 5.2.2.3-1 and are as follows:

- Case 1: Profile 2032-100, Hector Mine ATH
- Case 2: Profile 2032-100, Darfield ATH
- Case 3: Profile 560-500, Hector Mine ATH
- Case 4: Profile 900-200, Nahanni ATH
- Case 5: Profile 900-100, Northridge ATH

The first four cases were selected based on the first principle (maximum total sliding), and the fifth based on the second principle, to include SP 900-100 and the Northridge ATH, that were not included in the first four cases.

The five representative cases screened for validation of the LMSM with cracked concrete section are analyzed with the FE model. To limit the number the FE model analyses, the same five cases are selected for the validation of the LMSM with uncracked concrete section. In this way, the results of the FE model analyses can be used to decide which concrete section (cracked, uncracked, or both) is used in the final sliding analyses (see also Section 5.2.2.5).

5.2.2.4 Sliding Analysis for Representative Cases

The results of sliding analyses for representative cases, performed with the FE model, are listed in Table 5.2.2.4-1 in terms of maximum total sliding, along with the corresponding results obtained with the non-validated LMSM, for both cracked and uncracked concrete sections. For both concrete sections, cracked and uncracked, the requirements for LMSM validation stated in Section 4.3.2.3 are not met in two out of five cases. Fine tuning is therefore necessary for both LMSMs (see Section 5.2.4).

5.2.2.5 Cracked vs. Uncracked Section

The sliding analyses are performed for five time histories compatible with the CSDRS. During these seismic events, the concrete structure sections are considered to crack, with resulting reduction of the stiffness and increase in damping (Section 5.2.2.2). Uncracked section structures are also analyzed, to obtain the response of structures that may not crack under these seismic events, and the results from the two analyses are enveloped. A sensitivity study is performed using the FE model to investigate if either the cracked section properties or the

uncracked section properties govern sliding of the R/B complex. Five cases are selected for this sensitivity study, corresponding to the cases screened for LMSM validation (Section 5.2.2.3), that are most likely to represent the governing cases for sliding analysis in terms of maximum total sliding.

The results of the sliding analyses for the R/B complex with cracked and uncracked concrete section properties for all five selected cases are summarized in the second and fourth columns of Table 5.2.2.4-1, and the time histories of the calculated total sliding are plotted in Figure 5.2.2.5-1 through Figure 5.2.2.5-5.

The ratio between the maximum total sliding values (see Equation 4.5.5-1), $\delta_{\max}^{UC}$ (uncracked) and $\delta_{\max}^{CR}$ (cracked) is calculated for each case analyzed as:

$$Ratio = \delta_{\max}^{UC} \Big/ \delta_{\max}^{CR} \qquad \text{Equation 5.2.2.5-1}$$

The maximum sliding of the R/B complex with cracked concrete section is higher than the maximum sliding of the R/B complex with uncracked concrete section in two of the five cases in Table 5.2.2.4-1, with minimum ratio close to 0.3. For the other three cases, the ratio is between 1.09 and 1.29. A conclusion cannot be made regarding the effect of concrete section properties on calculated sliding of R/B complex, based on the analysis results presented in Table 5.2.2.4-1. Therefore the sliding analyses are performed for both cases.

Regarding the unusual aspect of the plots in Figure 5.2.2.5-1a, with apparent movement of the two structures in opposite directions, this is due to the fact that the values represented here are total (vector) sliding, resulting from vector addition of the sliding displacements in the X and Y directions. As can be seen in Figure 5.2.2.5-1b, showing sliding in X and in Y directions separately, the two structures slide in the same direction during each sliding event. The large differences in total sliding between times 9 seconds and 21 seconds are due to the fact that, at certain instants, the X and Y sliding displacements of the structure with cracked section (blue lines) cross the *y*=0 axis (change sign), while the X and Y sliding displacements of the structure with uncracked section (red lines) have a constant sign.

5.2.3 Development of the LMSM

Two LMSMs are developed for the R/B complex with cracked and uncracked concrete sections. They are calibrated to accurately reproduce the mass, stiffness and lower modes of the detailed structures, and validated based on the corresponding FE models to reproduce, within reasonable limits (as discussed in Section 4.3.2.3), the amount of sliding calculated using the FE model. The calibration method is described in detail in Appendix A. Validation of the two LMSMs is discussed in Section 5.2.4.

5.2.4 Fine Tuning and Validation

5.2.4.1 Cracked Section

Five cases are selected, as discussed in Section 5.2.2.3, to fine-tune the calibrated LMSM for the R/B complex with cracked section properties, to meet the validation requirements listed in Section 4.3.2.3. Fine tuning is performed by trial-and-error, by modifying the vertical and horizontal stiffness of the beams in all stick models representing the superstructure (PCCV, CIS and ARPSB). After increasing the horizontal stiffness by 10% and reducing the vertical stiffness by 38% for all the beam elements and link elements in the superstructure, the LMSM for R/B complex with cracked concrete section meets the validation criterion set in Section

4.3.2.3 for all five representative cases. The analysis results in terms of maximum total sliding obtained with the validated LMSM are listed in Table 5.2.4.1-1 and compared with the results from the corresponding FE model analyses. Calculated time histories of total sliding for the FE model and the validated LMSM are compared in Figure 5.2.4.1-1 through Figure 5.2.4.1-5, for the representative cases used for LMSM validation.

5.2.4.2 Uncracked Section

Five cases are also selected, as discussed in Section 5.2.2.3, to fine-tune the calibrated LMSM for the R/B complex with uncracked section properties, to meet the validation requirements listed in Section 4.3.2.3. Fine tuning is performed by trial-and-error, by modifying the vertical and horizontal stiffness of the beams in all stick models representing the superstructure (PCCV, CIS and ARPSB). After increasing the horizontal stiffness by 15% and reducing the vertical stiffness by 40% for all the beam elements and link elements in the superstructure, the LMSM for R/B complex with uncracked concrete section meets the validation criterion set in Section 4.3.2.3 for all five representative cases. The analysis results in terms of maximum total sliding obtained with the validated LMSM are listed in Table 5.2.4.2-1 and compared with the results from the corresponding FE model analyses. Calculated time histories of total sliding for the FE model and the validated LMSM are compared in Figure 5.2.4.2-1 through Figure 5.2.4.2-5, for the representative cases used for LMSM validation.

5.2.5 Sliding Analysis Results for the R/B Complex

Several sets of sliding analysis results are obtained and processed as discussed below:

1. Representative cases (Cracked and Uncracked, FE model and validated LMSM): Two sets of results have been obtained after screening and LMSM validation, consisting of five cases for each type of concrete section (cracked and uncracked). Each of these cases is analyzed with both the FE model and the validated LMSM. These results are listed in Table 5.2.4.1-1 and Table 5.2.4.2-1 in terms of δ_{max} for the cracked and the uncracked concrete sections, respectively.
2. All cases, Cracked and Uncracked, validated LMSM: Next, all the remaining combinations of SP, ATH, and section types (cracked and uncracked) are analyzed with the validated LMSM. The results in terms of maximum total sliding are listed in Table 5.2.5-1 through Table 5.2.5-6.
3. Governing cases, Cracked or Uncracked, FE model: For each case, the maximum total sliding for that combination of SP and ATH, $\delta_{max}^{SP,TH}$, is selected as the envelope of results obtained with the LMSM for the cracked and the uncracked section. There are 30 values of $\delta_{max}^{SP,TH}$, as *SP* spans all six SPs and *TH* spans all ATHs. These results are listed in the last lines of Table 5.2.5-1 through Table 5.2.5-6. The maximum value for each SP, $\delta_{max}^{SP,allTH}$, defines the governing case for that SP for all ATHs. This is the screening process mentioned in the Sections 4.0 and 4.3.1. Nonlinear sliding analyses using the FE model are performed for each governing case. For each governing case, the FE model analysis is performed considering either the cracked or the uncracked concrete section properties. The cracked or the uncracked section is selected based on the maximum value obtained with the LMSM for that case. Some of the FE model analyses for the governing cases have already been performed during the validation process (Group 1).

4. For the reasons outlined in Section 5.4.1, two more cases, namely CC55CR and CC55UC, are added to the representative cases of sliding analyses performed using the FE model.

All the sliding analysis results obtained are listed in terms of maximum total sliding (δ_{max} in Equation 4.5.5-1) in Table 5.2.5-1 through Table 5.2.5-6. The selection process described in Item 3 above ensures that nonlinear sliding analyses using the FE model, that minimize the modeling errors, are available for all governing cases that define the maximum sliding for each SP.

Statistical processing is performed in Section 5.4.1 for all results in terms of maximum total sliding values obtained using the FE model, for both cracked and uncracked concrete section properties. These results, obtained from analyses that minimize the modeling errors, include all governing cases, as selected based on the LMSM sliding analyses. The results in this sample are shown highlighted in Table 5.2.5-1 through Table 5.2.5-6.

The 30 values listed in the last lines of Table 5.2.5-1 through Table 5.2.5-6 represent the envelope of sliding analysis results obtained with the LMSM for cracked and uncracked sections. A discussion of these results is presented in Appendix C.

5.3 Turbine Building

5.3.1 Loads

5.3.1.1 Seismic Loads

The translational and rotational ground ATHs used as input for the sliding analyses are derived based on nodal ATHs calculated inform the SSI analyses of the T/B at selected locations at the basemat-subgrade interface. The SSI analyses for the T/B are performed in a similar manner with the SSI analyses for the R/B that are documented in Reference 5. The locations of the structural nodes in the FE model used in the SSI analyses where the acceleration results from the SSI are processed are shown in Figure 5.3.1.1-1. The results consist of 60 sets of ATHs (for six SPs times five time histories times two types of concrete sections) at each of the nine nodes shown in Figure 5.3.1.1-1. The translational and rotational accelerations prescribed to the subgrade in the nonlinear sliding analyses are derived in a similar manner as described in Section 5.2.1.1 for the R/B complex.

A sensitivity study was performed for the T/B with uncracked concrete section to check if the conclusions of the sensitivity studies investigating the effect of rocking performed for the R/B complex and described in Sections 5.2.1.1 apply to the sliding analysis of the T/B. The four sets of locations for defining rocking motion are located on the perimeter of the T/B basemat in a similar manner as for the R/B complex (shown in Figure 4.5.2-1), i.e., set R1 including the nodes located at the basemat level at the South-East corner, center of the North side and South-West corner, etc. This study is performed using the FE model for the T/B with uncracked concrete section and is limited to two cases:

1. Profile 2032-100, Hector Mine ATH (HM21UC)
2. Profile 900-200, Northridge ATH (NR92UC)

The results in terms of total sliding time histories are presented in Figure 5.3.1.1-2 and Figure 5.3.1.1-3, and are summarized in Table 5.3.1.1-1 in terms of maximum total sliding.

From the results presented in Table 5.3.1.1-1 and Figure 5.3.1.1-2 and Figure 5.3.1.1-3, it is concluded that accounting for rocking or not does not make a significant difference for the sliding analysis results for the T/B. An explanation for slightly larger effect of rocking on the sliding analysis results for the R/B complex than for the T/B can be found in the interplay between the vibration characteristics of the structure and the dominant frequency of the rocking motion. The rocking motion, with relatively high frequency, has stronger effect on the R/B complex (a concrete structure with lowest mode frequencies of 3Hz to 5Hz), than on the T/B (a steel structure with lowest mode frequencies of about 1.3Hz). For consistency, the same type of input is used for the T/B as is used for the R/B complex, namely rocking input evaluated based on the vertical accelerations calculated in the SSI analyses at nodes located at the basemat level at the South-East corner, center of the North side and South-West corner.

5.3.1.2 Live Loads

The results of the sensitivity study on the effect of Live Loads on the sliding analysis results performed for the R/B complex and discussed in Appendix B, Section B.1.1 indicated that including or not including the amount of Live Loads recommended by SRP 3.7.2 (Reference 24) does not have a significant effect on the results of the nonlinear sliding analyses. Therefore, the Live Loads are included in the analysis, namely 25% of the floor design live load and 75% of the roof design snow load, as also included in the SSI analyses used to infer the ground input accelerations for sliding.

5.3.1.3 Lateral Earth Pressures

As stated by Assumptions 3 and 4 (Section 4.5.1), no lateral earth pressures from backfill, acting on the vertical walls of the basement, are considered in the nonlinear sliding analyses presented in this TeR. Assumption 3 is discussed in Section 4.5.3. Assumption 4, related to dynamic soil pressures acting on fixed (non-moving) walls when the structure does not slide, is discussed in this section based on a quantitative assessment for the T/B (see also Section 5.2.1.3 for general considerations).

5.3.2 Development of the FE Model and Analysis

5.3.2.1 Contact Formulation

The modeling of the contact between basemat and subgrade by means of compression only contact elements with Coulomb friction is described in detail in Section 4.2.3. The minimum stiffness of the contact elements necessary to avoid spurious vibrations induced by rigid body motion of the entire structure is determined as described in Section 4.2.3. The T/B has a total mass of 10,500 kilo-slugs and rests on the basemat with area of 68,322.6 ft^2. Using Equations 4.5.2-1 and 4.5.2-2 and assuming 5% structural damping ratio, the minimum contact stiffness per unit area of the basemat needed to avoid rigid body vibrations for frequencies of the input motion of at least 50Hz is about 1.2×10^6 kips/ft/ft^2.

5.3.2.2 Damping Formulation and Verification

Selection of the Frequency Ranges Relevant for Sliding

The same type of modal analyses are performed for the T/B as described for the R/B complex in Section 5.2.2.2. The frequency range that is relevant for sliding analysis, *F1* - *F2*, is determined in a similar manner with the R/B complex. The lower bound of the frequency range is selected to correspond to more than 99.9% of the total modal mass in any direction. The resulting values are *F1* = 1.33 Hz for the T/B with cracked concrete section properties (Figure 5.3.2.2-1) and *F1* = 1.38 Hz for the T/B with uncracked section (Figure 5.3.2.2-2).

As the T/B superstructure vibrates in vertical direction at much lower frequencies than the basement, *F2* is selected only based on the modal analysis results for the superstructure (E/R plus T/B). Moreover, since the superstructures of the two models (with cracked and with uncracked section) are identical, the upper bound, *F2*, is the same for both cases. The selection criteria are that *F2* includes a cumulative modal mass ratio of the superstructure of at least 80% in the vertical direction, and of at least 90% in any horizontal direction. The upper bound is selected as *F2* = 13.5 Hz. This corresponds to approximately 83% of the modal mass of the superstructure in the vertical direction and more than 95% of the modal mass of the superstructure in any horizontal direction (Figure 5.3.2.2-3).

The frequency ranges selected for calculating the Rayleigh damping coefficients and the damping ratios $\zeta(F)$ are presented in Figure 5.3.2.2-4 and Figure 5.3.2.2-5 for the T/B with cracked and with uncracked section, respectively. The selected ranges of modal frequencies relevant to sliding, the corresponding Rayleigh damping coefficients calculated for a target damping ratio ζ_0 = 5% using Equations 4.2.2-1 and 4.2.2-2, and the average damping ratio over the relevant frequency interval (termed here as “original frequency range”) are listed in Table 5.3.2.2-1.

Verification of the Frequency Ranges

The lower bound, *F1*, is established to allow the inclusion of more than 99% of the modal mass in any direction (first part of this section), therefore validation of the lower bound of the frequency range is not necessary.

The validation of the upper bound, *F2*, is accomplished by comparing the results of two sliding analyses in terms of maximum total sliding, as follows:

- One analysis is performed with Rayleigh damping coefficients calculated based on the original frequency range, *F1* to *F2*.
- A second analysis is performed with Rayleigh damping coefficients calculated based on the extended frequency range, from *F1* to *F2'* (with *F2'* approximately 1.5 to 2 times *F2*).

As described in Section 5.2.2.2, the selected upper bound *F2* is considered validated if the difference between these two analyses is less than 5%. The extended frequency range for the two T/B models is shown in Table 5.3.2.2-2 along with the corresponding Rayleigh damping coefficients. Two potential governing cases for the sliding analysis of the T/B are selected for validation: NR21CR and HM21UC (the notations are explained in Section 5.2). The sensitivity analysis results are listed in terms of maximum total sliding in Table 5.3.2.2-3, and the time histories of the total sliding are plotted in Figure 5.3.2.2-6 and Figure 5.3.2.2-7.

The percent differences listed in Table 5.3.2.2-3 are calculated as:

$$\Delta(\%) = \frac{\left|\delta_{\max}^{\text{Extended Range}} - \delta_{\max}^{\text{Original Range}}\right|}{\delta_{\max}^{\text{Original Range}}} \times 100 \qquad \text{Equation 5.3.2.2-1}$$

As shown in Table 5.3.2.2-3, the maximum percent difference of each case is less than 5%. The selected frequency range listed in Table 5.3.2.2-1 is verified for the sliding analyses of the T/B.

5.3.2.3 Cracked vs. Uncracked Section

Five cases, as listed in Table 5.3.2.3-1, are selected to investigate the effect of concrete cracking on the results of nonlinear sliding analysis for T/B FE model. Four of these five cases are the governing cases (i.e., resulting in maximum total sliding) from the 30 cases considered for sliding of the T/B with uncracked concrete section. The fifth case (NH55) is the governing case for soil profiles. The comparison between the results for the T/B FE model with cracked and uncracked concrete section properties for all five cases is summarized in Table 5.3.2.3-1 in terms of maximum total sliding, and the time histories of total sliding are plotted in Figure 5.3.2.3-1 through Figure 5.3.2.3-5.

The ratio between the maximum total sliding values, $\delta_{\max}^{UC}$ (uncracked) and $\delta_{\max}^{CR}$ (cracked), as listed in Table 5.3.2.3-1, is calculated for each case analyzed as:

$$Ratio = \delta_{\max}^{UC} / \delta_{\max}^{CR} \qquad \text{Equation 5.3.2.3-1}$$

For all the five cases listed in Table 5.3.2.3-1, the T/B FE model with uncracked concrete section shows higher maximum sliding values compared to the T/B FE model with cracked concrete section. The average ratio is 1.8.

The results could be explained based on the interplay between dynamic structural properties and spectral amplitudes in the CSDRS. For the T/B, the dominant modal frequencies in horizontal direction are typically less than 2 Hz, and most of the modal mass is excited by frequencies corresponding to the steeply ascending branch of the CSDRS (Frequency < 2.5 Hz, as shown in Figure 4.1.2-1). Since the model with uncracked section has larger modal frequencies, it corresponds to larger spectral amplitudes in the input and is expected to result in larger sliding.

Based on this sensitivity study, the T/B model with uncracked concrete section consistently yields larger sliding, therefore providing more conservative results. The sliding analyses for the T/B will be therefore conducted considering the uncracked concrete section only.

5.3.3 Sliding Analysis Results for the T/B

The sliding analysis results for all the 30 cases (5 sets of ATHs times 6 SPs), performed with the T/B FE model with uncracked concrete section properties, are listed in Table 5.3.3-1. The maximum values for each profile are shown in boldface. The maximum calculated sliding for the T/B is less than 0.2 in. The maximum value is 0.18 in and is obtained for SP 2032-100 and Hector Mine ATH.

5.4 Statistical Processing of Sliding Analysis Results

SRP 3.7.2 (Reference 24) requires more than four time histories be used in nonlinear dynamic analyses. Five sets of time histories are generated for the nonlinear sliding analyses. The generation of these time histories, as outlined in Section 5.1, represents seismic events with energy levels that exceed realistic earthquake values. Each of these five sets therefore represent conservative input values for the purposes of this analysis.

Each set of time histories is used in conjunction with SSI analyses performed for six different SPs for both the R/B complex and T/B. These SSI analyses provide the actual ATHs at the base of the structure, to be used as input to the nonlinear sliding analyses. The samples of governing results in terms of maximum sliding that are selected for statistical processing are larger than five for each of the structures considered (R/B complex or T/B).

5.4.1 R/B Complex

Result processing is performed to estimate the maximum expected amount of sliding. The set of data used for this purpose consists of the results of nonlinear sliding analysis using the FE model. The results, in terms of maximum total sliding, have been obtained for 17 cases (combinations of SP and ATH, as well as type of concrete section - cracked and/or uncracked) selected out of the total of 60 cases as follows:

The 17 results of nonlinear sliding analyses performed with the FE model and used here for statistical processing are shown highlighted in Table 5.2.5-1 through Table 5.2.5-6. Histograms of these results, helping to infer the type of sample probability distribution, are presented in Figure 5.4.1-1 for (1) all maximum total sliding results, (2) results for soil profiles (270-500, 270-200 and 560-500), and (3) results for rock profiles (900-200, 900-100 and 2032-100). For each group, the number of bins in the histogram is selected to be approximately equal to the group sample size divided by two. The sample means and standard deviations, as well as the minimum and maximum values in each group, are also shown in Figure 5.4.1-1.

A common measure of the maximum expected value for normally distributed results is the mean plus two times the standard deviation, which has a probability of being exceeded of 2.5% (see e.g., Reference 25). For non-normal distributions, however, the maximum values with a given exceedance probability do not necessarily correspond to the mean plus two times the standard deviation and have to be calculated based on the respective cumulative distribution function. By visual examination, the two samples consisting of sliding analysis results for soil profiles and for rock profiles in Figure 5.4.1-1 follow a Lognormal distribution. For these samples, the maximum expected value with a probability of being exceeded of 2.5% is calculated first for the corresponding normal distribution, obtained by taking the natural logarithm of the results in each sample, and then the maximum value is transformed back to the Lognormal distribution by exponentiation. Denoting the results in each sample by X, the maximum expected value, $X_{max}^{2.5\%}$, is obtained as follows:

$$Y = ln(X) \qquad \text{Equation 5.4.1-1a}$$

$$Y_{max}^{2.5\%} = mean(Y) + 2 * stdev(Y) \qquad \text{Equation 5.4.1-1b}$$

$$X_{max}^{2.5\%} = exp\{ Y_{max}^{2.5\%}\} \qquad \text{Equation 5.4.1-1c}$$

The expected maximum values with a probability of exceedance of 2.5% resulted as:

The results in terms of maximum total sliding obtained with the validated LMSM are discussed in Appendix C. The results of statistical processing for the LMSM in terms of ranges, sample statistics and maximum expected values are remarkably close to the corresponding results obtained from statistical processing of the FE model values, for both soil and rock profiles.

5.4.2 Turbine Building

The results of nonlinear sliding analyses in terms of maximum total sliding presented in Table 5.3.3-1 are grouped by SP in Figure 5.4.2-1. For each profile, the five values of maximum sliding obtained using five ATHs are represented by three-bin histograms showing the range of results (blue lines, as well as numbers on the figure) and their grouping. Each range of results (for each SP) is divided into three equal intervals, and the numbers of results falling in each interval are shown by the height of the respective bin in the histogram. While a statistical analysis of the results in each profile is not possible due to small samples (five results), the means and sample standard deviations are shown in Figure 5.4.2-1 to help in the following discussion.

Two conclusions are made from the results of sliding analyses for the T/B presented in Figure 5.4.2-1:

The results of nonlinear sliding analyses in terms of maximum total sliding are grouped in Figure 5.4.2-2. The maximum sliding results for each group are represented by histograms with various numbers of bins showing the range of results (blue lines, as well as numbers on the figure) and their grouping. For each group, the number of bins is selected to be approximately equal to the group sample size divided by two. The means and sample standard deviations are also shown in Figure 5.4.2-2. The results in Group 1 appear to follow a Lognormal distribution, while the results in Group 2A are normally distributed.

Table 5.1-1 Correlation Coefficients of the Modified Time Histories Components

Earthquake	Components		
Chi Chi	N-E	N-V	E-V
	-0.0222	-0.1039	0.0033
Darfield	S17E-S73W	S17E-V	S73W-V
	0.065	-0.1219	0.0533
Hector Mine	090-360	090-V	360-V
	0.0813	0.1158	0.0014
Nahanni	270-360	270-V	360-V
	0.0535	0.1574	0.0996
Northridge	180-090	180-V	090-V
	-0.0428	-0.0818	-0.054

Table 5.1-2 Modified Time Histories Characteristics

Earthquake	Station	Absolute Maximum Acceleration (g)			Total Duration (sec)	Δt (sec)
		H1 (NS)	H2 (EW)	Vertical (UP)		
Chi Chi	ILA067	0.313	0.306	0.306	24.00	0.005
Darfield	DFHS	0.315	0.314	0.304	25.00	0.005
Hector Mine	Amboy	0.317	0.312	0.305	23.00	0.005
Nahanni	Site 3	0.32	0.312	0.307	21.00	0.005
Northridge	Mt. Baldy	0.313	0.314	0.305	22.08	0.005

Table 5.1-3 Duration Properties of the Modified Time Histories

Earthquake	Component	Total Duration (sec)	Rise Time (sec)	Strong Motion Duration (sec)	Decay Time (sec)
ChiChi	**H1(N)**	**24.00**	6.38	**10.13**	7.50
	H2(E)	**24.00**	6.29	**9.96**	7.76
	V	**24.00**	5.21	**9.78**	9.02
Darfield	**H1(S17E)**	**25.00**	3.41	**14.88**	6.72
	H2(S73W)	**25.00**	2.78	**14.44**	7.79
	V	**25.00**	2.32	**14.21**	8.48
Hector Mine	**H1(090)**	**23.00**	3.13	**11.35**	8.52
	H2(360)	**23.00**	3.39	**10.54**	9.08
	V	**23.00**	1.47	**11.87**	9.67
Nahanni	**H1(270)**	**21.00**	2.81	**8.25**	9.95
	H2(360)	**21.00**	2.73	**8.08**	10.20
	V	**21.00**	2.95	**7.48**	10.58
Northridge	**H1(180)**	**22.08**	3.00	**8.13**	10.96
	H2(090)	**22.08**	2.73	**10.10**	9.26
	V	**22.08**	1.34	**10.38**	10.37

Table 5.1-4 Magnitude and Distance Bins and Strong Motion Duration Criteria

(NUREG/CR-6728, Table 3-2, Reference 7)

M	*R* (km)	Durations (sec)	
		Rock	Soil
6.5 (6 - 7)	10 – 50	**3.1** – 7.0	3.6 – 8.2
	50 – 100	5.1 – 11.6	5.7 – 12.8
	100 -200	8.1 – 18.3	8.7 – 19.5
7.5 (7+)	10 – 50	6.6 – 14.0	7.2 – 16.1
	50 – 100	8.7 – 19.5	12.2 – 27.5
	100 -200	11.7 – 26.3	16.2 – **36.5**

Table 5.1-5 Central and Eastern United States V/A & AD/V^2 Mean Ratios ± One Standard Deviation

Distance Bin	M	V / A (cm/sec/g), σ_{ln} (1)	AD / V^2, σ_{ln} (1)	V/A / $e^{(\sigma_{ln})}$ (in/sec/g) (2)	V/A * $e^{(\sigma_{ln})}$ (in/sec/g) (2)	AD/V^2 / $e^{(\sigma_{ln})}$	AD/V^2 * $e^{(\sigma_{ln})}$
10 - 50, Rock	6.32	31.75, 0.51	6.58, 0.70	**7.51**	20.82	3.27	13.25
10 - 50 Soil	6.41	51.74, 0.35	3.49, 0.47	14.35	28.91	2.18	5.58
50 - 100, Rock	6.38	32.59, 0.33	4.66, 0.52	9.22	17.85	2.77	7.84
50 - 100, Soil	6.57	56.04, 0.36	3.01, 0.48	15.39	31.62	**1.86**	4.86
10 - 50, Rock	7.38	58.24, 0.72	7.78, 0.63	11.16	47.11	4.14	14.61
10 - 50 Soil	7.47	128.74, 0.27	3.57, 0.35	38.69	**66.4**	2.52	5.07
50 - 100, Rock	7.49	50.29, 0.56	10.60,0.46	11.31	34.66	6.69	**16.79**

(1) See NUREG/CR-6728, Table 3-6, Reference 7.
(2) Units are changed to facilitate comparison to time history results

Table 5.1-6 V/A and AD/V^2 Values of the Modified Time Histories

Earthquake	Component	A (g)	V (in/sec)	D (in)	V/A (in/s/g)	AD/V^2
ChiChi	**H1(N)**	0.313	16.08	9.48	**51.28**	**4.44**
	H2(E)	0.306	18.11	10.60	**59.12**	**3.82**
	V	0.306	16.54	7.33	**54.10**	**3.17**
Darfield	**H1(S17E)**	0.315	18.55	11.40	**58.84**	**4.03**
	H2(S73W)	0.314	17.49	9.74	**55.64**	**3.87**
	V	0.304	12.51	4.81	**41.16**	**3.61**
Hector Mine	**H1(090)**	0.317	16.08	7.42	**50.68**	**3.52**
	H2(360)	0.312	17.50	10.23	**56.14**	**4.02**
	V	0.305	12.76	5.30	**41.80**	**3.83**
Nahanni	**H1(270)**	0.320	14.68	10.76	**45.87**	**6.17**
	H2(360)	0.312	18.95	9.77	**60.80**	**3.27**
	V	0.307	13.44	5.40	**43.78**	**3.55**
Northridge	**H1(180)**	0.313	18.14	7.05	**57.86**	**2.59**
	H2(090)	0.314	17.93	10.83	**57.04**	**4.09**
	V	0.305	13.26	7.55	**43.50**	**5.05**

Table 5.2.1.1-1 Effect of Rocking: Sensitivity Study Results in Terms of Maximum Total Sliding (in inches) for the R/B Complex with Cracked Concrete Section; Preliminary Analysis Results Using the Non-validated LMSM

Table 5.2.1.1-2 Effect of Rocking: Sensitivity Study Results in Terms of Maximum Total Sliding (in inches) for the R/B Complex with Cracked Concrete Section Using the Validated LMSM

Table 5.2.1.1-3 Effect of Rocking: Sensitivity Study Results in Terms of Maximum Total Sliding (in inches) for the R/B Complex with Uncracked Concrete Section Using the Validated LMSM

Table 5.2.2.2-1 Frequency Ranges and Rayleigh Damping Coefficients for the Nonlinear Sliding Analysis of the R/B Complex

Table 5.2.2.2-2 Extended Frequency Ranges and Rayleigh Damping Coefficients used in the Sensitivity Analyses for the Range of Relevant Frequencies for the R/B Complex

Table 5.2.2.2-3 R/B Complex: Results of the Sensitivity Analyses for the Range of Relevant Frequencies in Terms of Maximum Total Sliding

Table 5.2.2.3-1 Nonlinear Sliding Analysis Results for the R/B Complex with Cracked Concrete Section, Calculated Using the Non-validated LMSM, and Used for Screening for Validation

Table 5.2.2.4-1 R/B Complex: Maximum Total Sliding (in inches) Calculated Using the FE Model and the Non-validated LMSM for the Representative Cases

Table 5.2.4.1-1 LMSM Validation for the R/B Complex with Cracked Concrete Section: Maximum Total Sliding Calculated Using the FE Model and the Validated LMSM

Table 5.2.4.2-1 LMSM Validation for the R/B Complex with Uncracked Concrete Section: Maximum Total Sliding Calculated Using the FE Model and the Validated LMSM

Table 5.2.5-1 Nonlinear Sliding Analysis Results for the R/B Complex in Terms of Maximum Total Sliding (in inches) for Subgrade Profile 270-500 (FE Model and Validated LMSM)

Table 5.2.5-2 Nonlinear Sliding Analysis Results for the R/B Complex in Terms of Maximum Total Sliding (in inches) for Subgrade Profile 270-200 (FE Model and Validated LMSM)

Table 5.2.5-3 Nonlinear Sliding Analysis Results for the R/B Complex in Terms of Maximum Total Sliding (in inches) for Subgrade Profile 560-500 (FE Model and Validated LMSM)

Table 5.2.5-4 Nonlinear Sliding Analysis Results for the R/B Complex in Terms of Maximum Total Sliding (in inches) for Subgrade Profile 900-200 (FE Model and Validated LMSM)

Table 5.2.5-5 Nonlinear Sliding Analysis Results for the R/B Complex in Terms of Maximum Total Sliding (in inches) for Subgrade Profile 900-100 (FE Model and Validated LMSM)

Table 5.2.5-6 Nonlinear Sliding Analysis Results for the R/B Complex in Terms of Maximum Total Sliding (in inches) Subgrade Profile 2032-100 (FE Model and Validated LMSM)

Table 5.3.1.1-1 Effect of Rocking: Sensitivity Study Results in Terms of Maximum Total Sliding (in inches) for the T/B with Uncracked Concrete Section

Table 5.3.2.2-1 Frequency Ranges and Rayleigh Damping Coefficients for the Nonlinear Sliding Analysis for the T/B FE Model

Table 5.3.2.2-2 Extended Frequency Ranges and Rayleigh Damping Coefficients Used in the Sensitivity Analysis for the Range of Relevant Frequencies for the T/B FE Model

Table 5.3.2.2-3 T/B: Results of the Sensitivity Analyses for the Range of Relevant Frequencies in Terms of Maximum Total Sliding

Table 5.3.2.3-1 Effect of Concrete Cracking: Sensitivity Study Results in Terms of Maximum Total Sliding for the T/B: Cracked vs. Uncracked Concrete Section

Table 5.3.3-1 Analysis Results for the T/B with Uncracked Concrete Section in Terms of Maximum Total Sliding (in inches)

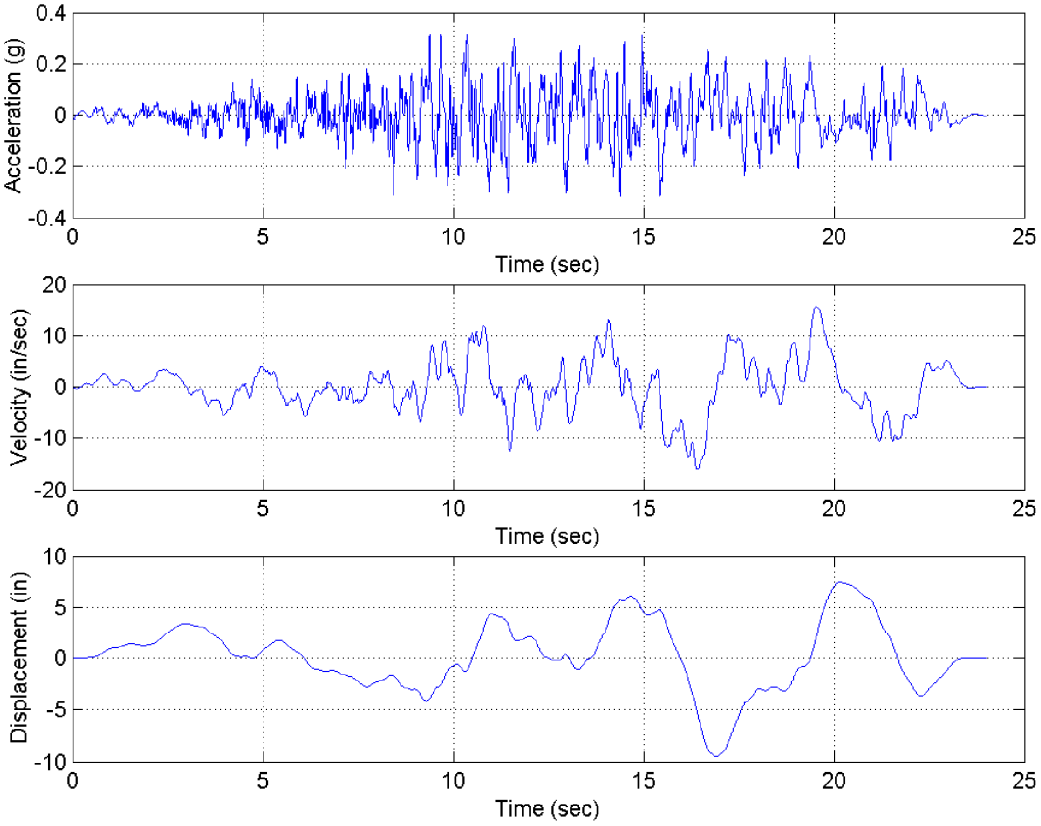

Figure 5.1-1 Acceleration, Velocity, and Displacement of Modified Chi-Chi Time History – H1 (NS) Component

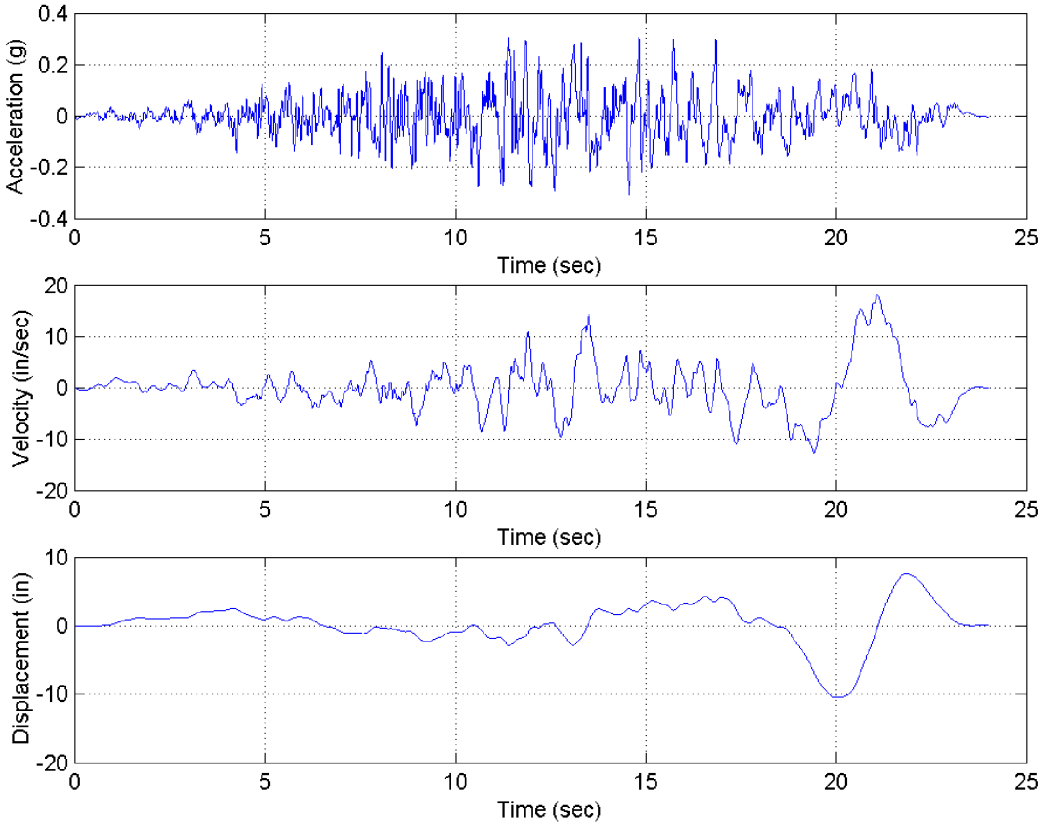

Figure 5.1-2 Acceleration, Velocity, and Displacement of Modified Chi-Chi Time History – H2 (EW) Component

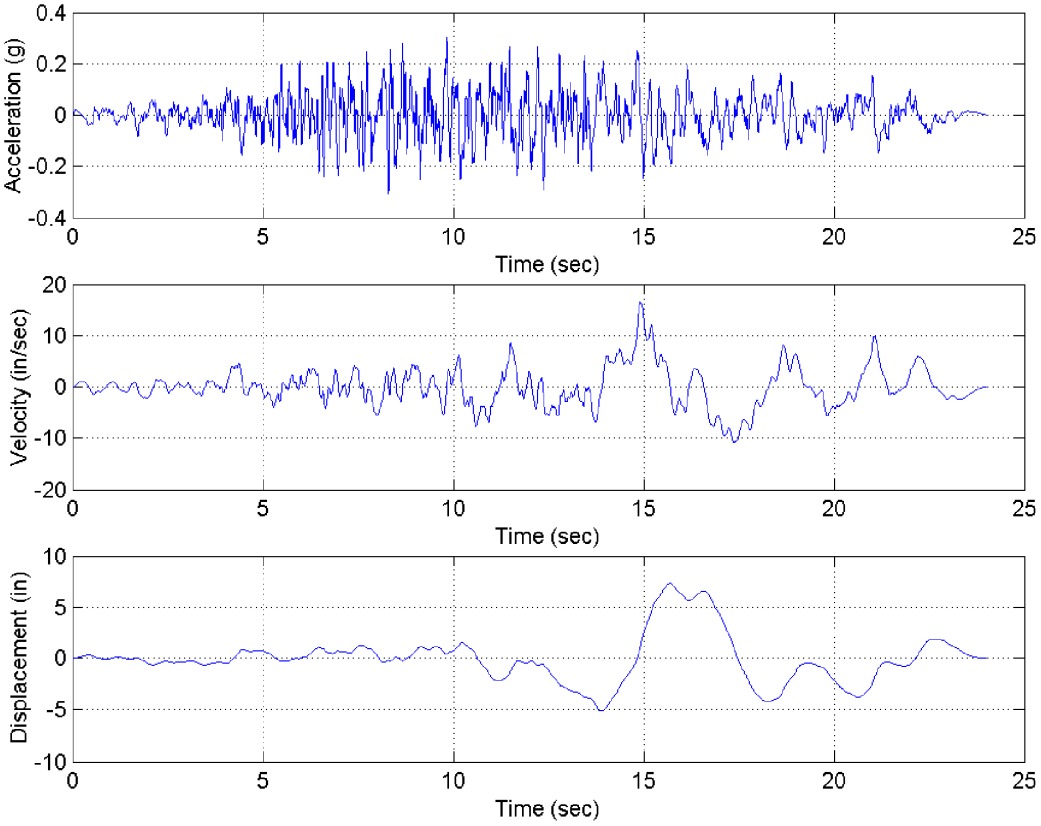

Figure 5.1-3 Acceleration, Velocity, and Displacement of Modified Chi-Chi Time History – Vertical (UP) Component

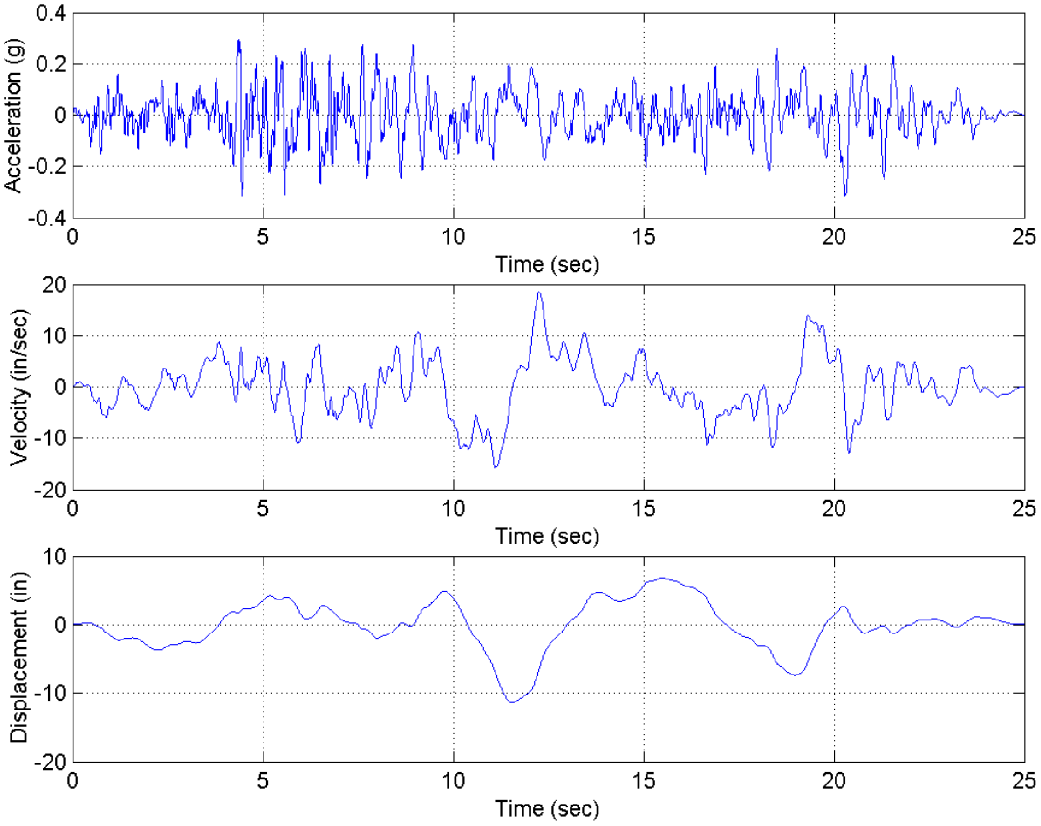

Figure 5.1-4 Acceleration, Velocity, and Displacement of Modified Darfield Time History – H1 (NS) Component

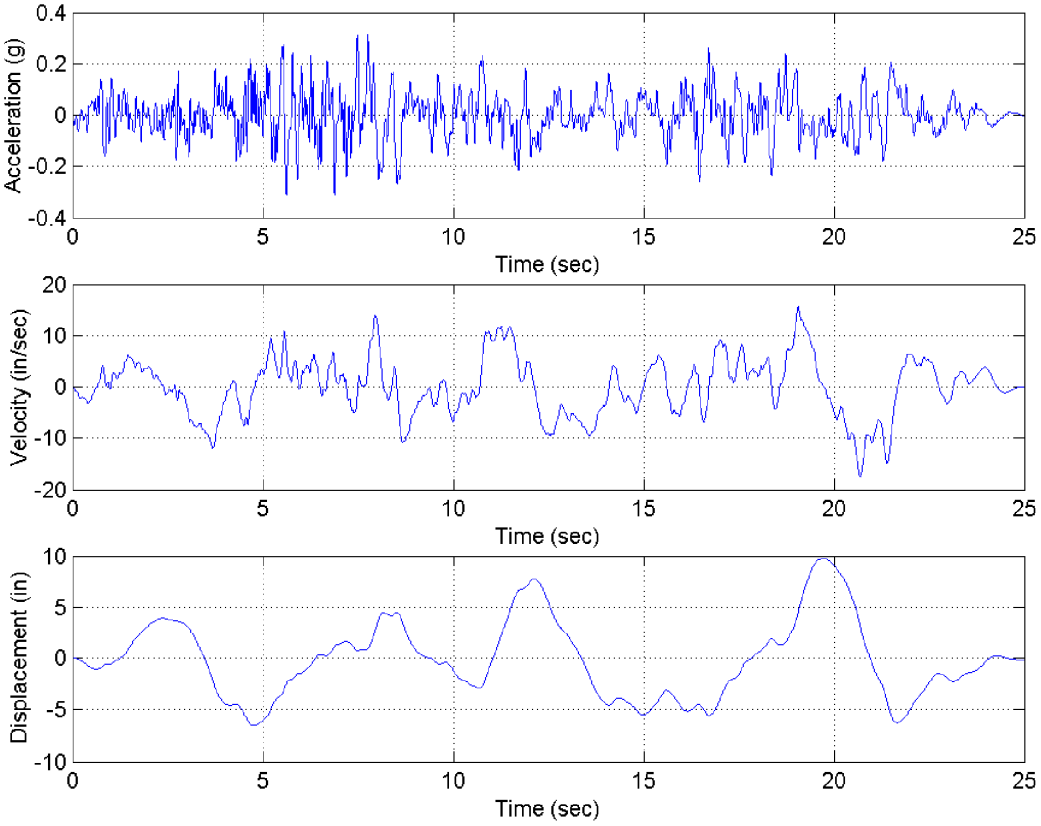

Figure 5.1-5 Acceleration, Velocity, and Displacement of Modified Darfield Time History – H2 (EW) Component

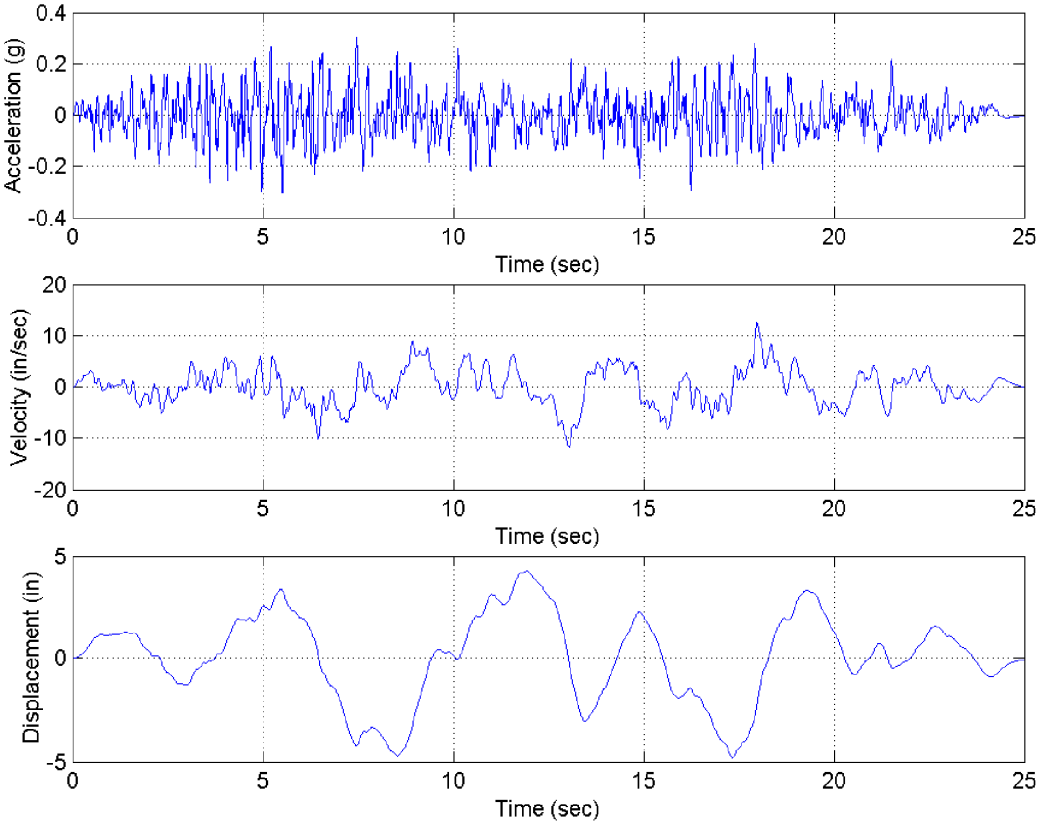

Figure 5.1-6 Acceleration, Velocity, and Displacement of Modified Darfield Time History – Vertical (UP) Component

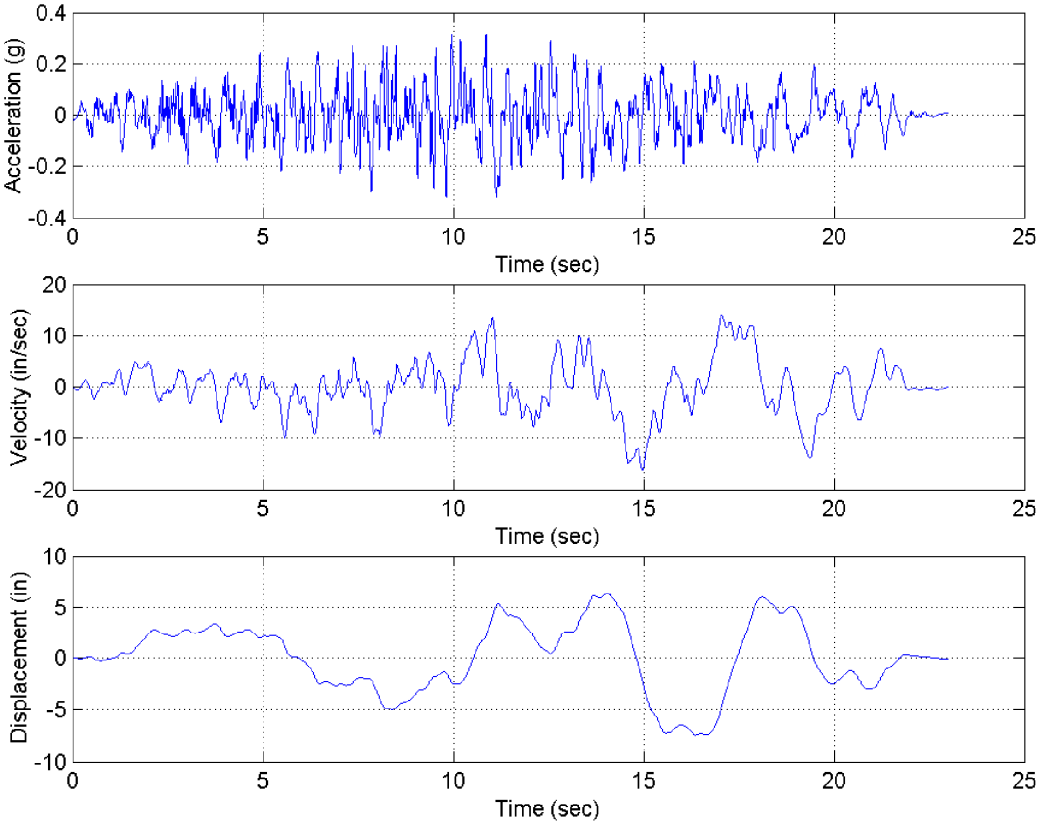

Figure 5.1-7 Acceleration, Velocity, and Displacement of Modified Hector Mine Time History – H1 (NS) Component

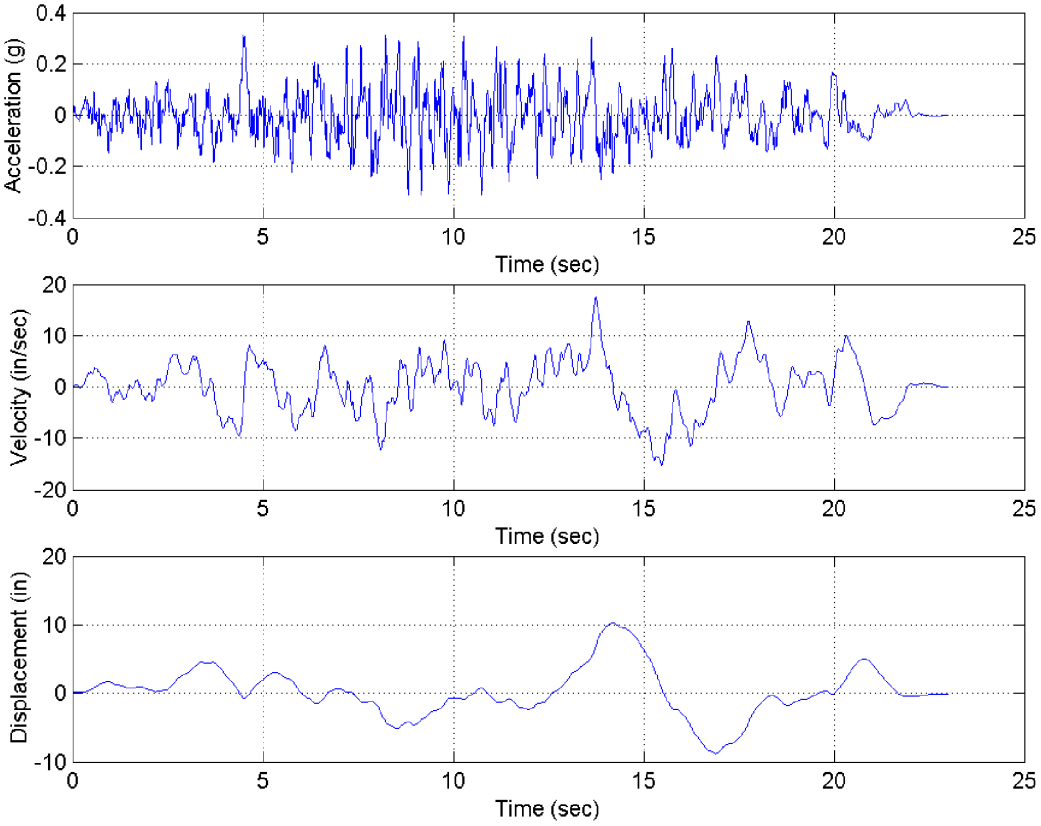

Figure 5.1-8 Acceleration, Velocity, and Displacement of Modified Hector Mine Time History – H2 (EW) Component

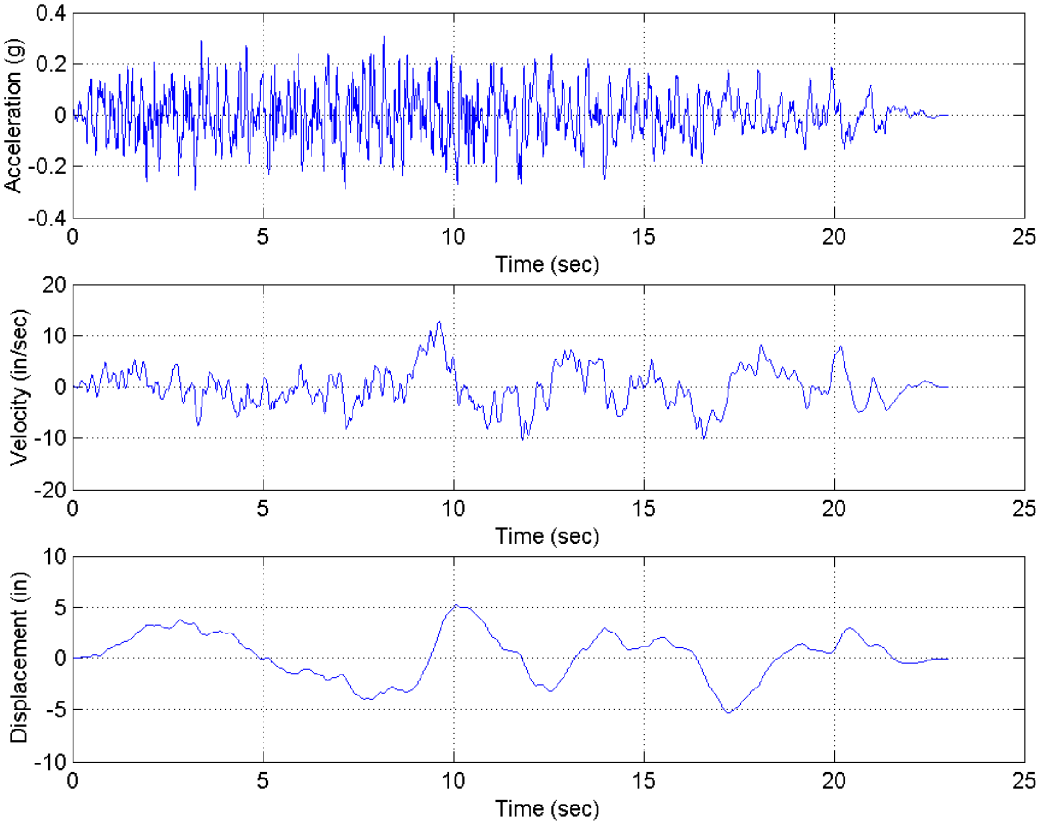

Figure 5.1-9 Acceleration, Velocity, and Displacement of Modified Hector Mine Time History – Vertical (UP) Component

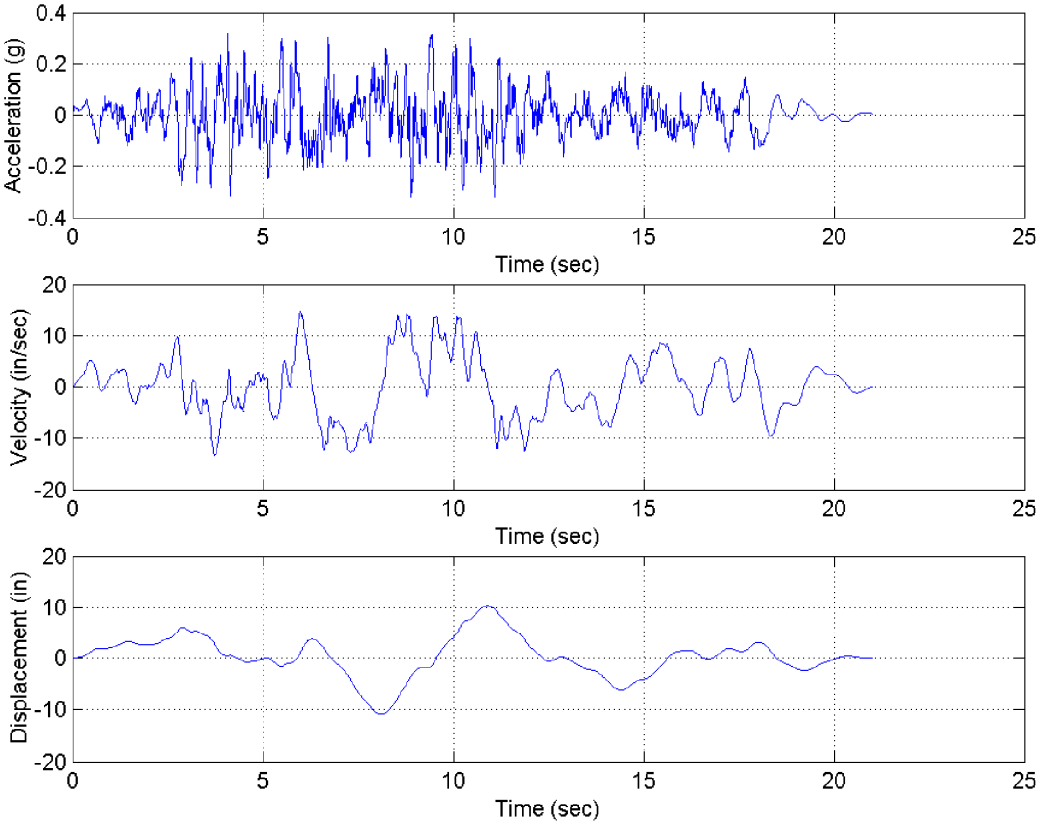

Figure 5.1-10 Acceleration, Velocity, and Displacement of Modified Nahanni Time History – H1 (NS) Component

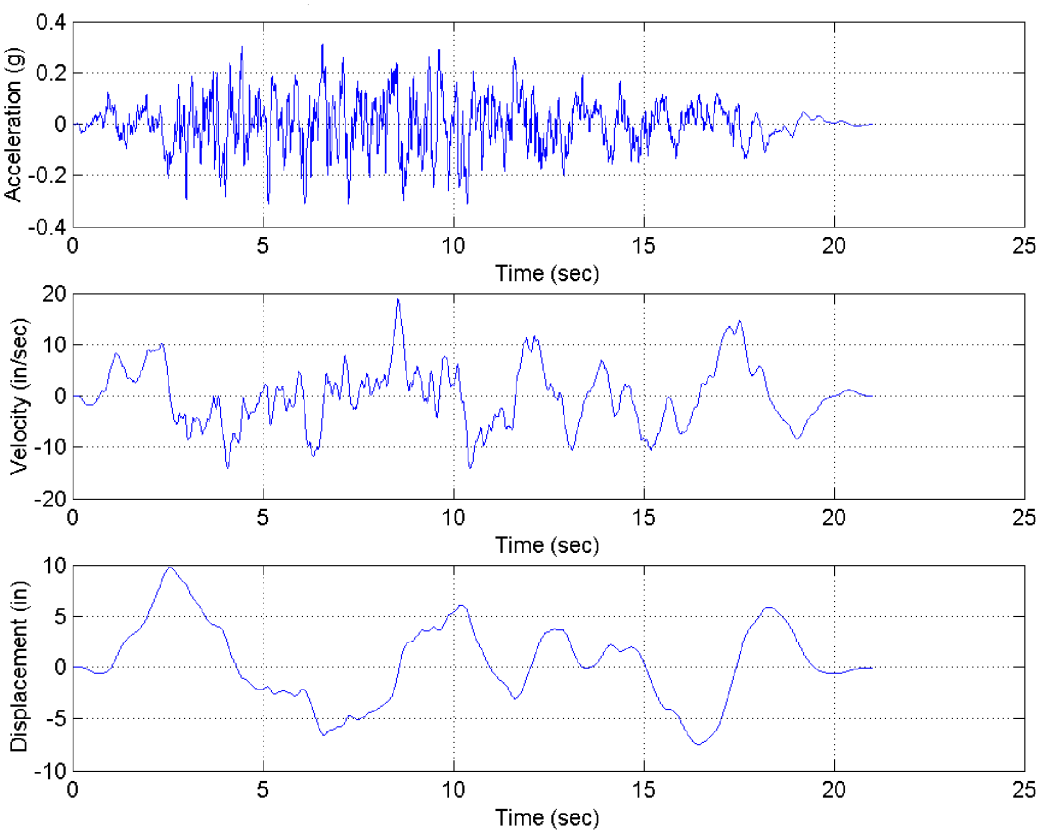

Figure 5.1-11 Acceleration, Velocity, and Displacement of Modified Nahanni Time History – H2 (EW) Component

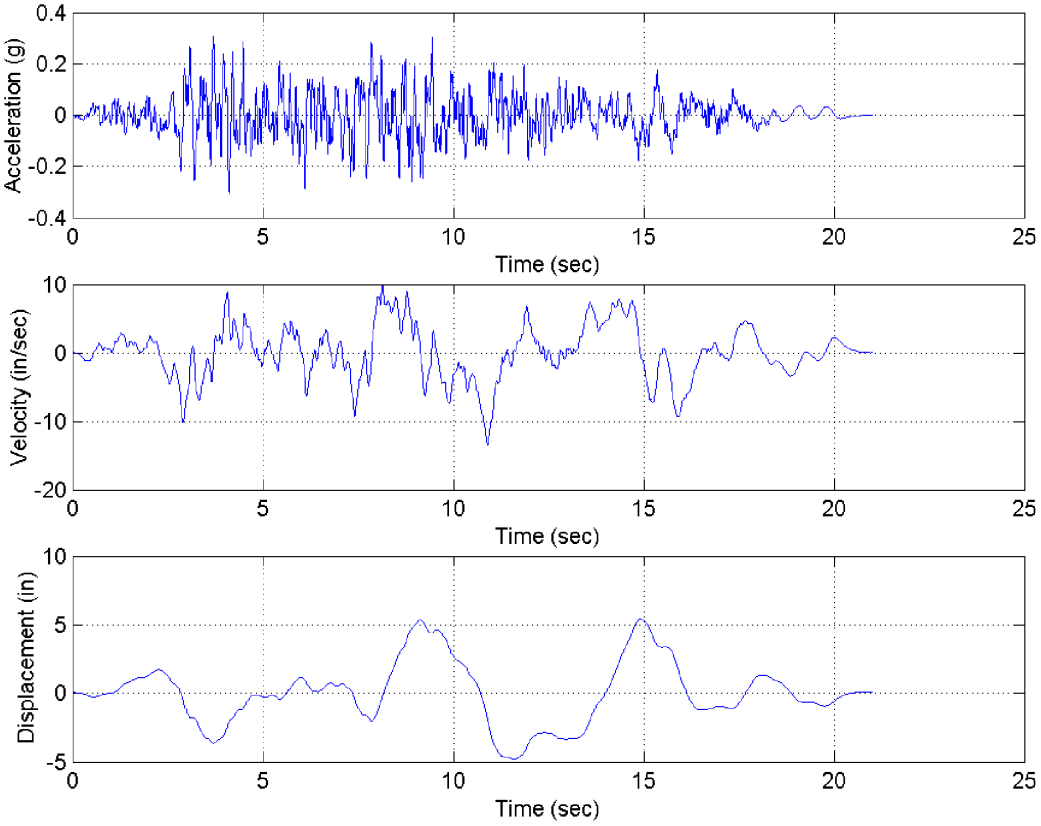

Figure 5.1-12 Acceleration, Velocity, and Displacement of Modified Nahanni Time History – Vertical (UP) Component

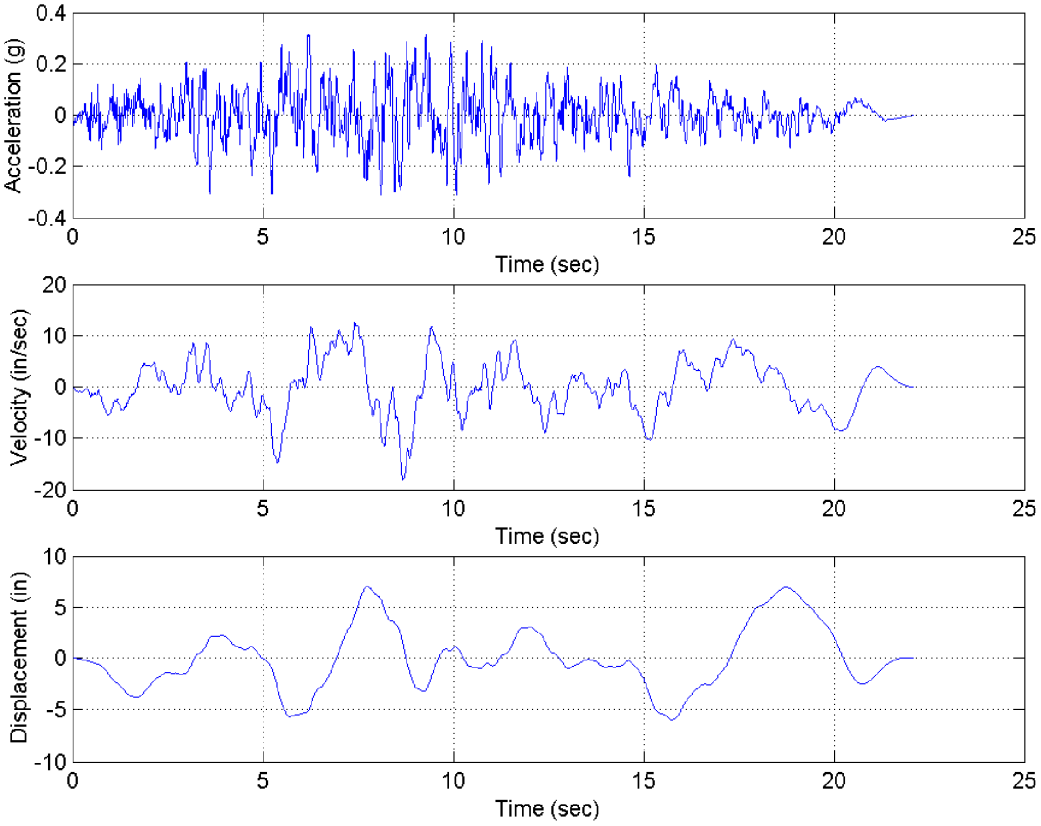

Figure 5.1-13 Acceleration, Velocity, and Displacement of Modified Northridge Time History – H1 (NS) Component

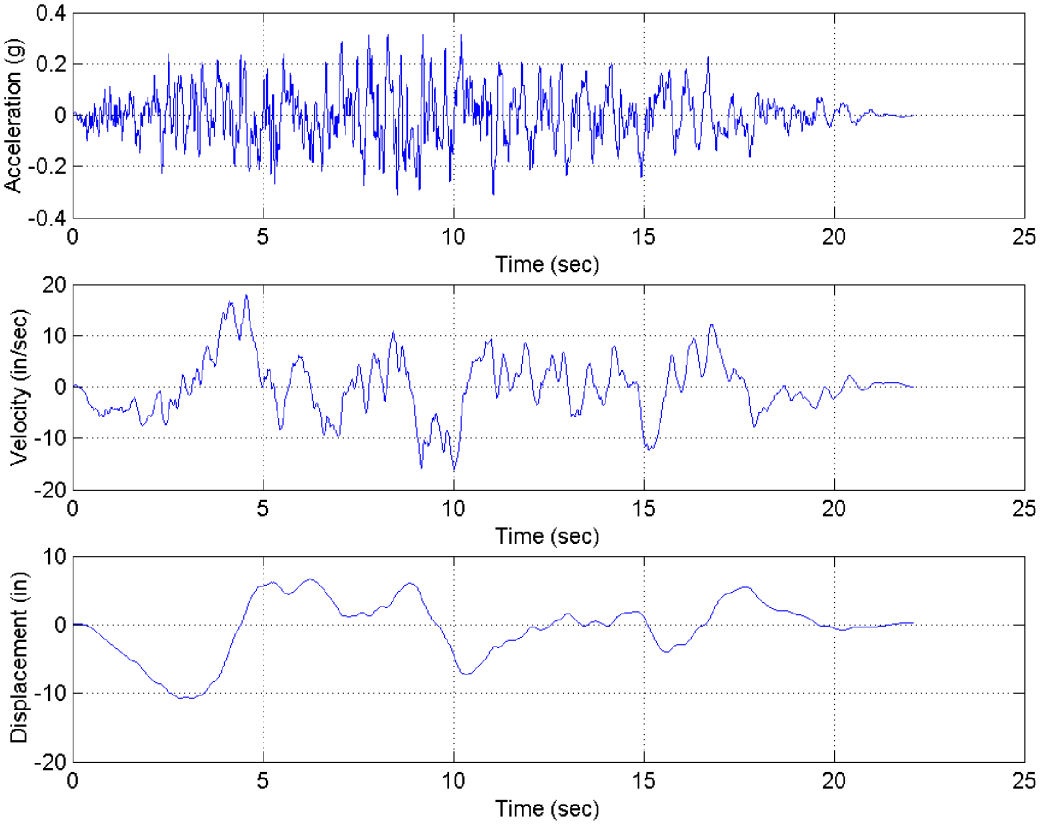

Figure 5.1-14 Acceleration, Velocity, and Displacement of Modified Northridge Time History – H2 (EW) Component

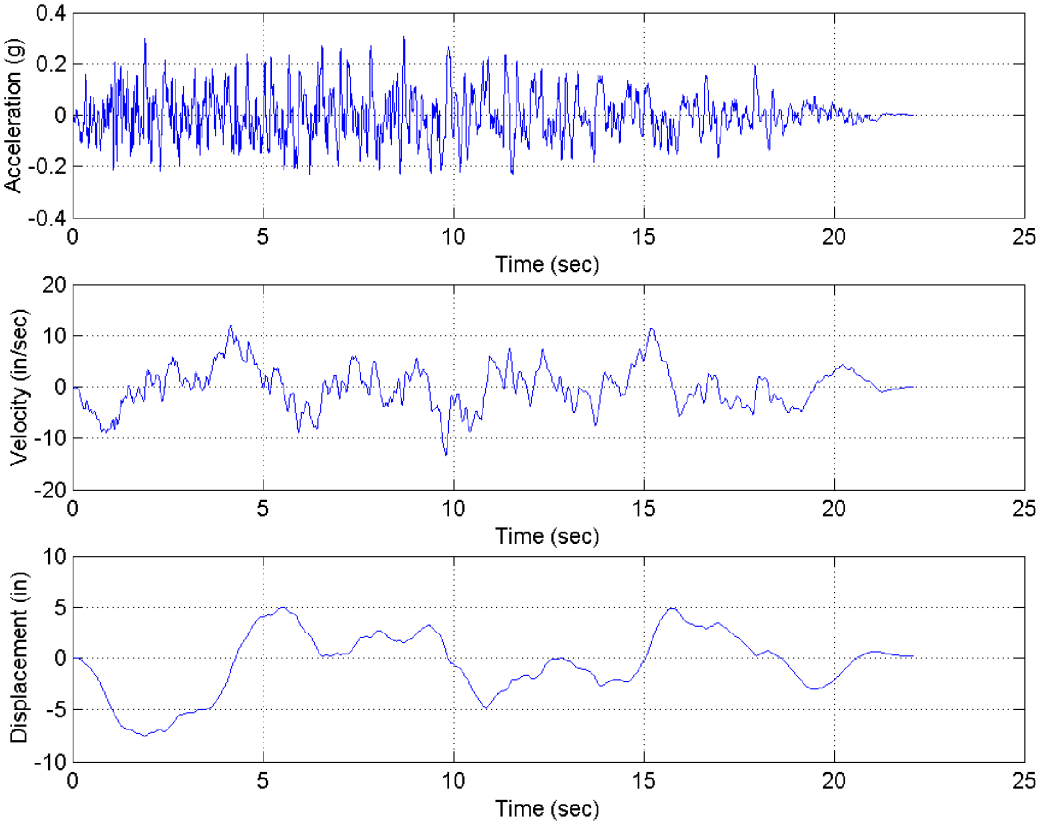

Figure 5.1-15 Acceleration, Velocity, and Displacement of Modified Northridge Time History – Vertical (UP) Component

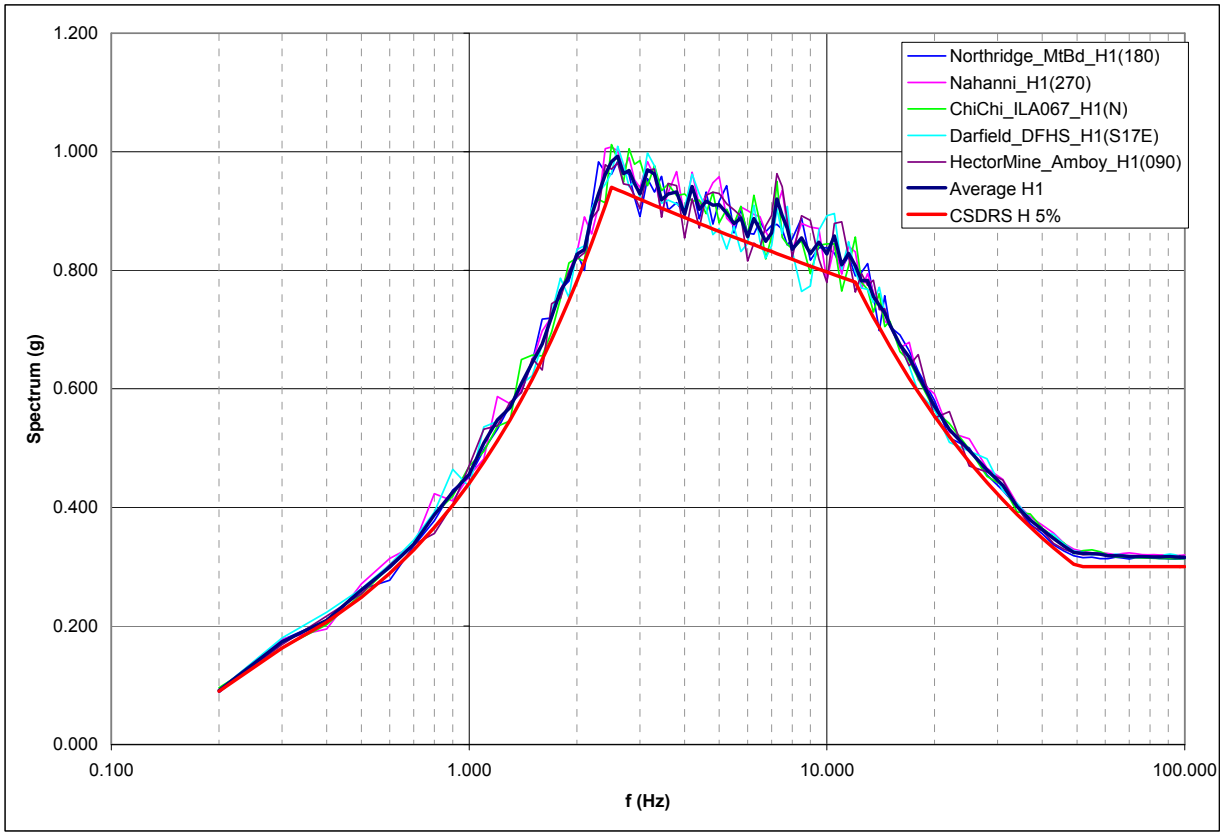

Figure 5.1-16 Response Spectra of H1 (NS) Component vs. CSDRS for 5% Damping

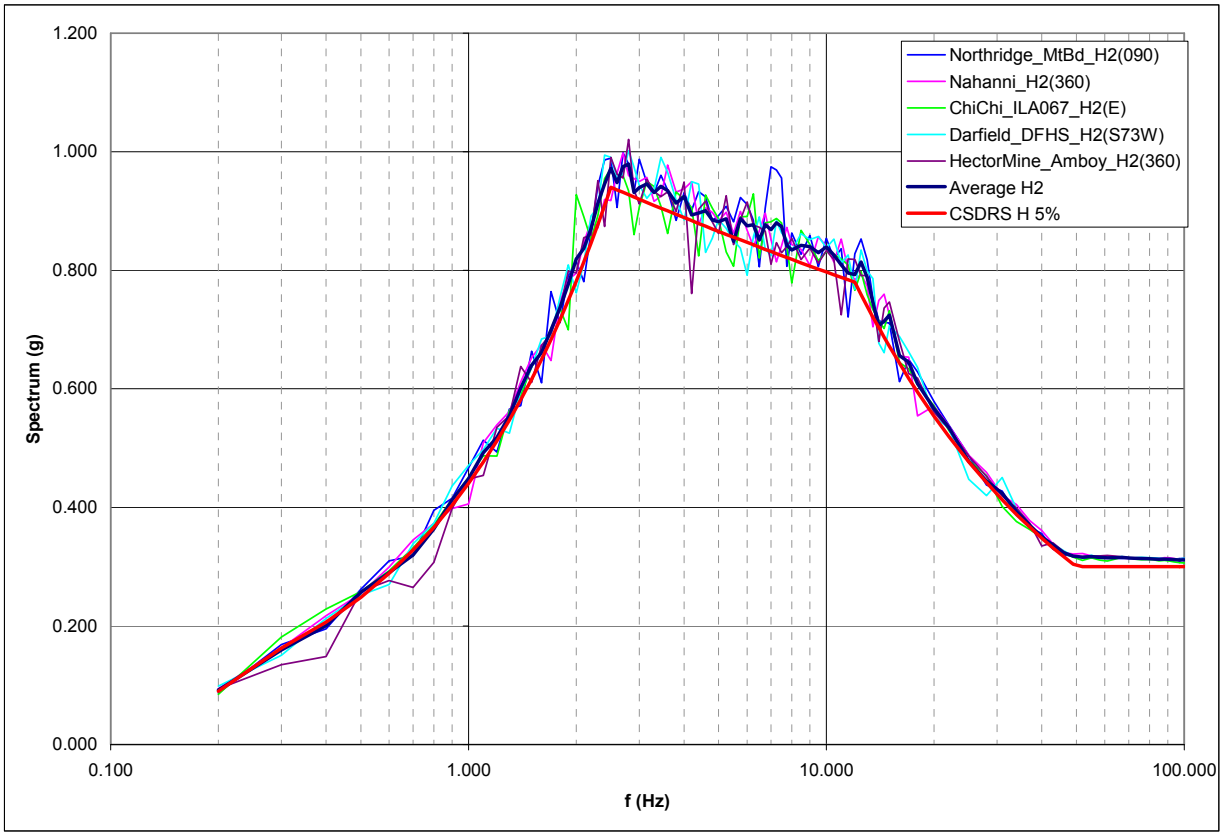

Figure 5.1-17 Response Spectra of H2 (EW) Component vs. CSDRS for 5% Damping

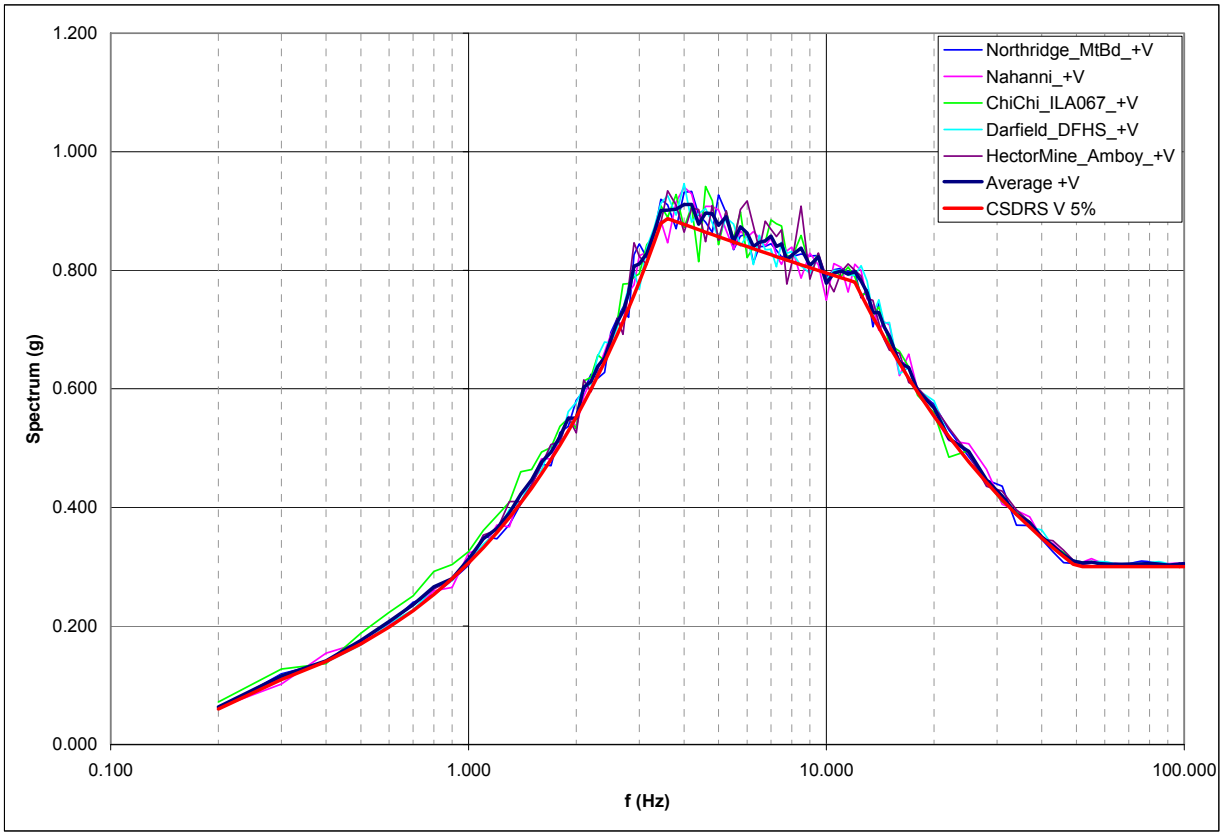

Figure 5.1-18 Response Spectra of Vertical (UP) Component vs. CSDRS for 5% Damping

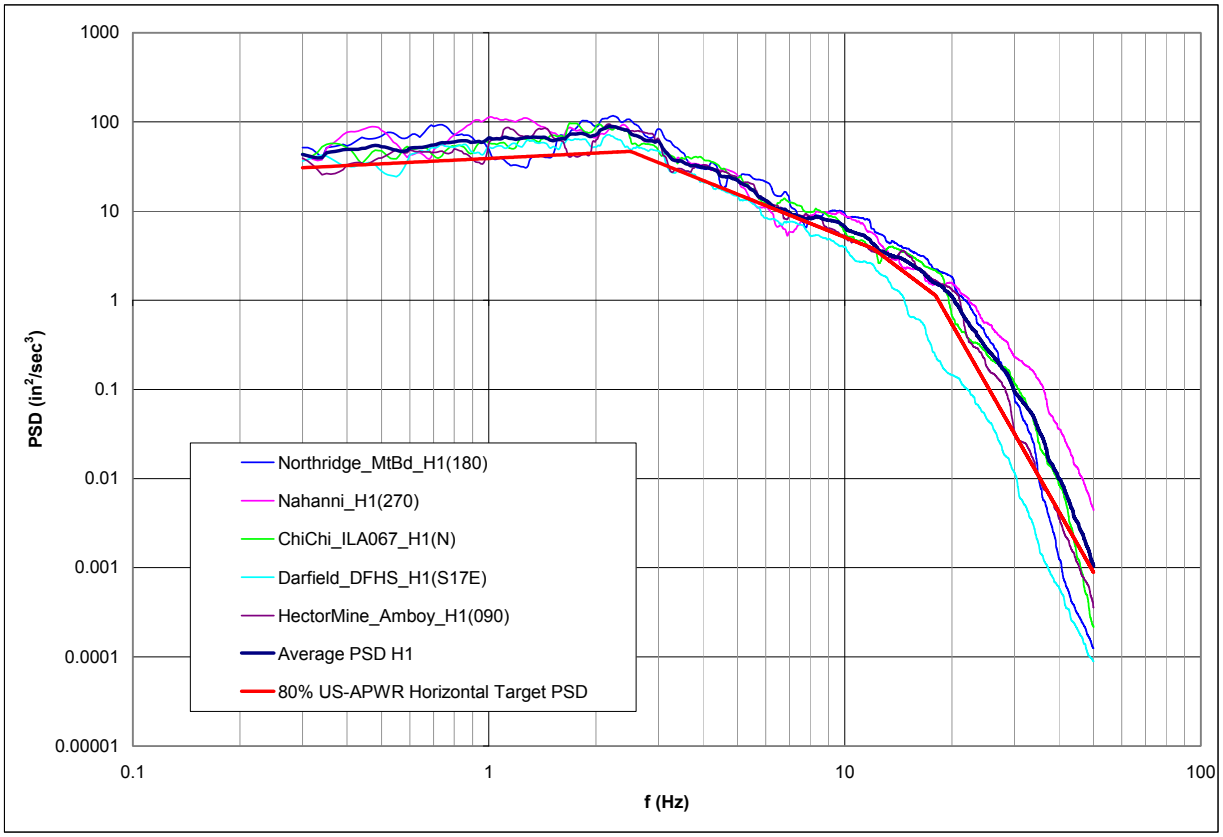

Figure 5.1-19 PSD for H1 (NS) Component vs. Horizontal Target PSD

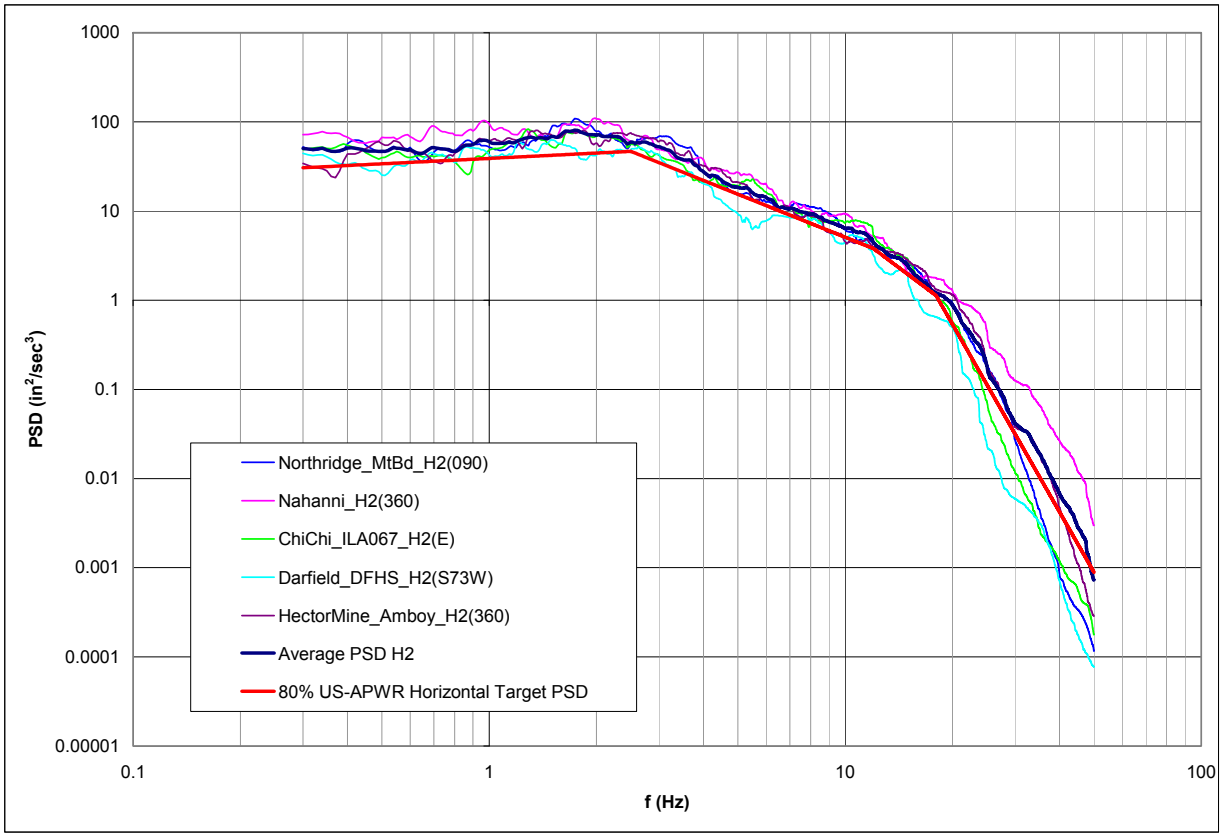

Figure 5.1-20 PSD for H2 (EW) Component vs. Horizontal Target PSD

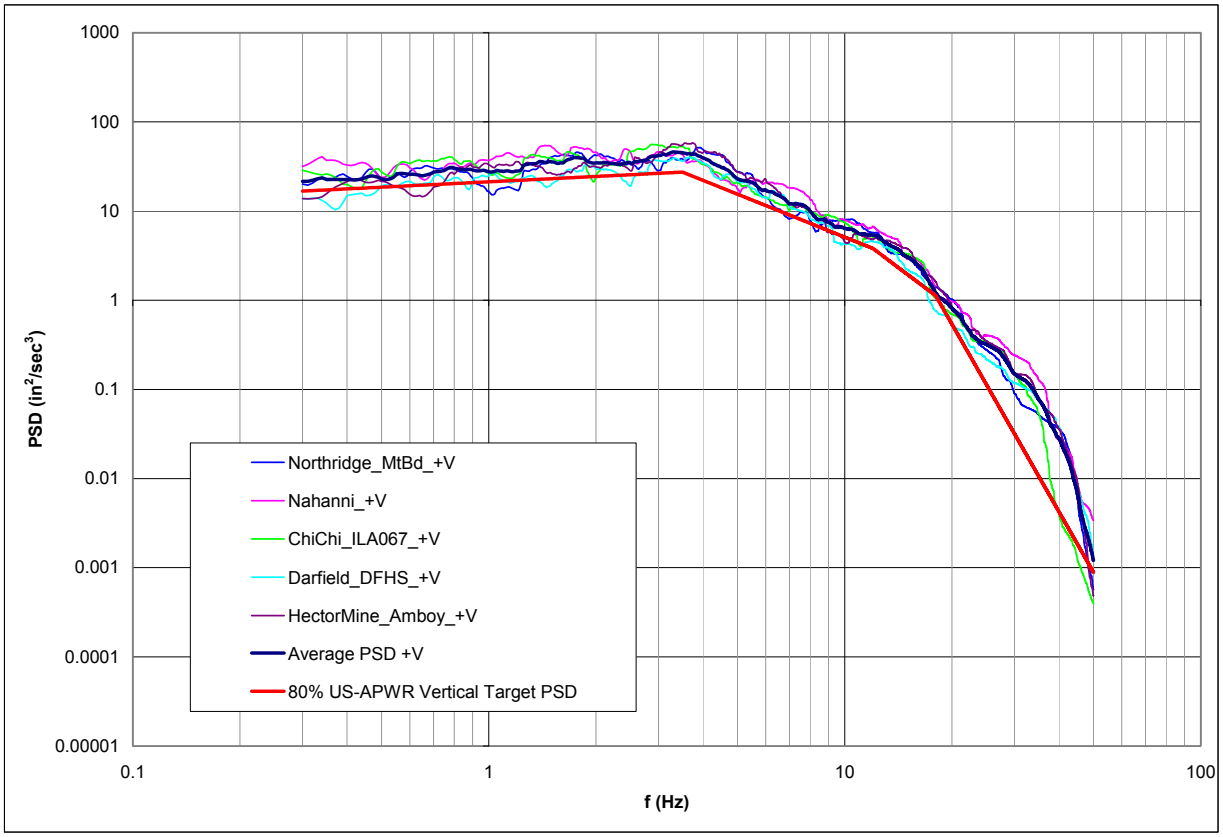

Figure 5.1-21 PSD for Vertical (UP) Component vs. Vertical Target PSD

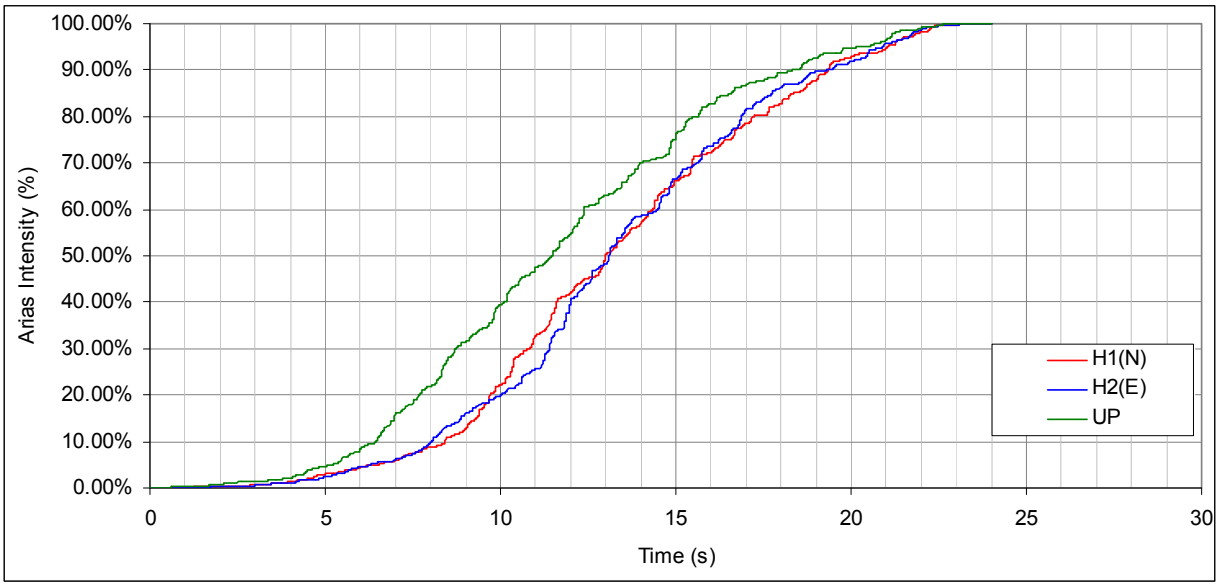

Figure 5.1-22 Normalized Arias Intensity for Modified Chi-Chi Time History

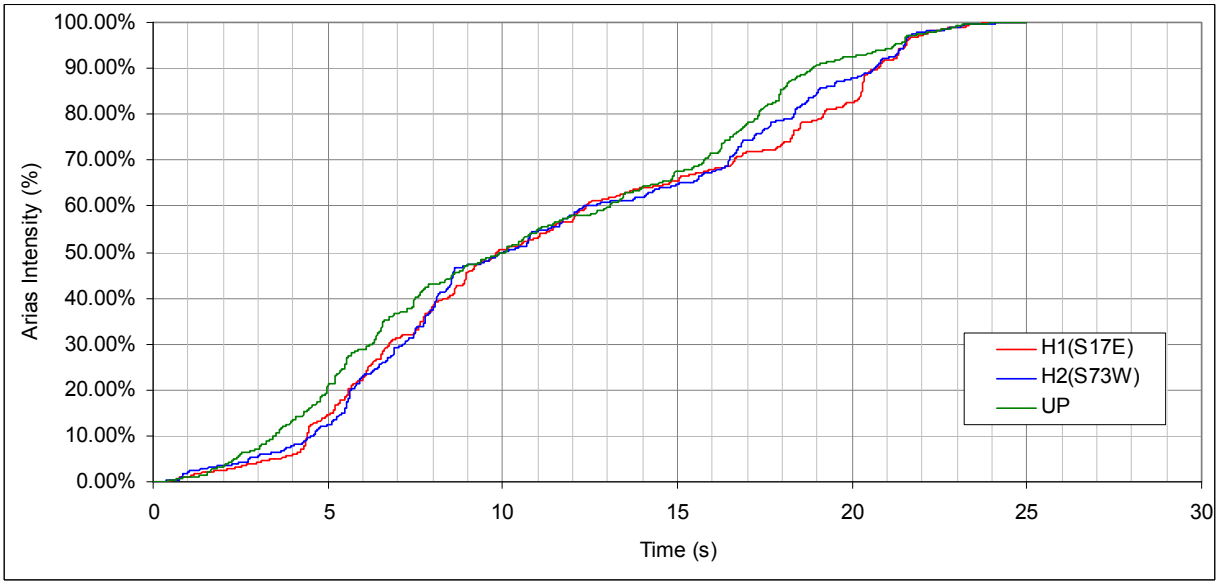

Figure 5.1-23 Normalized Arias Intensity for Modified Darfield Time History

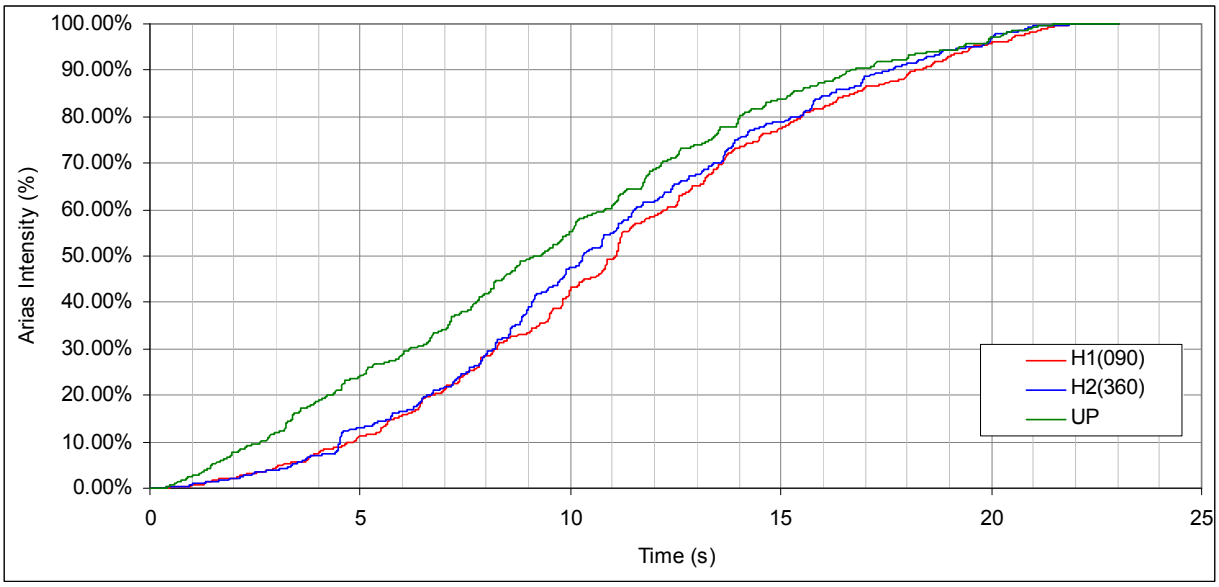

Figure 5.1-24 Normalized Arias Intensity for Modified Hector Mine Time History

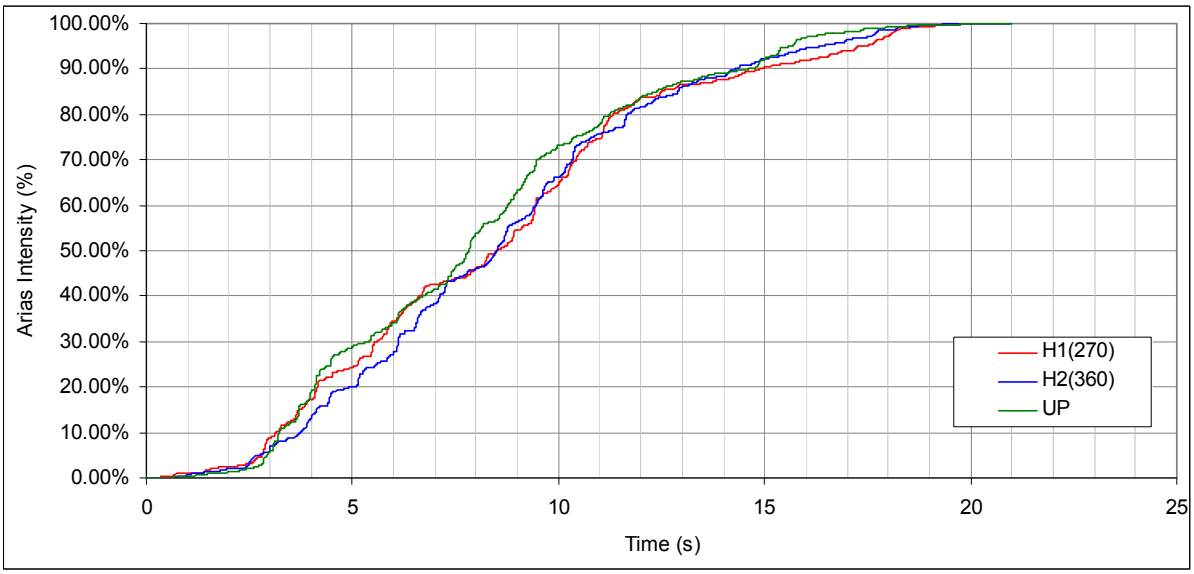

Figure 5.1-25 Normalized Arias Intensity for Modified Nahanni Time History

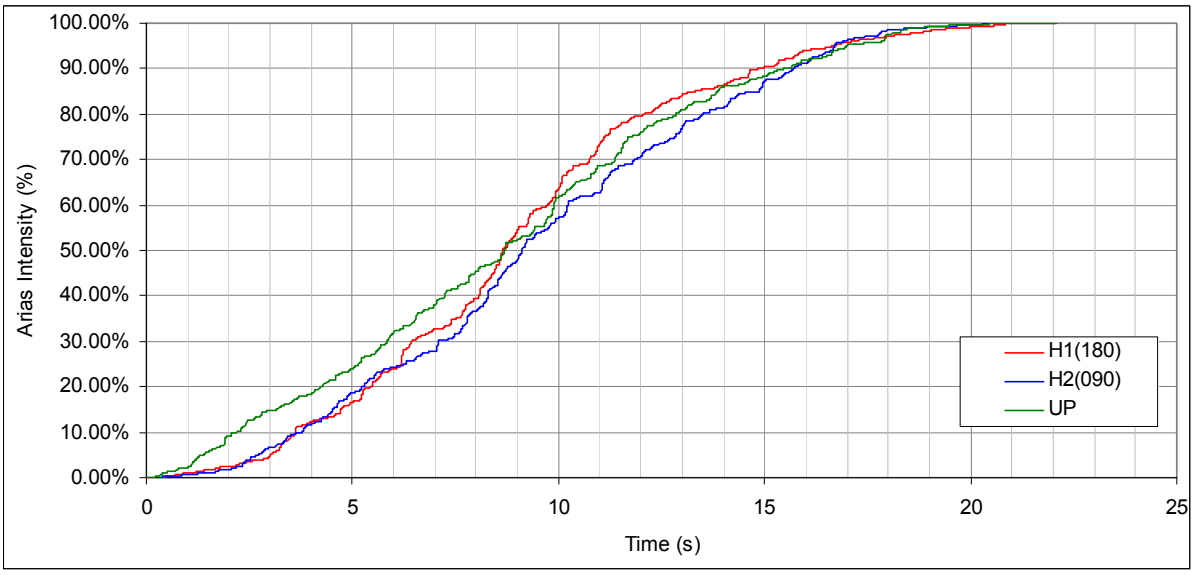

Figure 5.1-26 Normalized Arias Intensity for Modified Northridge Time History

Figure 5.2.1.1-1 Nodes in the Dynamic FE Model for SSI Analysis used for R/B Complex Sliding Analysis Input

Figure 5.2.1.1-2 Sensitivity Study for Rocking Effects - R/B Complex - Cracked Section, Subgrade Profile 2032-100, Darfield Acceleration Time History

Figure 5.2.1.1-3 Sensitivity Study for Rocking Effects - R/B Complex - Cracked Section, Subgrade Profile 2032-100, Hector Mine Acceleration Time History

Figure 5.2.1.1-4 Sensitivity Study for Rocking Effects - R/B Complex - Cracked Section, Subgrade Profile 560-500, Hector Mine Acceleration Time History

Figure 5.2.1.1-5 Sensitivity Study for Rocking Effects - R/B Complex - Cracked Section, Subgrade Profile 900-200, Nahanni Acceleration Time History

Figure 5.2.1.1-6 Sensitivity Study for Rocking Effects - R/B Complex - Cracked Section, Subgrade Profile 900-100, Northridge Acceleration Time History

Figure 5.2.1.1-7 Sensitivity Study for Rocking Effects - R/B Complex - Uncracked Section, Subgrade Profile 2032-100, Hector Mine Acceleration Time History

Figure 5.2.1.1-8 Sensitivity Study for Rocking Effects - R/B Complex - Uncracked Section, Subgrade Profile 900-100, Northridge Acceleration Time History

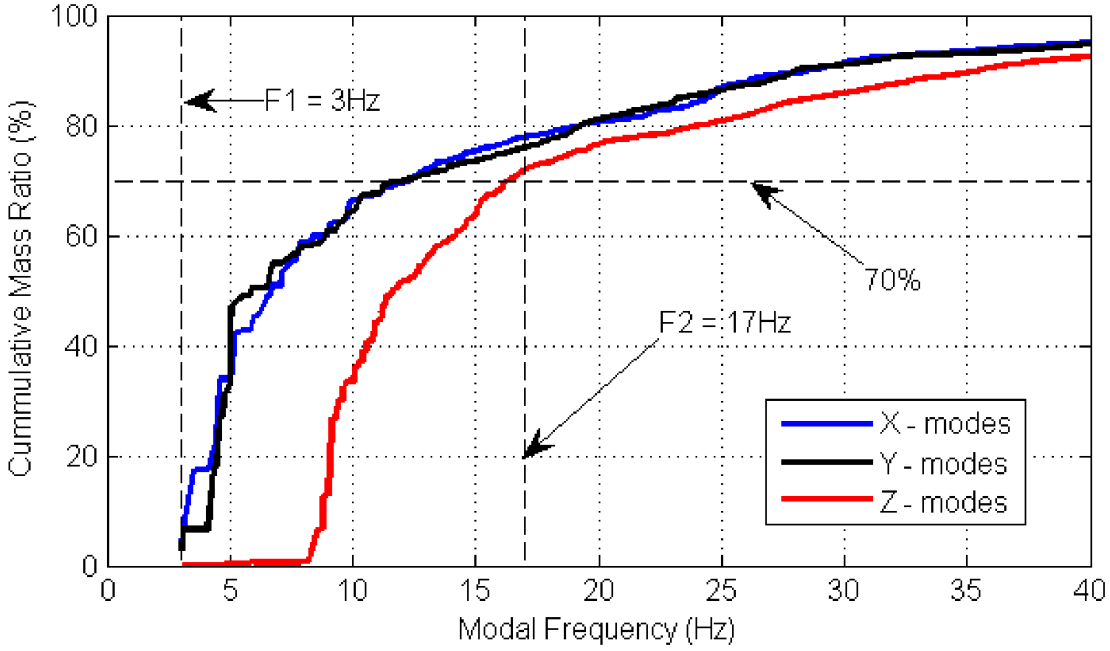

Figure 5.2.2.2-1 Cumulative Effective Mass Ratio for the R/B Complex with Cracked Section (FE Model) - Entire Structure (including basemat)

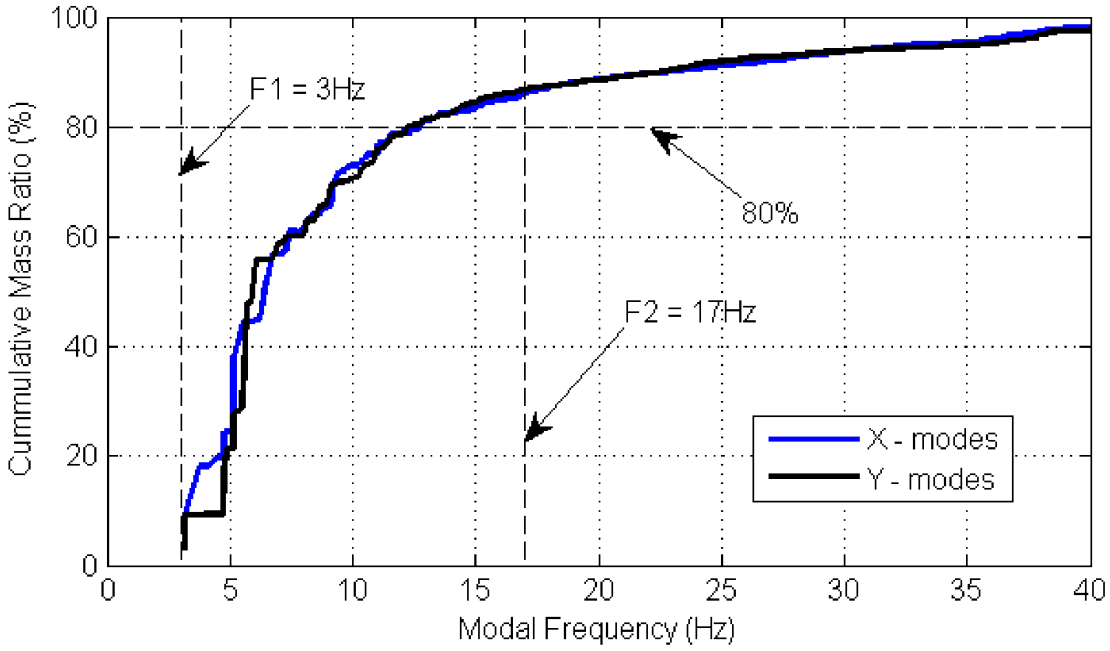

Figure 5.2.2.2-2 Cumulative Effective Mass Ratio for the R/B Complex with Cracked Section (FE Model) - Superstructure Only (above basemat)

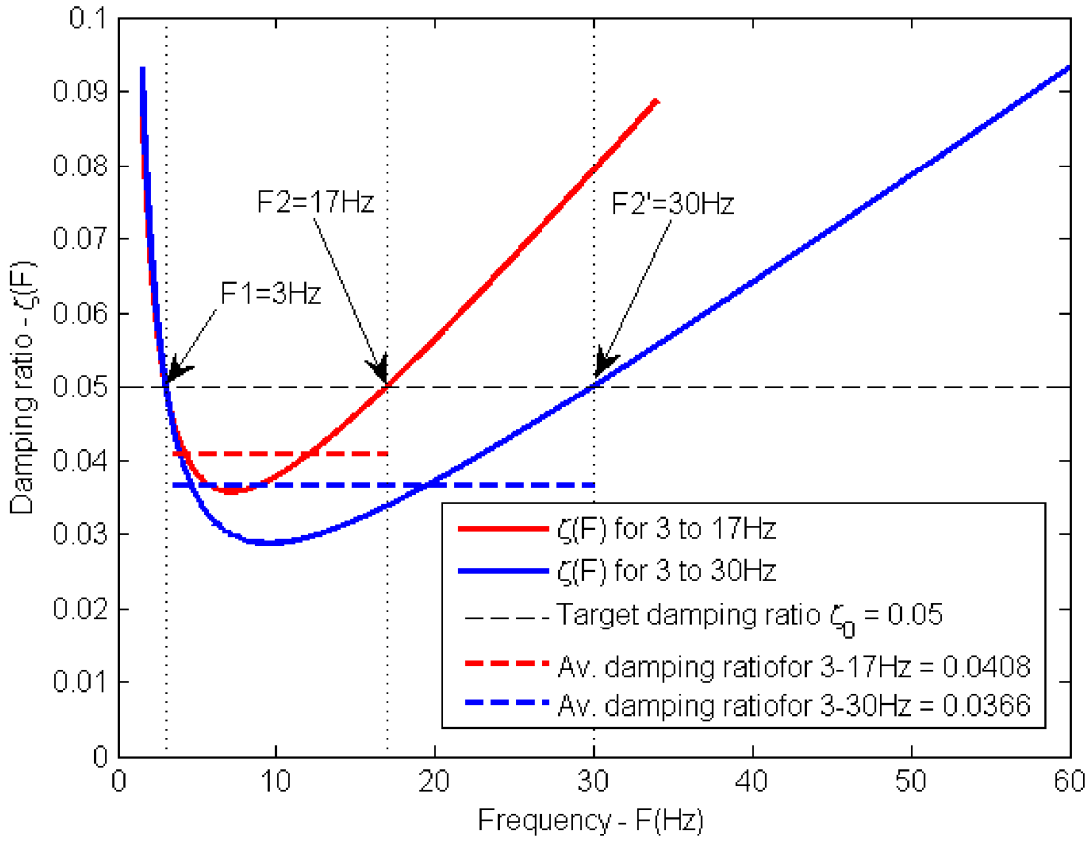

Figure 5.2.2.2-3 Damping Ratios Used in the Sensitivity Studies for Frequency Range for the R/B Complex with Cracked Concrete Section

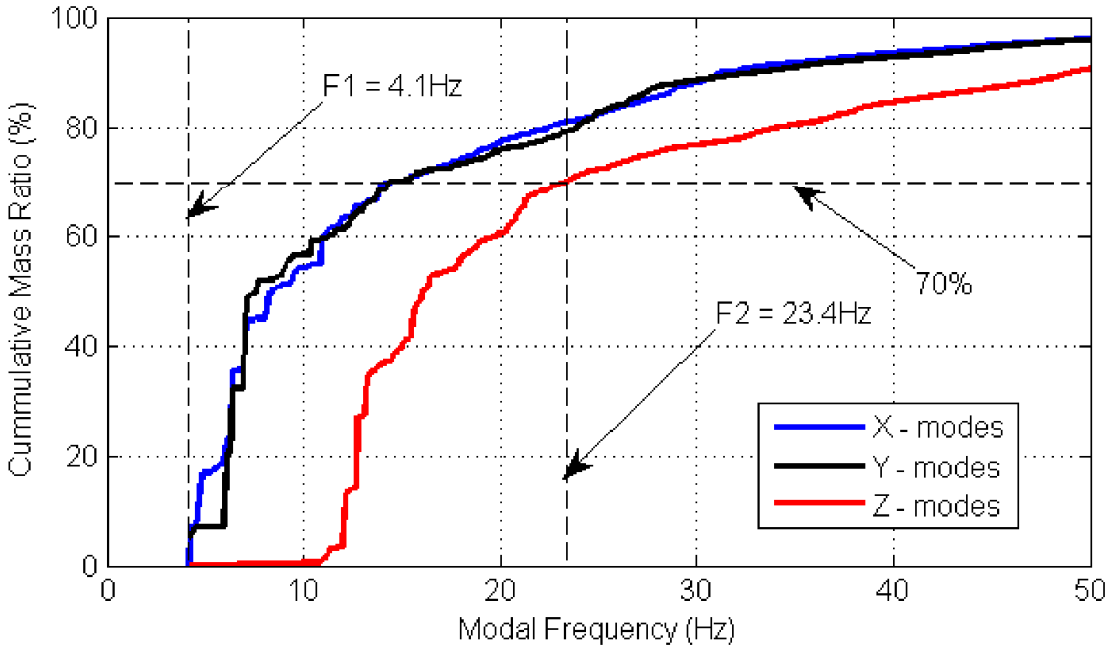

Figure 5.2.2.2-4 Cumulative Effective Mass Ratio for the R/B Complex with Uncracked Section (FE Model) - Entire Structure (including basemat)

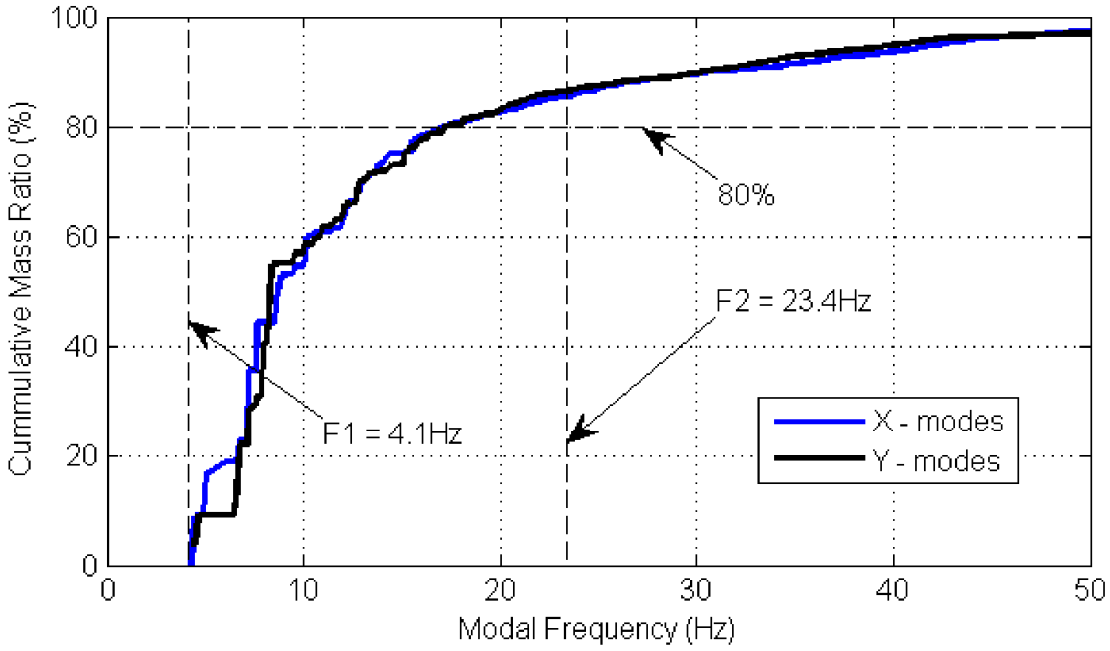

Figure 5.2.2.2-5 Cumulative Effective Mass Ratio for the R/B Complex with Uncracked Section (FE Model) - Superstructure Only (above basemat)

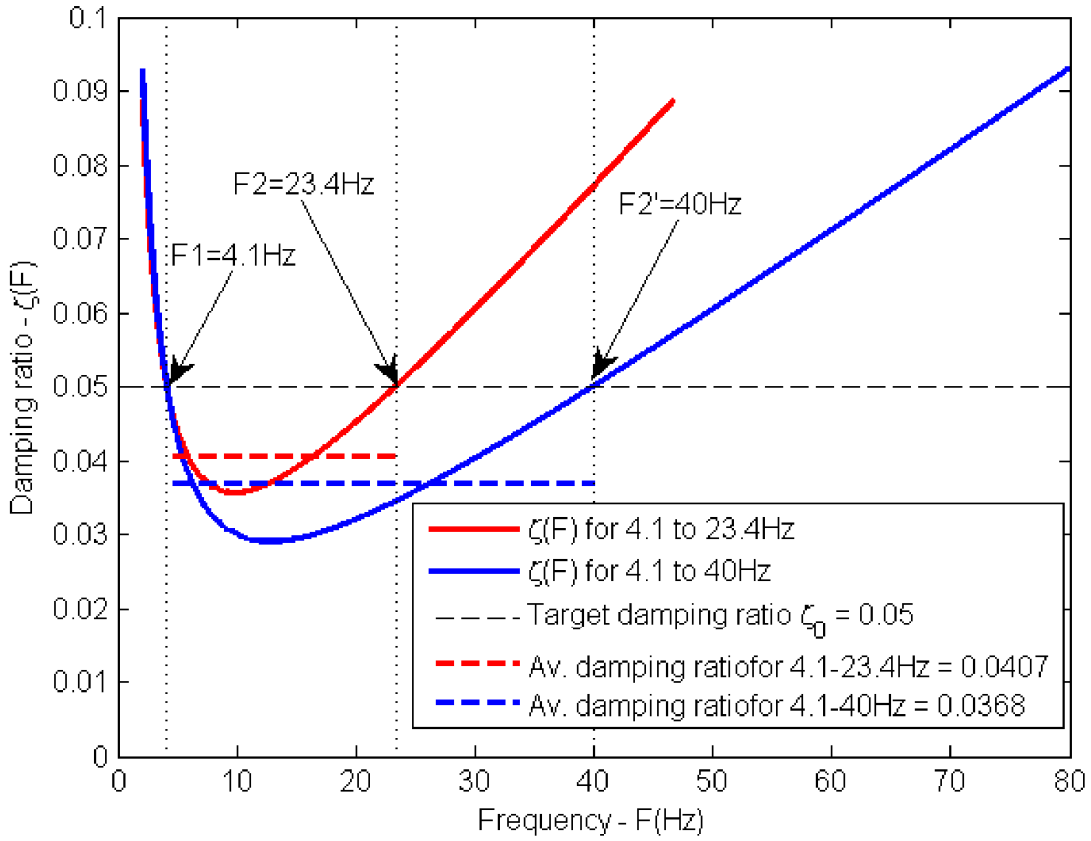

Figure 5.2.2.2-6 Damping Ratios Used in the Sensitivity Studies for Frequency Range for the R/B Complex with Uncracked Concrete Section

Figure 5.2.2.2-7 Sensitivity Study for Frequency Range Analysis Results for the R/B Complex, Profile 2032-100, Hector Mine Input Acceleration, Uncracked Concrete Section

Figure 5.2.2.5-1a Effect of Concrete Cracking: Analysis Results for the R/B Complex, Subgrade Profile 2032-100, Darfield Input Acceleration Time History

Figure 5.2.2.5-1b Analysis Results for the R/B Complex, Profile 2032-100, Darfield Input Acceleration, in Terms of Relative Sliding in the X and Y Directions

Figure 5.2.2.5-2 Effect of Concrete Cracking: Analysis Results for the R/B Complex, Subgrade Profile 2032-100, Hector Mine Input Acceleration Time History

Figure 5.2.2.5-3 Effect of Concrete Cracking: Analysis Results for the R/B Complex, Subgrade Profile 560-500, Hector Mine Input Acceleration Time History

Figure 5.2.2.5-4 Effect of Concrete Cracking: Analysis Results for the R/B Complex, Subgrade Profile 900-200, Nahanni Input Acceleration Time History

Figure 5.2.2.5-5 Effect of Concrete Cracking: Analysis Results for the R/B Complex, Subgrade Profile 900-100, Northridge Input Acceleration Time History

Figure 5.2.4.1-1 LMSM Validation: Analysis Results for the R/B Complex with Cracked Section, FE Model vs. Validated LMSM, Profile 2032-100, Darfield Input Acceleration

Figure 5.2.4.1-2 LMSM Validation: Analysis Results for the R/B Complex with Cracked Section, FE Model vs. Validated LMSM, Profile 2032-100, Hector Mine Input Acceleration

Figure 5.2.4.1-3 LMSM Validation: Analysis Results for the R/B Complex with Cracked Section, FE Model vs. Validated LMSM, Profile 560-500, Hector Mine Input Acceleration

Figure 5.2.4.1-4 LMSM Validation: Analysis Results for the R/B Complex with Cracked Section, FE Model vs. Validated LMSM, Profile 900-200, Nahanni Input Acceleration

Figure 5.2.4.1-5 LMSM Validation: Analysis Results for the R/B Complex with Cracked Section, FE Model vs. Validated LMSM, Profile 900-100, Northridge Input Acceleration

Figure 5.2.4.2-1 LMSM Validation: Analysis Results for the R/B Complex with Uncracked section, FE Model vs. Validated LMSM, Profile 2032-100, Darfield Input Acceleration

Figure 5.2.4.2-2 LMSM Validation: Analysis Results for the R/B Complex with Uncracked section, FE Model vs. Validated LMSM, Profile 2032-100, Hector Mine Input Acceleration

Figure 5.2.4.2-3 LMSM Validation: Analysis Results for the R/B Complex with Uncracked section, FE Model vs. Validated LMSM, Profile 560-500, Hector Mine Input Acceleration

Figure 5.2.4.2-4 LMSM Validation: Analysis Results for the R/B Complex with Uncracked section, FE Model vs. Validated LMSM, Profile 900-200, Nahanni Input Acceleration

Figure 5.2.4.2-5 LMSM Validation: Analysis Results for the R/B Complex with Uncracked section, FE Model vs. Validated LMSM, Profile 900-100, Northridge Input Acceleration

Figure 5.3.1.1-1 Nodes in the Dynamic FE Model for SSI Analysis Used for the T/B Sliding Analysis Input

Figure 5.3.1.1-2 Sensitivity Study for Rocking Effects - T/B - Uncracked Concrete Section, Subgrade Profile 2032-100, Hector Mine Acceleration Time History

Figure 5.3.1.1-3 Sensitivity Study for Rocking Effects - T/B - Uncracked Concrete Section, Subgrade Profile 900-200, Northridge Acceleration Time History

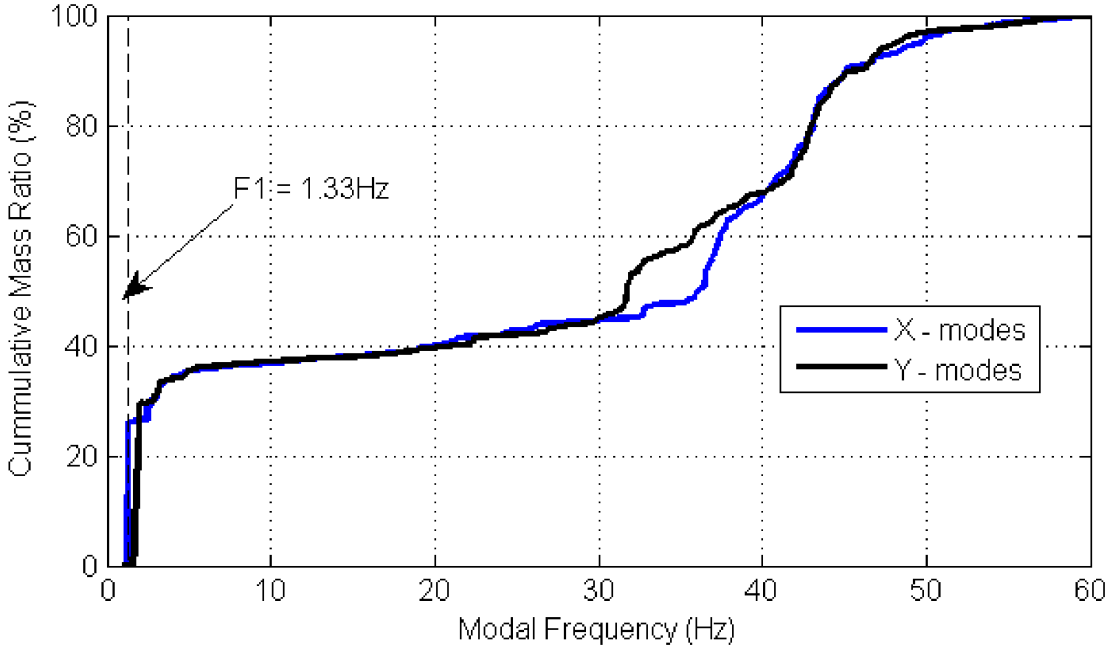

Figure 5.3.2.2-1 Cumulative Effective Mass Ratio for the T/B with Cracked Section - Entire Structure (including basemat)

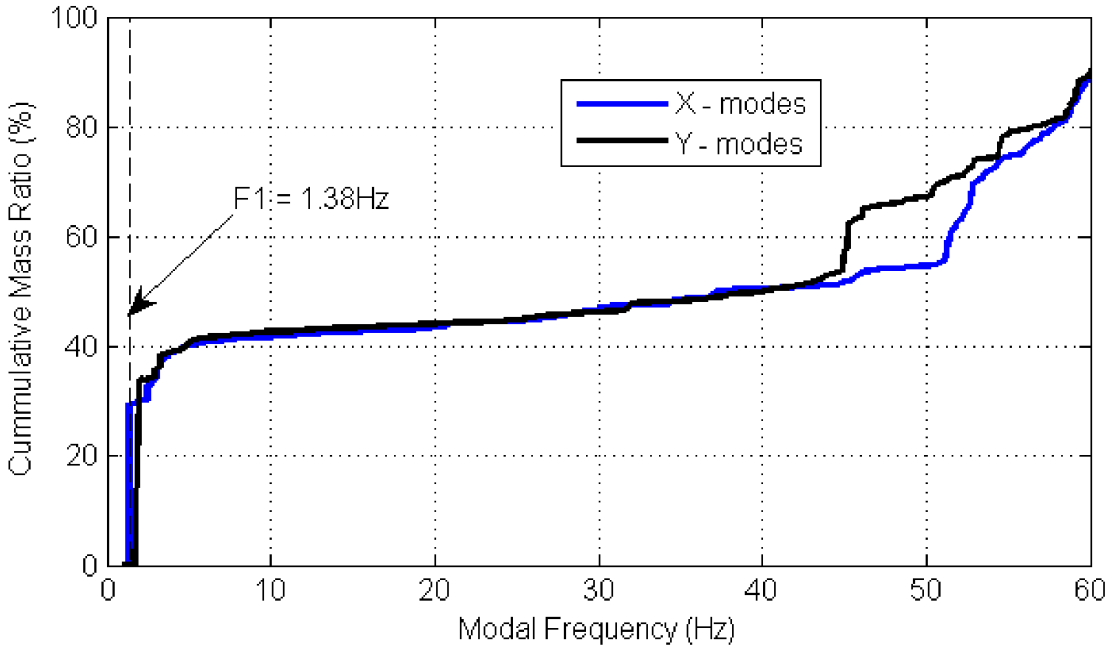

Figure 5.3.2.2-2 Cumulative Effective Mass Ratio for the T/B with Uncracked Section - Entire Structure (including basemat)

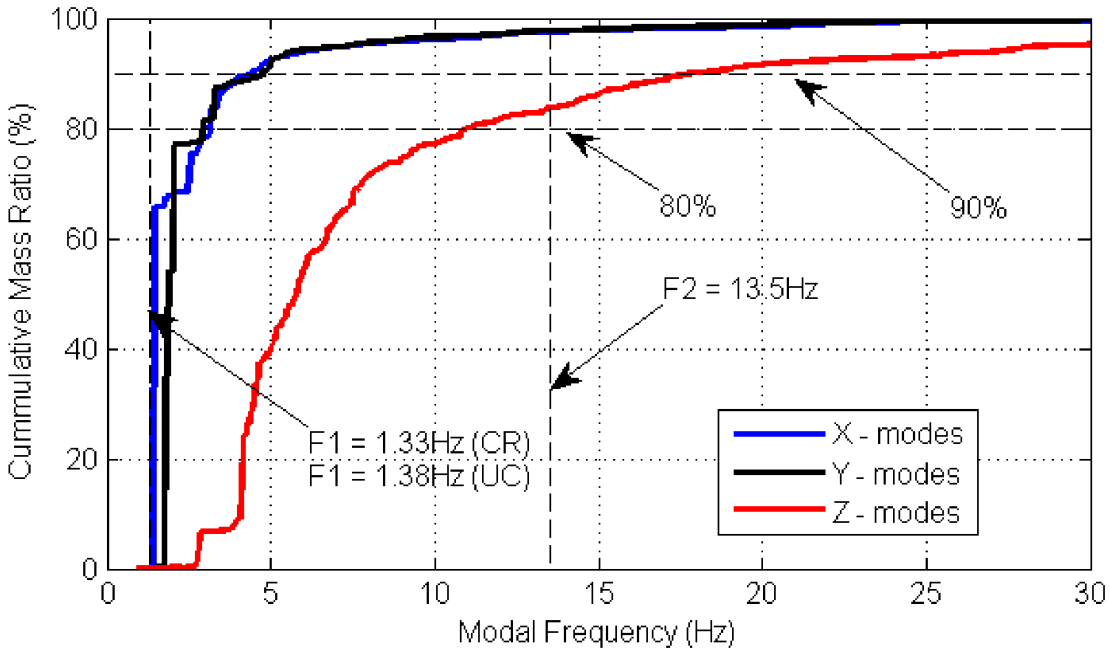

Figure 5.3.2.2-3 Cumulative Effective Mass Ratio for the T/B with Cracked or Uncracked Section - Superstructure (without basemat)

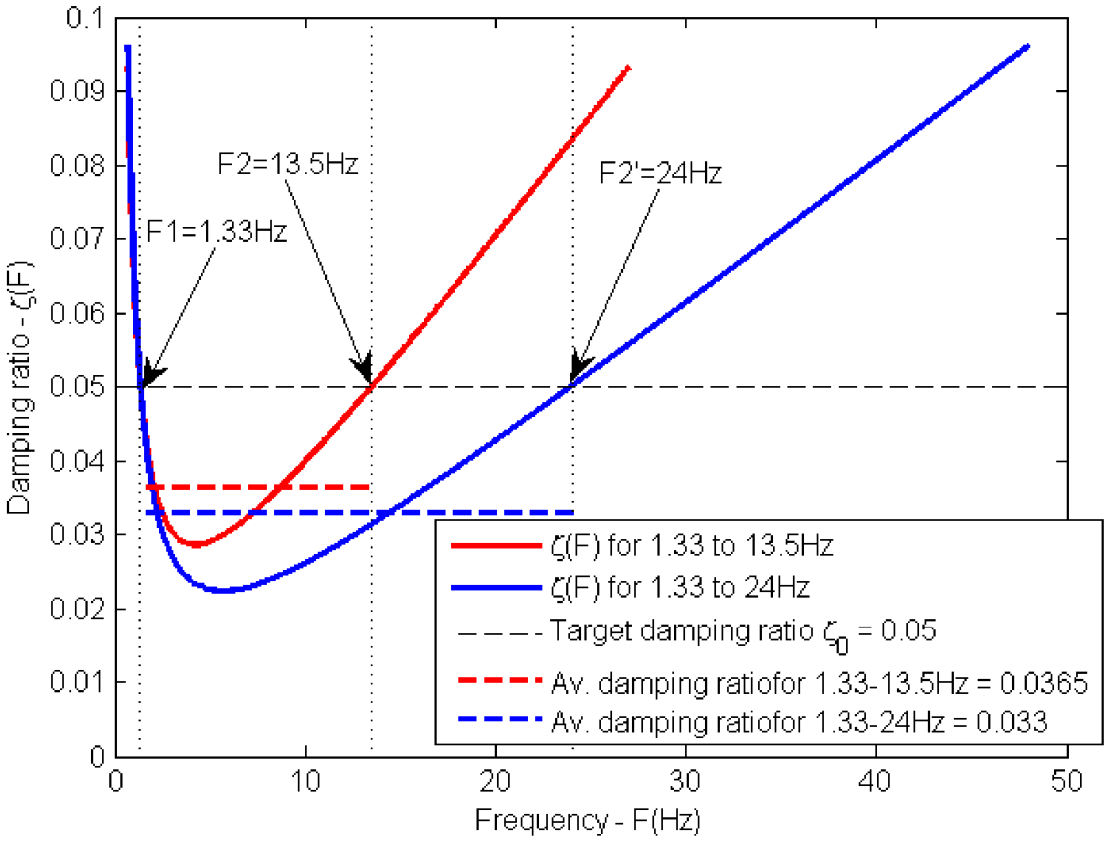

Figure 5.3.2.2-4 Damping Ratios Used in the Sensitivity Studies for the T/B with Cracked Concrete Section

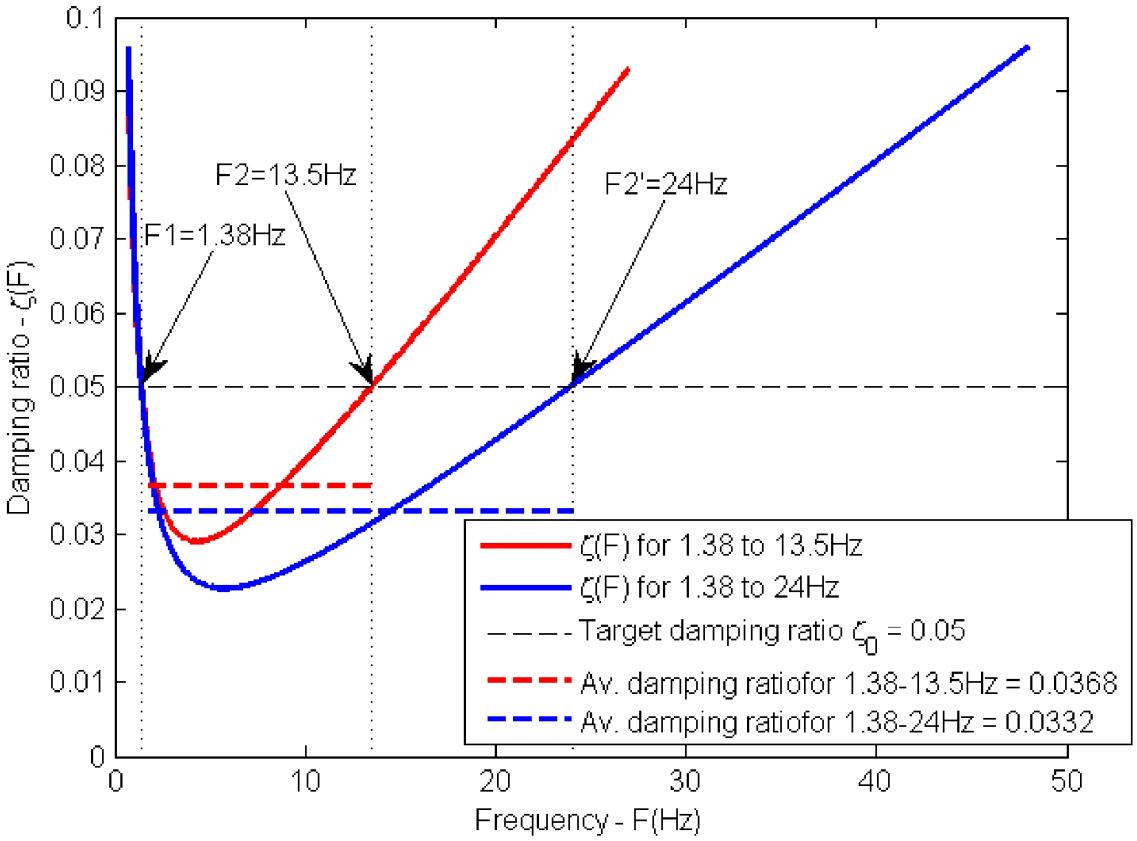

Figure 5.3.2.2-5 Damping Ratios Used in the Sensitivity Studies for the T/B with Uncracked Concrete Section

Figure 5.3.2.2-6 Sensitivity Study for Frequency Range: Analysis Results for the T/B, Profile 2032-100, Northridge Input Acceleration, Cracked Concrete Section

Figure 5.3.2.2-7 Sensitivity Study for Frequency Range: Analysis Results for the T/B, Profile 2032-100, Hector Mine Input Acceleration, Uncracked Concrete Section

Figure 5.3.2.3-1 Effect of Concrete Cracking: Analysis Results for the T/B, Profile 2032-100, Hector Mine Input Acceleration

Figure 5.3.2.3-2 Effect of Concrete Cracking: Analysis Results for the T/B, Profile 900-100, Hector Mine Input Acceleration

Figure 5.3.2.3-3 Effect of Concrete Cracking: Analysis Results for the T/B, Profile 900-200, Hector Mine Input Acceleration

Figure 5.3.2.3-4 Effect of Concrete Cracking: Analysis Results for the T/B, Profile 560-500, Nahanni Input Acceleration

Figure 5.3.2.3-5 Effect of Concrete Cracking: Analysis Results for the T/B, Profile 2032-100, Northridge Input Acceleration

Figure 5.4.1-1 R/B Complex: Distribution of Sliding Analysis Results Obtained with the FE Model, in Terms of Maximum Total Sliding

Figure 5.4.2-1 Distribution of Sliding Analysis Results for the T/B for Each Subgrade Profile

Figure 5.4.2-2 Grouping of Sliding Analysis Results for the T/B by Soil Profiles and Rock Profiles

6.0 ONCLUSION

6.1 R/B Complex

6.2 Turbine Building

6.3 Nonlinear Sliding Analysis Conservatisms

For each of the six generalized layered soil profiles, the net displacements from seismic induced sliding are computed as follows:

1. **Calculation**: Use five time histories all developed to be compatible with the CSDRS and in compliance with Option 2, using Option 1, Approach 1 requirements. Run five sliding analyses using a series of conservative assumptions that are discussed in the following.
2. **Result Processing**: The results are processed in terms of the absolute maximum sliding in each run. The resulting sliding displacement is calculated separately for soil profiles (270-500, 270-200 and 560-500) and for rock profiles (900-200, 900-100 and 2032-100). The sliding for each type of subgrade (soil or rock) is the envelope of two results: maximum value in each sample, and the maximum expected value with probability of being exceeded of 2.5%.
3. **Final Results**: The net sliding values calculated in Step 2 for each type of subgrade are once more enveloped over both subgrade types to obtain the maximum net sliding for the Standard Plant.

Based on the results presented in this TeR, with most result samples non-normally distributed and skewed to the right, the maximum expected value with exceedance probability of 2.5% is equivalent to doubling the mean value in each group. Furthermore, the net displacements are computed using much more rigorous technology than American Society of Civil Engineers (ASCE) 43-05 assumes (Reference 26). Also, the FoS of 2 to 3 recommended in Reference 26 is applied to the results of one analysis (which is equivalent to using the average results in the present nonlinear sliding analysis). Therefore, the FoS to be applied to the envelope of resulted sliding can be 1.0 when using conservative inputs. Besides the method for results processing described above, the following conservative factors are identified and quantified[1]:

[1] The quantitative values presented here are based on the results of the sensitivity studies performed with the validated LMSM for cracked concrete section, discussed in Appendix B.

1. All dynamic inputs are factored by 1.1. As discussed in Appendix B, Section B.1.4, due to the nonlinear character of the sliding phenomenon, use of a factor of 1.0 produces, on average, sliding results of approximately 47% of the results obtained using the factor 1.1. This is equivalent to applying a FoS to the sliding results, $FoS_1 \approx 2$.
2. Based on evidence from laboratory and full scale tests, a reasonable value for the kinetic friction coefficient at the basemat-subgrade interface for the set of subgrade properties considered for the Standard Plant is $\mu_k = 0.55$. A more conservative value ($\mu_k = 0.50$) is used in the sliding analyses. As discussed in Appendix B, Section B.1.3, use of the friction coefficient $\mu_k = 0.55$ result in a reduction of the sliding analysis results, on average, by 38%. This is equivalent to applying a FoS to the sliding results, $FoS_2 \approx 1.5$.

The reduction factors discussed above are based on results from all SPs. In general, the reduction in sliding results for rock profiles is lower than for soil profiles. Based on the sensitivity studies presented in Appendix B, the corresponding equivalent FoS for rock profiles are: $FoS_1 \approx 1.7$ and $FoS_2 \approx 1.4$.

When considering the two above conservative inputs discussed above and their effect on the sliding analysis results, one could simply infer an equivalent factor of safety $FoS = FoS_1\ FoS_2 \approx 2$ to 3. This effect of conservative inputs is applied to the envelope of the results, not to the mean.

In addition to the two conservative inputs that, as discussed above, could be considered equivalent with a FoS of at least 2 applied to the maximum expected value of calculated net sliding displacements, the method for nonlinear sliding analysis used employs a series of additional conservative assumptions whose effects are more difficult to quantify:

1. The GWL is taken at one foot below grade – the highest elevation considered for design. As discussed in Appendix B, Section B.1.2, sliding calculated with GWL at one foot below grade resulted, on average, three times larger than calculated assuming GWL at 20 feet below grade (mid distance between grade level and basemat bottom level for the R/B complex).
2. The ATHs developed to the CSDRS are a very conservative seismic analysis input.
3. The kinetic friction coefficient is used under both static and kinetic conditions (i.e., before the initiation of sliding).
4. The passive soil reactions are neglected.
5. The effect of friction forces on the lateral basement walls is not accounted for.

It is therefore considered reasonable not to apply any additional FoS to the maximum sliding values resulting from statistical processing of the results (Section 5.4).

7.0 REFERENCES

1 Foundations, NUREG-0800 Standard Review Plan, SRP Section 3.8.5, Revision 3, U.S. Nuclear Regulatory Commission, Washington, DC, May 2010.

2 Structural Design Challenges in Design Certification Applications for New Reactors, PVP2011-57600, Proceedings of the American Society of Mechanical Engineers 2011 Pressure Vessels & Piping Division Conference, Miranda, M., Braverman, J., Wey, X., Hofmayer, H., and Xu, J., Baltimore, MD, July, 2011.

3 Seismic Design Parameters, NUREG-0800 Section 3.7.1, Revision 3, U.S. Nuclear Regulatory Commission, Washington, DC, March 2007.

4 US-APWR Standard Design Seismic Design Criteria, Mitsubishi Heavy Industries, N0-CF00001, Revision 4, October, 2012.

5 Soil Structure Interaction Analyses and Results for the US-APWR Standard Plant, Mitsubishi Heavy Industries, Ltd., Technical Report MUAP-10006, Revision 3, November, 2012.

6 A Measure of Earthquake Intensity, Seismic Design for Nuclear Power Plants, pages 438-483, Arias, A., R.J. Hansen, Massachusettes Institute of Technology Press, Cambridge, Massachusetts, 1970.

7 Technical Basis for Revision of Regulatory Guidance on Design Ground Motions: Hazard- and Risk-Consistent Ground Motions Spectra Guidelines, NUREG/CR-6728, Prepared for Division of Engineering Technology, Washingtion, D.C., 2001.

8 Design Response Spectra for Seismic Design of Nuclear Power Plants, Regulatory Guide 1.60 Revision 1, U.S. Nuclear Regulatory Commission, Washington, DC, December, 1973.

9 PEER Next Generation Attenuation Strong Motion Database, Pacific Earthquake Engineering Research Center, http://peer.berkeley.edu/nga/, University of California, Berkeley, CA, 2006.

10 GeoNet New Zealand Seismograph Network, GNS Science, http://geonet.org.nz/.

11 ANSYS, Release 13.0, SAS IP, Inc., 2010.

12 ACS SASSI, Version 2.3.0 including “Option A” & Nuclear Quality Assurance “Option FS,” “An Advanced Computational Software for 3-D Dynamic Analysis Including Soil Structure Interaction,” User Manuals Revision 7.0, Ghiocel Predictive Technologies, Inc., September 26, 2012.

13 T/B Model Properties, SSI Analyses, and Structural Integrity Evaluation, Mitsubishi Heavy Industries, Ltd., Technical Report MUAP-11002, Revision 2, February, 2013.

14 Dynamics of Structures, 2nd Edition, Clough, R.W. and Penzien, J., Mcgraw-Hill, 1993.

15 Code Requirements for Nuclear Safety-Related Concrete Structures, ACI 349-06, American Concrete Institute, September, 2007.

16 Uplift Pressures, Shear Strengths, and Tensile Strengths for Stability Analysis of Concrete Gravity Dams, Volume 1, prepared by Stone and Webster Engineering Corporation for EPRI, Denver, Colorado, August, 1992.

17 Foundation Analysis and Design, 5th Edition, Bowles, J.E., Mcgraw-Hill, 1996.

18 Working Group on Sliding Safety of Existing Gravity Dams, Final Report, ICOLD European Club, G. Ruggieri (coordinator), 2004.

19 The Stress Dilatancy Relation for Static Equilibrium of an Assembly of Particles in Contact, Proc. Royal Society of London, Series A, pp. 500-527, P.W. Rowe, 1962.

20 A State Parameters for Sands, Geotechnique, 35(2):99-107, Been. K and M.G. Jefferies, 1985.

21 Constant Volume Cyclic Simple Shear Testing, Proceedings of the 2nd International Conference on Microzonation, San Francisco, CA, Finn, W.D.L., Laid, Y.P. and Bhatia, S.K.,pg 839-851, 1978.

22 Simplified Procedures for Estimating Earthquake-Induced Deviatoric Slope Displacements, Journal of Geotechnical and Geoenvironmental Engineering, ASCE 133(4): 381-392, Bray. J.D. and Travasarou, T., 2007.

23 Seismic Analysis of Safety-Related Nuclear Structures and Commentary, ASCE 4-98, American Society of Civil Engineers, 1998.

24 Seismic System Analysis, NUREG-0800 Standard Review Plan, SRP Section 3.7.2, Revision 3, U.S. Nuclear Regulatory Commission, Washington, DC, May 2007.

25 Probability and Statistics for Engineering and the Sciences, Devore, J.L., Brooks/Cole, 2000.

26 Seismic Design Criteria for Structures, Systems, and Components in Nuclear Facilities, ASCE/Seismic Engineering Institute 43-05, American Society of Civil Engineers, 2005.

27 Simplified Seismic Slope Displacement Procedures in Earthquake Geotechnical Engineering, pp 327-353, Bray J.D. and K.D. Pitilakis (ed.), Springer, 2007.

28 Nonlinear Coupled Seismic Sliding Analysis of Earth Structures, Journal of Geotechnical and Geoenvironmental Engineering, ASCE 126(11):1002-1014, Rathje, E.M. and Bray, J.D., 2000.

Appendix A

Development of the R/B Complex Lumped Mass Stick Models

APPENDIX A TABLE OF CONTENTS

LIST OF FIGURES

LIST OF TABLES

A.1.0 CALIBRATION METHODOLOGY

The LMSM for sliding analysis of the R/B complex (Figure A.1.0-1) consists of a basemat of the same size and shape as the actual basemat of the R/B complex and three Lumped Mass Stick (LMS) sub-models, representing the CIS, PCCV, and the ARPSB). The three LMS sub-models act independently. In the LMSM representing the R/B complex, these sub-models are attached to the common basemat at points corresponding to the location of their centers of mass in the horizontal plane. Two different LMSMs are developed for the R/B complex: one corresponding to the uncracked section properties and the other corresponding to the cracked section properties.

The first phase in building the LMSM is deciding on the number and locations of lumped masses. As the largest part of the structural mass is generally located at the floor levels, lumped masses are located at the main floor elevations. Next, the walls and columns from each floor are assigned to the neighboring floor levels. This operation is illustrated in Figure A.1.0-2 for one of the LMS sub-models.

A.1.1 Basemat Modeling

The basemat of the R/B complex is modeled by two rigid plates connected by solid elements plus some structural masses in between. The reason for including the bottom rigid plate (termed as the “upper surface” in Section 4.2.3 in conjunction with the contact formulation) is to avoid spurious vertical vibration induced at local loss of contact between basemat and the subgrade, also modeled as a rigid surface. More detail is provided in Section 4.2.3. The rigid plate at the top is necessary to attach the LMS sub-models of the superstructure to the basemat. As discussed in Section 4.2.3 for the FEM, the LMSM basemat flexibility to shear in two vertical planes and to overall vertical deformations is not affected by the presence of the rigid plates. The solid elements used to model the basemat in between the two rigid plates represent the actual basement of the R/B Complex, including the empty spaces in the actual structure. The stiffness of the solid elements used in the LMSM is calibrated to reproduce the stiffness of the actual R/B complex basement, as described in Section A.1.3.

The basemat of the LMSM is modeled entirely with brick elements. The basemat is divided into several areas in the horizontal plane and the mass distribution to these areas is calculated from the FE model and adjusted so that the mass center and moments of inertia of the LMSM basemat match the corresponding quantities of the FE model basemat in all three directions.

A.1.2 Mass Analysis

Each sub-structure of the FE model (namely CIS, PCCV and ARPSB) is divided into a number of main floors, as illustrated in Figure A.1.0-2. The stick model representing each sub-structure consists of beams, representing the walls, and concentrated masses at the levels of the main floors of the FE model. The lumped masses are placed at the elevation of the main floors. After selecting the structural elements associated with the seismic mass at each level, the lumped masses (both translational and rotational masses – or mass moments of inertia) are calculated from the FE model. The center of mass location at each level is also obtained and used for determining the elevation of each lumped mass. The mass eccentricities are captured by including the mass moments of inertia with respect to three orthogonal directions. These are calculated based on the corresponding mass moments of inertia in the FE model and assigned to each lumped mass in the LMSM as rotational masses.

A.1.3 Stiffness Analysis

The stiffness of each story level of the LMSM (i.e., the stiffness of the beam between two adjacent concentrated masses) is calculated based on the corresponding story stiffness of the dynamic FE model. Due to much larger stiffness of the floors as compared to walls and columns, most lateral resistance is provided by the walls in shear. The shear stiffness of story level "*k*" along DOF "*j*" is calculated with ANSYS (Reference 11) using the conventional static method from the FE model. A unit displacement in direction "*j*" is applied at the top of level "*k*" along with restraining all DOF at the lower levels. All but one DOF (namely "*j*") are also restrained at the top of story level "*k*" and all the levels above (see Figure A.1.3-1). The shear stiffness of story level "*k*" along DOF"*j*", K_{jk}^{SH}, is provided by ANSYS as the sum of all forces along DOF "*j*" at the lower levels, F_{ji}.

$$K_{jk}^{SH} = \sum_{i=1}^{k-1} F_{ji} \qquad \text{Equation A.1.3-1}$$

To account for the additional flexibility of the structure due to axial deformations of walls and columns leading to some general bending of the structure (with the floor sloping), a "total stiffness" is approximately calculated at each story level by applying a unit deformation as described above, but with allowance for rotation about the horizontal axis normal to the direction of unit displacement and for vertical displacement at the story level "*k*" and all the levels above (see Figure A.1.3-2). The total stiffness at each story level and in each horizontal direction, "*j*", K_{jk}^{T}, is obtained with ANSYS in the same way as the shear stiffness in Equation A.1.3-1. The LMSM is considered to have, at each story level, "*k*", a shear stiffness equal to K_{jk}^{SH} in Equation A.1.3-1, and a bending stiffness, K_{jk}^{B}, calculated based on K_{jk}^{T} as follows:

$$K_{jk}^{B} = \left(\frac{1}{K_{jk}^{T}} - \frac{1}{K_{jk}^{SH}} \right)^{-1} \qquad \text{Equation A.1.3-2}$$

The stiffness in the vertical direction at each story level is calculated with ANSYS similarly to the level shear stiffness, with unit displacements applied in the vertical direction. The rotational stiffness about the vertical axis at each level is calculated in the same manner, by applying unit rotations and summing up all moment reactions.

A.1.4 Modal Analysis

Modal analysis of the Dynamic FE model is performed to identify the lower modes of vibration in each direction. Use of the first mode in each direction is supported by published evidence that the effect of higher modes on calculated sliding is negligible (References 22, 27, and 28). The natural frequencies and mode shapes of the LMSM are also calculated based on the models with structural characteristics determined as shown in Sections A.1.2 and A.1.3.

Two of the elements of the superstructure in the FE model (CIS and ARPSB) have a relatively complicated structural layout and therefore a large number of mode shapes. By contrast, the corresponding LMS sub-models have a small number of mode shapes. To obtain equivalent dynamic behavior for the LMSM and the FE model in the lower modes, the modes in the FE model corresponding to the first modes in the LMSM are selected to obtain the same modal effective mass in both models. The tables shown in Figure A.1.4-1 (for the X and Y directions) and Figure A.1.4-2 (for the Z direction) are extracted from the modal analysis results obtained for the ARPSB with cracked section. The ranges of modes in the FE model whose effective masses sum up to the corresponding effective masses of the first modes in the LMSM are

highlighted. Therefore, for the ARPSB with cracked section, the ranges of modal frequencies in the FE model corresponding to the first modes in the LMSM are:

- From 3.73 Hz to 9.81 Hz for the X direction.
- From 4.77 Hz to 6.50 Hz for the Y direction.
- From about 8 Hz to 22.84 Hz for the Z direction. While there is some small effective mass in the Z direction in all modes, only the modes with significant effective mass in the Z direction are shown.

A first calibration of the LMSM is performed to match an “average fundamental frequency” calculated using an approximate formula (Equation A2.1-2) for the group of lower modes in each horizontal direction identified as shown in Figure A.1.4-1. This is done by adjusting the total story stiffness at each level, to match the fundamental frequencies and corresponding modal masses in the x and y-directions.

Next, an equivalent fundamental frequency in the vertical direction of the Dynamic FE model is estimated by considering a number of modes in the Dynamic FE model such that the sum of modal masses equals the modal mass of the first mode in the vertical direction of the LMSM (Figure A.1.4-2).

As shown in Figure A.1.4-2, a wide range of the modal frequencies of the FE model had to be included to obtain a sum of modal masses for the FE model equivalent to the modal mass corresponding to the first mode of the LMSM (i.e., to obtain the same effective mass ratios for both FE model and LMSM). This is due to the fact that, while the vertical vibration modes in the LMSM include only longitudinal vibration of the beams (representing structural walls), there are two groups of modal masses in the FE model, corresponding to two different responses: (1) vertical vibration of the frame walls, taking place at relatively high frequencies, and (2) vertical vibration of the horizontal floor slabs, including modes with lower frequencies than those of the vertical walls (two of these modes are illustrated for the ARPSB in Figure A.1.4-2).

To address this aspect, two sets of modal analyses are performed for the FE model structures:

1. A first analysis for the structure without floor slabs, to obtain the fundamental frequency for the vertical wall frame, and;
2. A second analysis for the structure with floor slabs isolated at each elevation by fixing the vertical displacement DOF for the walls. This analysis provides modal masses vibrating in the vertical direction at lower frequencies that cannot be modeled by the original stick model.

As the floors vibrate upon the entire wall frame, the concentrated mass in the LMSM model at each floor is separated into two masses, M1 and M2. The masses M1 represent the mass of the walls plus some of the floor mass that vibrates along with the walls. These masses are connected between floors by beam elements representing the structural walls. The masses M2 represent the fraction of the floor masses that vibrate at a lower frequency than the first modal frequency of the walls. They are located at the same locations as the corresponding masses M1. The procedure to determine the actual values of the masses M1 and M2 at each floor is explained in Sections A.2.3 and A.2.4.

For each floor level of the LMSM, the mass M2 is bound in the two horizontal directions to the beams representing the walls. In the vertical direction, each mass M2 is linked only to the corresponding mass M1 (located at the same elevation) by a link element whose stiffness models the stiffness of the floors in their first mode of vibration. In this way the LMSM can capture the first out-of-plane vibration mode for the slabs at each floor. As only the lower frequencies are important for the sliding analysis, only the out-of-plane vibration modes which

are smaller than the first dominant vertical frequency of the vertical wall frame are considered, and the corresponding effective modal mass is modeled by the additional mass M2. The sum of masses M1 and M2 at each floor equals the total mass assigned to that floor as discussed in Section A.1.2.

Same as for the horizontal direction, the vertical stiffness at each level in the LMSM is adjusted to match an “average fundamental frequency” approximately estimated from the FE model using Equation A.2.1-2. For the cases when floor masses are divided into M1 and M2 (namely for the CIS and the ARPSB) the vertical stiffness adjustment is iterative, as described in Sections A.2.3 and A.2.4.

Since matching of fundamental modal frequencies in both horizontal and vertical directions is done by using approximate averaging formulas for the FE model modes, fine tuning of fundamental vibration frequency in both directions is performed using actual sliding analysis result comparison (Section 4.3.2).

Figure A.1.0-1 LMSM of the R/B Complex - ANSYS Model

Figure A.1.0-2 Mass Analysis for the LMSM Calibration of the ARPSB

Figure A.1.3-1 Stiffness Analysis for Estimating Shear Stiffness in the LMSM of the ARPSB

Figure A.1.3-2 Stiffness Analysis for Estimating Total and Bending Stiffness in the LMSM of the ARPSB

Figure A.1.4-1 Modal Analysis of the FE Model (ARPSB) – Horizontal Modes of Vibration

Figure A.1.4-2 Modal Analysis of the FE Model (ARPSB) – Vertical Modes of Vibration

(Modes 29 and 31 Illustrated in the Figure are for Floor Slabs Only)

A.2.0 R/B COMPLEX LMSM DEVELOPMENT

A.2.1 Basemat Modeling

The FE model for the basemat of the R/B complex is shown in Figure A.2.1-1. The basemat is divided into five groups: three floors at elevations -39.67 ft, -26.33 ft, and 2.58 ft, respectively and two inter-floor layers in between.

Mass Analysis

The basemat has the following overall dimensions: L = 330.75 ft, B = 409.67 ft, H = 42.25 ft, and an area $Abase$ = 124,955.1 ft^2. It is modeled by two rigid plates connected by solid elements plus several structural masses placed at elevation -26.33 ft, modeled by MASS21 elements (Reference 11). The plates are placed at the top (Z = 2.58 ft) and the bottom (Z = -39.67 ft). The two inter-floor layers are modeled by SOLID45 elements (Reference 11). The mass distribution between rigid plates and solid elements is designed for matching the center of mass in the vertical direction (ZCB) as well as the mass moments of inertia about the two horizontal axes (I_{xx} and I_{yy}) of the FE model basemat.

To match the mass center of the FE model in horizontal direction (namely XCB and YCB) and the mass moment of inertia about the vertical axis (I_{zz}), the area of the floor is divided into 22 zones in the LMSM. The mass density in each zone is calculated from the FE model and adjusted to match the mass center in X and Y directions and I_{zz}. The mass distribution in the basemat is identical in the two FE models with cracked and uncracked concrete section. The main results of the mass analysis for the basemat are listed in Table A.2.1-1. All masses and centers of mass calculated for the LMSM match the corresponding quantities in the FE model within less than 0.1%, as shown in Table A.2.1-1. Also listed in Table A.2.1-1 are the mass moments of inertia that are matched within 1% between LMSM and FE model.

Stiffness Analysis

For the stiffness evaluation, the top and bottom solid elements can be treated as one interlayer. The shear stiffness in the two horizontal directions (KX and KY) and the stiffness in vertical direction (KZ) for this interlayer are calculated from the FE model by applying unit displacements in each direction to the LMSM basemat with fixed base and fixing all other DOF for nodes at the top plate. Since the top and bottom plates of the LMSM are rigid, the shear stiffness of the interlayer, for example, KX, is calculated with unrestrained vertical displacement and no rotational restraint in the Y direction, that is UZ and ROTY are set to free for all the nodes in the interlayer. The material properties of the solid elements in the interlayer (namely axial and shear moduli for orthotropic material properties) are then calculated as shown below for the LMSM, with cracked concrete section:

The other material properties for solid elements are assigned as follows: GXY = 5.0×10^4 ksf, EX = EY = 1.3×10^5 ksf, μ = 0.17.

Similarly, the calculated shear and tension stiffnesses from FE model with uncracked concrete section are:

Modal Analysis

The total masses participating in the modal analysis in each direction, $M^{tot}_{LMSM\alpha}$, are shown in Table A.2.1-2 for the two models with cracked and uncracked sections. The symbol α in the subscript indicates the Cartesian direction and takes values of X, Y or Z. Also listed in Table A.2.1-2 are the first modal frequencies in the three directions, $F_{\alpha LMSM}$, and the corresponding effective modal masses, $M^{eff}_{LMSM\alpha}$, for the LMSM basemat. The total modal masses for the first 4000 modes for the FE model, $M^{tot}_{FEM\alpha}$, are also shown in Table A.2.1-2.

First modes could be identified for the FE model in the two horizontal directions, but the corresponding effective masses are much smaller than the effective masses obtained for the LMSM, due to much larger complexity of the FE model compared to the LMSM. A clear first mode could not be identified for the FE model in the vertical direction. To obtain "first mode" frequencies for the FE model equivalent to the modes calculated for the LMSM (i.e., for the same effective mass ratios), the effective masses in the FE model corresponding to the ones in the LMSM are first calculated as follows:

$$M^{eff}_{FEM\alpha} = M^{eff}_{LMSM\alpha} \times M^{tot}_{FEM\alpha} \Big/ M^{tot}_{LMSM\alpha} \qquad \text{Equation A.2.1-1}$$

Next, for each direction, α, the number of modes, $N_{\alpha 1}$, corresponding to the cumulative modal effective mass $M^{eff}_{FEM\alpha}$ is identified in the output file of the modal analysis, and a weighted average of the modal frequency in the FE model corresponding to the modal effective mass from Equation A.2.1-1 is calculated by an approximate weighted averaging formula as:

$$F_{\alpha FEM} = \sum_{i=1}^{N_{\alpha 1}} F_i M_{\alpha i} \Big/ M^{eff}_{FEM\alpha} \qquad \text{Equation A.2.1-2}$$

Where F_i are all modal frequencies for i = 1, …, $N_{\alpha 1}$, and $M_{\alpha i}$ are their corresponding effective masses in direction α.

The resulting fundamental frequencies of the FE model, corresponding to the effective masses of the fundamental modes of the LMSM, are listed in Table A.2.1-2. There are relatively large differences between the first fundamental frequencies in the X-direction (FE model vs. LMSM). These modal frequencies are larger than 25Hz for the model with cracked section and larger than 30Hz for the model with uncracked section. As these values are well outside the range of frequencies that are relevant for the sliding analysis (see Section 5.2.2 and Table 5.2.2.2-1), no further adjustment is considered necessary.

A.2.2 LMSM for PCCV

The FE model of the PCCV is shown in Figure A.2.2-1. The PCCV is divided into four floors and three inter-floor layers. The LMSM for the PCCV is attached to the top plate of the basement (elevation *ZPC* = 2.58 ft) at the horizontal coordinates *XPC* = 0 and *YPC* = 0, which are very close to the center of mass coordinates in the FE model. The PCCV is modeled as a three-level stick with one finite element (BEAM4, Reference 11) at each level.

Mass Analysis

The masses in the LMSM are calculated from the FE model masses, as described in Section A.1.2. The walls and columns between each floor are assigned to the neighboring floor levels. The ratio of the inter-floor mass added to the upper floor and to the lower floor is adjusted so that the Center of Mass (CM) of the LMSM model matches the CM of the FE model in Z direction. The mass distribution in the PCCV is identical in the two FE models with cracked and uncracked concrete sections. The final adjusted lumped masses, mass centers and mass

moments of inertia are summarized in Table A.2.2-1. The mass moments of inertia are assigned in ANSYS as rotational masses to the MASS21 (Reference 11) elements modeling the lumped masses at each floor.

Stiffness Analysis

The shear and bending stiffness in the two horizontal directions, axial stiffness and torsion stiffness about the vertical axis are calculated from the FE model as described Section A.1.3. The values obtained from the FE model with cracked concrete section are listed in Table A.2.2-2. The notations in Table A.2.2-2 are as follows:

- KX_shear and KY_shear represent the total shear stiffness of the PCCV in the X and Y directions, respectively;
- KZ_axial is the axial stiffness of the PCCV;
- KX_bend and KY_bend represent the total bending stiffness of the PCCV in the X and Y directions, respectively;
- KZ_torsion is the torsional stiffness of the PCCV about the vertical axis.

Based on the stiffness values listed in Table A.2.2-2, assuming an arbitrary value for the Young's modulus (E_{beam} = 10^7 ksf) and for the Poisson's ratio, μ_{beam} = 0.17, the structural dimensions of the beam elements resulted as listed in Table A.2.2-3.

The quantities shown in Table A.2.2-3 are used to assign the real constants for the BEAM4 finite elements in ANSYS (Reference 11), and are as follows:

- Abeam - cross-sectional area, used to define stiffness in the axial direction of the element (global Z - direction);
- Izz and Iyy are the cross-section moments of inertia in the element local coordinate system. In this analysis, the local ZZ axis corresponds to the global X axis, and the local YY axis corresponds to the global Y axis;
- Ashz and Ashy are the areas used for calculating the shear stiffness of the beam element in ZZ and YY local directions, corresponding to X and Y global directions, respectively;
- Ixx is the cross-section moment of inertia in the axial direction (global Z-direction);
- h is the inter-floor beam length.

Similarly, the values obtained from the FE model with uncracked concrete section are listed in Table A.2.2-4. The geometric properties of the beam elements used in the LMSM with uncracked concrete section are listed in Table A.2.2-5.

Modal Analysis

The first mode frequencies (in all three directions) for the LMSM are calculated by modal analysis and are listed in the 7th column of Table A.2.2-6 for the two models with cracked and uncracked concrete sections . For the PCCV FE model, the first modes could be identified in the two horizontal directions, but the corresponding effective masses were smaller than the effective masses obtained for the LMSM. A clear first mode could not be identified in the vertical direction. To obtain "first mode" frequencies for the FE model equivalent to the ones calculated for the LMSM (i.e., for the same effective mass ratios), the effective masses in the FE model corresponding to the ones in the LMSM are first calculated using Equation A.2.1-1 and the corresponding FE model modal frequencies are calculated using Equation A.2.1-2 - see Section A.2.1 for equations and explanation of the symbols. The resulting fundamental

frequencies of the FE model, corresponding to the effective masses of the fundamental modes of the LMSM, are listed in the 4th column of Table A.2.2-6.

The procedure described by Equations A.2.1-1 and A.2.1-2 results in very close matching of the modal masses in the first modes in each direction (see the 11th column in Table A.2.2-6). To match the frequencies of the first modes in each direction, the stiffness of the LMSM is adjusted by the stiffness correction factors listed in the last column of Table A.2.2-6). For example, for the model with cracked concrete section, the geometric properties of the beam elements listed in Table A.2.2-3 are modified as follows:

- *Iyy* and Ashy are multiplied by 0.803.
- *Izz* and Ashz are multiplied by 0.789.
- *Abeam* is multiplied by 0.972.

These corrections for beam stiffness result in an exact match of the first mode frequencies in all directions between the LMSM and the FE model (the new modal frequencies for the LMSM are listed in the 8th column of Table A.2.2-6).

A.2.3 LMSM for CIS

The FE model of the CIS is shown in Figure A.2.3-1. The CIS is divided into four floors and three inter-floor layers. The LMSM for the CIS is attached to the top plate of the basement (elevation *ZPC* = 2.58 ft) at the horizontal coordinates *XCS* = 0 and *YCS* = 0 (the same as for the PCCV), which are very close to the center of mass coordinates in the FE model. The CIS is modeled as three-level stick with one finite element (BEAM4) at each level.

Mass Analysis

The masses in the LMSM are calculated from the FE model masses, as described in Section A.1.2. The walls and columns between each floor are assigned to the neighboring floor levels. The ratio of the inter-floor mass added to the upper floor and to the lower floor is adjusted so that the CM of the LMSM model matches the CM of the FE model in Z direction. The mass distribution in the CIS is identical in the two FE models with cracked and uncracked concrete sections. The final adjusted lumped masses, mass centers and mass moments of inertia are summarized in Table A.2.3-1. The mass moments of inertia are assigned in ANSYS as rotational masses to the MASS21 elements modeling the lumped masses at each floor.

Stiffness Analysis

The shear and bending stiffness in the two horizontal directions, axial stiffness and torsion stiffness about the vertical axis, are calculated from the FE model as described Section A.1.3. The values obtained from the FE model with cracked concrete section are listed in Table A.2.3-2. The notations in Table A.2.3-2 are explained in Section A.2.2.

Based on the stiffness values listed in Table A.2.3-2, assuming an arbitrary value for the Young's modulus (E_{beam} = 10^7 ksf) and for the Poisson's ratio, μ_{beam} = 0.17, the structural dimensions of the beam elements resulted as listed in Table A.2.3-3.

The quantities shown in Table A.2.3-3 are used to assign the real constants for the BEAM4 finite elements in ANSYS. Their signification is explained in Section A.2.2.

Similarly, the values obtained from the FE model with uncracked concrete section are listed in Table A.2.3-4. The geometric properties of the beam elements used in LMSM with uncracked concrete section are listed in Table A.2.3-5.

Modal Analysis

Modal analysis of the LMSM for CIS provided the first mode frequencies in the horizontal directions, as listed in the 7th column of Table A.2.3-6 for the models with cracked and uncracked concrete sections. For the CIS FE model, the first modes could be identified in the two horizontal directions, but the corresponding effective masses were smaller than the effective masses obtained for LMSM. To obtain "first mode" frequencies for the FE model equivalent to the ones calculated for the LMSM (i.e., for the same effective mass ratios), the effective masses in the FE model corresponding to the ones in the LMSM are first calculated using Equation A.2.1-1 and the corresponding FE model modal frequencies are calculated using Equation A.2.1-2. The resulting fundamental frequencies of the FE model in the two horizontal directions, corresponding to the effective masses of the fundamental modes of the LMSM, are listed in Table A.2.3-6 for both cracked and uncracked concrete sections.

The procedure described by Equations A.2.1-1 and A.2.1-2 results in very close matching of the modal masses in the first modes in the horizontal directions (see the 11th column in Table A.2.3-6) To match the frequencies of the first modes in horizontal directions, the stiffness of the LMSM is adjusted by the stiffness correction factors listed in the last column of Table A.2.3-6. For example, for the model with cracked concrete section, the geometric properties of the beam elements listed in Table A.2.3-3 are modified as follows:

- *Iyy* and Ashy are multiplied by 0.670.
- *Izz* and Ashz are multiplied by 0.609.

Based on the modal analysis results in vertical direction, the lumped masses of the CIS with cracked concrete section are divided into two sets, as described in Section A.1.4: (1) masses *M1*, including the mass of walls plus part of the floor mass vibrating along with the walls (for the CIS the masses *M1* include all modal masses vibrating in vertical direction with frequency larger than 17.55 Hz - as calculated in the modal analysis of the FE model without floors), and (2) masses *M2*, representing the fraction of floor mass that vibrates at frequencies lower than 17.55 Hz. For the CIS, the sum of masses *M2* is 138 k-slugs and the average vibration frequency in vertical direction for *M2* is 14.25 Hz - as calculated from the FE model using Equation A.2.1-2. The distribution of *M2* over the CIS floors is shown in Table A.2.3-7. The masses *M2* are connected in the vertical direction to the corresponding masses *M1* at each floor by LINK180 elements (Reference 11) whose stiffness is calculated to capture the vibration frequency in the FE model (namely 14.25Hz). The other five DOF of the masses *M2* are slaved to the corresponding DOF of the main lumped masses (*M1*) at each floor. Similar procedure is applied to the model with uncracked concrete section and the distribution of *M2* over the CIS floors and corresponding vibration frequency are also shown in Table A.2.3-7.

The first mode frequency and corresponding effective mass for the LMSM of CIS in the vertical direction are listed in the 7th and 9th columns of Table A.2.3-8 for models with cracked and uncracked concrete sections. To obtain "first mode" frequencies for the FE model equivalent to the ones calculated for the LMSM (i.e., for the same effective mass ratios), the effective masses in the FE model corresponding to the ones in the LMSM are first calculated using Equation A.2.1-1 and the corresponding FE model modal frequencies are calculated using Equation A.2.1-2. The resulting fundamental frequencies of the FE model, corresponding to the effective masses of the fundamental modes of the LMSM, are listed in the 4th column of Table A.2.3-8 for both cracked and uncracked concrete sections.

The procedure described by Equations A.2.1-1 and A.2.1-2 results in very close matching of the modal masses in the first modes in the vertical direction (see the 11th column in Table A.2.3-8). A trial-and-error procedure with adjusting the stiffness of the beam elements and the link elements is performed so that the first dominant frequency of the LMSM in *Z* direction is

equal to the first mode frequency in the FE model and at the same time keeping the cumulative effective masses corresponding to their frequencies identical in the FE model and LMSM. For example, for the model with cracked concrete section, at the end of the trial-and-error process, the geometric properties of the beam elements listed in Table A.2.3-3 and the stiffness of the link elements are modified as follows:

- The cross-sectional area of all beams (Abeam) is multiplied by 0.715.
- The stiffness of the LINK180 elements is multiplied by 0.95.

These corrections for beam and link stiffness result in an exact match of the first modal frequency in Z direction, as listed in Column 10 of Table A.2.3-8. Therefore, the new modal frequencies for the LMSM in all three directions match exactly with those of the FE model and are listed in Column 8 of Table A.2.3-6 and Table A.2.3-8 for the horizontal and vertical directions, respectively.

A.2.4 LMSM for ARPSB

The FE model of the ARPSB is shown in Figure A.2.4-1. The ARPSB is divided into six floors and five inter-floor layers. The LMSM for the ARPSB is attached to the top plate of the basement (*ZAR*=2.58 ft) at the horizontal coordinates of its center of mass in the FE model, which are *XAR* = 4.15 ft and *YAR* = -43.42 ft. The ARPSB is modeled as a five-level stick with one finite element (BEAM4) at each level.

Mass Analysis

The masses in the LMSM are calculated from the FE model masses, as described in Section A.1.2. The walls and columns between each floor are assigned to the neighboring floor levels. The ratio of the inter-floor mass added to the upper floor and to the lower floor is adjusted so that the CM of the LMSM model matches the CM of the FE model in Z direction. The mass distribution in the ARPSB is identical in the two FE models with cracked and uncracked concrete sections. The final adjusted lumped masses, mass centers and mass moment of inertia are summarized in Table A.2.4-1. The mass moments of inertia are assigned in ANSYS as rotational masses to the MASS21 elements modeling the lumped masses at each floor.

Stiffness Analysis

The shear and bending stiffness in the two horizontal directions, axial stiffness and torsion stiffness about the vertical axis, are calculated from the FE model as described Section A.1.3. The values obtained from the FE model with cracked concrete section are listed in Table A.2.4-2. The notations in Table A.2.4-2 are explained in Section A.2.2.

Based on the stiffness values listed in Table A.2.4-2, assuming an arbitrary value for the Young's modulus (E_{beam} = 10^7 ksf) and for the Poisson's ratio, μ_{beam} = 0.17, the structural dimensions of the beam elements resulted as listed in Table A.2.4-3.

The quantities shown in Table A.2.4-3 are used to assign the real constants for the BEAM4 finite elements in ANSYS. Their signification is explained in Section A.2.2.

Similarly, the values obtained from the FE model with uncracked concrete section are listed in Table A.2.4-4. The geometric properties of the beam elements used for LMSM with uncracked concrete section are listed in Table A.2.4-5.

Modal Analysis

Modal analysis of the LMSM for ARPSB provided the first mode frequencies in the horizontal directions, as listed in Column 7 of Table A.2.4-6 for the models with cracked and uncracked

concrete sections. For the ARPSB FE model, the first modes could be identified in the two horizontal directions, but the corresponding effective masses were smaller than the effective masses obtained for LMSM. To obtain "first mode" frequencies for the FE model equivalent to the ones calculated for the LMSM (i.e., for the same effective mass ratios), the effective masses in the FE model corresponding to the ones in the LMSM are first calculated using Equation A.2.1-1 and the corresponding FE model modal frequencies are calculated using Equation A.2.1-2. The resulting fundamental frequencies of the FE model in the two horizontal directions, corresponding to the effective masses of the fundamental modes of the LMSM are listed in the 4th column of Table A.2.4-6 for both cracked and uncracked concrete sections.

The procedure described by Equations A.2.1-1 and A.2.1-2 results in very close matching of the modal masses in the first modes in the horizontal directions (see the 11th column in Table A.2.4-6) To match the frequencies of the first modes in horizontal directions, the stiffness of the LMSM is adjusted by the stiffness correction factors listed in the last column of Table A.2.4-6. For example, for the model with cracked concrete section, the geometric properties of the beam elements listed in Table A.2.4-3 are modified as follows:

- *Iyy* and Ashy are multiplied by 0.757.
- *Izz* and Ashz are multiplied by 0.753.

Based on the modal analysis results in vertical direction, the lumped masses of the ARPSB with cracked concrete section are divided into two sets, as described in Section A.1.4: (1) masses *M1*, including the mass of walls plus part of the floor mass vibrating along with the walls (for the ARPSB the masses *M1* include all modal masses vibrating in vertical direction with frequency larger than 15.02 Hz - as calculated in the modal analysis of the FE model without floors), and (2) masses *M2*, representing the fraction of floor mass that vibrates at frequencies lower than 15.02 Hz. For example, as shown in Table A.2.4-7, the mass *M2* at level 3 is 82.92 kilo-slugs and the average vibration frequency in vertical direction for *M2* is 11.71Hz - as calculated from the FE model using Equation A.2.1-2. The masses *M2* at each floor of ARPSB are shown in Table A.2.4-7. The masses *M2* are connected in the vertical direction to the corresponding masses *M1* at each floor by LINK180 elements whose stiffness is calculated to capture the vibration frequency in the FE model (namely 11.71Hz at level 3). The other five DOF of the masses *M2* are slaved to the corresponding DOF of the main lumped masses (*M1*) at each floor. A similar procedure is applied to the model with uncracked concrete section. The distribution of the masses *M2* over the ARPSB floors and the corresponding vibration frequencies are also shown in Table A.2.4-7.

The first mode frequencies and corresponding effective masses for the LMSM of ARPSB in the vertical direction are listed in the 7th and 9th columns of Table A.2.4-8 for models with cracked and uncracked concrete sections. To obtain "first mode" frequencies for the FE model equivalent to the ones calculated for the LMSM (i.e., for the same effective mass ratios), the effective masses in the FE model corresponding to the ones in the LMSM are first calculated using Equation A.2.1-1 and the corresponding FE model modal frequencies are calculated using Equation A.2.1-2. The resulting fundamental frequencies of the FE model, corresponding to the effective masses of the fundamental modes of the LMSM, are listed in the 4th column of Table A.2.4-8 for both cracked and uncracked concrete sections.

The procedure described by Equations A.2.1-1 and A.2.1-2 results in very close matching of the modal masses in the first modes in the vertical direction (see the 11th column in Table A.2.4-8). A trial-and-error procedure with adjusting the stiffness of the beam elements and the link elements is performed so that the first dominant frequency of the LMSM in *Z* direction is equal to the first mode frequency in the FE model and at the same time keeping the cumulative effective masses corresponding to their frequencies identical in the FE model and

LMSM. For example, for the model with cracked concrete section, at the end of the trial-and-error process, the geometric properties of the beam elements listed in Table A.2.4-3 and the stiffness of the link elements are modified as follows:

- *Abeam* is multiplied by 0.788.
- The stiffness of the LINK180 elements is multiplied by 0.700.

These corrections for beam and link stiffness result in an exact match of the first modal frequency in Z direction, as listed in Column 10 of Table A.2.4-8. Therefore, the new modal frequencies for the LMSM in all three directions match exactly with those of the FE model and are listed in Column 8 of Table A.2.4-6 and Table A.2.4-8 for the horizontal and vertical directions, respectively.

A.2.5 LMSM Calibration for the R/B Complex

With the stiffness adjustment of all the beam and link elements in the superstructure using the stiffness reduction factors listed in Sections A.2.2 through A.2.4 for the PCCV, CIS, and ARPSB, respectively, the first mode frequencies in all directions of all the components of the superstructure in the LMSM match exactly the corresponding components in the FE model, as shown in the fourth and eighth columns of Table A.2.2-6 for PCCV, Table A.2.3-6 and Table A.2.3-8 for CIS, and Table A.2.4-6 and Table A.2.4-8 for ARPSB. It is mentioned that the modal matching between LMSM and FE model is done assuming validity of the weighted averaging Equation A.2.1-2.

Table A.2.1-1 Comparison of the Basemat Masses, Mass Centers and Moments of Inertia Between LMSM and FE Model

Quantity	FEM	LMSM	Difference
Total Mass (kslug)	17532.85	17532.85	0.00%
X - Center of Mass (ft)	17.57	17.57	0.01%
Y - Center of Mass (ft)	-45.71	-45.71	0.07%
Z - Center of Mass (ft)	-20.27	-20.27	0.00%
Inertia about X-axis (kslug-sqft)	2.14E+08	2.12E+08	-1.04%
Inertia about Y-axis (kslug-sqft)	1.52E+08	1.51E+08	-0.70%
Inertia about Z-axis (kslug-sqft)	3.59E+08	3.56E+08	-0.95%

Table A.2.1-2 Comparison of Modal Analysis Results for the Basemats of FE Model and LMSM

.

Table A.2.2-1 Lumped Masses, Mass Centers and Mass Moments of Inertia for the PCCV

Table A.2.2-2 Shear, Bending, Axial and Torsion Stiffness from the PCCV FE Model with Cracked Concrete Section

Table A.2.2-3 Geometric Properties of BEAM4 Elements in the PCCV LMSM Model with Cracked Concrete Section

Table A.2.2-4 Shear, Bending, Axial and Torsion Stiffness from the PCCV FE Model with Uncracked Concrete Section

Table A.2.2-5 Geometric Properties of BEAM4 Elements in the PCCV LMSM with Uncracked Concrete Section

Table A.2.2-6 Modal Analysis Results for PCCV: FE Model and LMSM

Table A.2.3-1 Lumped Masses, Mass Centers and Mass Moments of Inertia for the CIS

Table A.2.3-2 Shear, Bending, Axial and Torsion Stiffness from the CIS FE Model with Cracked Concrete Section

Table A.2.3-3 Geometric Properties of BEAM4 Elements in the CIS LMSM Model with Cracked Concrete Section

Table A.2.3-4 Shear, Bending, Axial and Torsion Stiffness from the CIS FE Model with Uncracked Concrete Section

Table A.2.3-5 Geometric Properties of BEAM4 Elements in the CIS LMSM with Uncracked Concrete Section

Table A.2.3-6 Modal Analysis Results for the CIS in Horizontal Direction: FE Model and LMSM

Table A.2.3-7 Separated Masses (M2) and Corresponding Modal Frequencies for the CIS LMSM

Table A.2.3-8 Modal Analysis Results for the CIS in Vertical Direction: FE Model and LMSM

Table A.2.4-1 Lumped Masses, Mass Centers and Mass Moments of Inertia for the ARPSB

Table A.2.4-2 Shear, Bending, Axial and Torsion Stiffness from the ARPSB FE Model with Cracked Concrete Section

Table A.2.4-3 Geometric Properties of BEAM4 Elements in the ARPSB LMSM Model with Cracked Concrete Section

Table A.2.4-4 Shear, Bending, Axial and Torsion Stiffness from the ARPSB FE Model with Uncracked Concrete Section

Table A.2.4-5 Geometric Properties of BEAM4 Elements in the ARPSB LMSM with Uncracked Concrete Section

Table A.2.4-6 Modal Analysis Results for the ARPSB in Horizontal Directions: FE Model and LMSM

Table A.2.4-7 Separated Masses (M2) and Corresponding Modal Frequencies for the ARPSB LMSM

Table A.2.4-8 Modal Analysis Results the for ARPSB in Vertical Direction: FE Model and LMSM

Figure A.2.1-1 FE Mesh of the R/B Complex Basemat

Figure A.2.2-1 FE Mesh of the PCCV in the R/B Complex FE Model

Figure A.2.3-1 FE Mesh of the CIS in the R/B Complex FE Model

Figure A.2.4-1 FE Mesh of the ARPSB in the R/B Complex FE Model

Appendix B

Sensitivity Analyses

APPENDIX B TABLE OF CONTENTS

LIST OF TABLES

B.1.0 SENSITIVITY ANALYSES

The sensitivity analyses discussed in the following address some of the uncertainties related to loads and with subgrade properties and help with assessing the degree of conservatism used in the nonlinear sliding analyses. All calculations presented in this Appendix are done with the validated LMSM of the R/B complex with cracked concrete section properties.

B.1.1 Effect of Live Load

As presented in Appendix A and Section 5.2.4, the LMSM for nonlinear sliding analysis of the R/B complex is calibrated and validated based on the FE model with Live Loads used in the SSI analyses. The Live Loads include 25% of the floor design live load and 75% of the roof design snow load. To assess the effect of Live Loads on sliding, the LMSM that has been validated as discussed in Section 5.2.4 is transformed by removing the masses corresponding to Live Loads at every level of the three stick models and at the basemat level. The new LMSM, without Live Loads, is termed here as LMSMnoLL.

The Live Loads used in the dynamic analysis (i.e., 25% of the floor design live load and 75% of the roof design snow load) are taken from Reference 5, and are subtracted from the concentrated masses of the LMSM to obtain the LMSMnoLL (i.e., the LMSM of the structure with zero Live Loads). No further validation of the LMSMnoLL is performed.

The analyses results using the LMSM without Live Loads (cracked concrete section) are listed in Table B.1.1-1 for all five sets of ATHs and for all six SPs. The maximum total sliding values obtained for the runs considering Live loads are also shown for comparison.

The absolute difference between the maximum sliding values, δ_{max}^{LL} (with Live Loads) and δ_{max}^{noLL} (without Live Loads) is calculated for each case analyzed as:

$$\Delta = \left| \delta_{max}^{noLL} - \delta_{max}^{LL} \right| \qquad \text{Equation B.1.1-1}$$

The average value of the absolute differences over all cases analyzed is zero. For all the cases analyzed, there are no differences between results larger than 0.02 in, which is about 3% of the maximum total sliding calculated for all cases analyzed.

Based on the results of this study, it is concluded that accounting for or not for the presence of Live Loads in the sliding analysis does not have a significant effect on the results. The explanation is that, even if the Live Loads may have a stabilizing effect by increasing the resisting friction force, they also may have a driving effect by increasing the inertia forces. As shown by the results of this study, these effects compensate each other. Therefore, only sliding analyses including presence of Live Loads (as specified in Reference 23 for dynamic analyses) are considered in this TeR.

B.1.2 Effect of Groundwater Level

For all the analysis results listed in Sections 5.2.5 and 5.3.3, the GWL is assumed at 1ft below grade - the highest elevation considered for design. The effect of this conservative assumption on the calculated seismic sliding displacements is assessed through a comparison between sliding values calculated for GWL at 1 ft below grade, and GWL at 20 ft below grade. The results in terms of maximum total sliding values are summarized in Table B.1.2-1 for the LMSM of R/B complex with cracked concrete section.

The percent difference between the maximum sliding values, δ_{max}^{-1} (GWL at 1 ft below grade) and δ_{max}^{-20} (GWL at 20 ft below grade) is calculated for each case analyzed as:

$$\Delta = \frac{\delta_{\max}^{-20} - \delta_{\max}^{-1}}{\delta_{\max}^{-1}} \times 100(\%)$$ Equation B.1.2-1

As shown in Table B.1.2-1, a reduction of the GWL by 19 ft (i.e., at half distance between the grade and the R/B complex basemat) results, on average, in a reduction of computed seismic sliding by 66% for the R/B complex. The average reduction in maximum total sliding for soil profiles (270-500, 270-200 and 560-500) is about 81%, while the average reduction in maximum total sliding for rock profiles (900-200, 900-100 and 2032-100) is about 52%.

B.1.3 Effect of Friction Coefficient

The kinetic friction coefficient considered for the basemat-subgrade interface was conservatively assessed as μ_k = 0.5, as discussed in Section 4.4. It is also pointed out in Section 4.4 that all tests performed for concrete vs. rock and concrete vs. concrete interfaces resulted in kinetic friction coefficients μ_k > 0.57. For soil, the majority of residual friction angles were found to be larger than 30°, corresponding also to μ_k > 0.57. It is therefore reasonable to investigate the effect that the selected value of the kinetic friction coefficient has on the sliding analysis results. For this purpose, a set of analyses is performed assuming a kinetic friction coefficient at the interface μ_k = 0.55 (still conservative), and using all five ATHs and six SPs. The results in terms of maximum total sliding values are summarized in Table B.1.3-1 for the LMSM of R/B complex with cracked concrete section. The maximum total sliding values obtained for the runs considering μ_k = 0.5 are also shown for comparison. In all analyses, presence of 25% Live loads and GWL at 1 ft below grade are assumed.

The percent difference between the maximum sliding values, $\delta_{max}^{0.5}$ (with μ_k = 0.5) and $\delta_{max}^{0.55}$ (with μ_k = 0.55) is calculated for each case analyzed as:

$$\Delta = \frac{\delta_{max}^{0.55} - \delta_{max}^{0.5}}{\delta_{max}^{0.5}} \times 100(\%)$$ Equation B.1.3-1

From the results of sliding analyses presented in Table B.1.3-1, it can be observed that an increase by 10% of the friction coefficient results, on average, in a reduction of calculated total sliding values of 38%. The average reduction in maximum total sliding for soil profiles (270-500, 270-200 and 560-500) is about 48%, while the average reduction in maximum total sliding for rock profiles (900-200, 900-100 and 2032-100) is about 27%. Given the experimental evidence discussed in Section 4.4 and pointing out to values of the kinetic friction coefficient of at least 0.55, it appears that the sliding results obtained for μ_k = 0.5 are very conservative.

B.1.4 Effect of Factor for the Input Acceleration

For all the analyses results listed in Sections 5.2.5 and 5.3.3, all components of the seismic input accelerations (including rotations) are amplified by a factor of 1.1, as explained in Section 1.0. The effect of this factor for the input acceleration is investigated by performing a set of analyses without amplifying the input acceleration and by comparing the results with those using an amplification factor of 1.1. The results in terms of maximum total sliding values are summarized in Table B.1.4-1 for the LMSM of R/B complex with cracked concrete section.

The percent difference between the maximum sliding values, $\delta_{max}^{1.1}$ (with amplification factor 1.1) and $\delta_{max}^{1.0}$ (without amplification) is calculated for each case analyzed as:

$$\Delta = \frac{\delta_{max}^{1.0} - \delta_{max}^{1.1}}{\delta_{max}^{1.1}} \times 100(\%)$$ Equation B.1.4-1

[.

]

Table B.1.1-1 Sliding Analysis Results in terms of Maximum Total Sliding (in inches) for the R/B Complex with Cracked Concrete Section, With and Without Considering Live Loads, Using the Validated LMSM

Table B.1.2-1 Sliding Analysis Results in terms of Maximum Total Sliding (in inches) for the R/B Complex with Cracked Concrete Section Using the Validated LMSM: Groundwater Level at 1 ft and 20 ft Below Grade

Table B.1.3-1 Sliding Analysis Results in terms of Maximum Total Sliding (in inches) for the R/B Complex with Cracked Concrete Section Using the Validated LMSM: Friction Coefficient = 0.5 and 0.55

Table B.1.4-1 Sliding Analysis Results in terms of Maximum Total Sliding (in inches) for the R/B Complex with Cracked Concrete Section Using the Validated LMSM: Factor of Input Acceleration = 1.0 and 1.1

Appendix C

Statistical Processing of R/B Complex LMSM Sliding Analysis Results

APPENDIX C TABLE OF CONTENTS

LIST OF FIGURES

LIST OF TABLES

C.1.0 STATISTICAL PROCESSING OF R/B COMPLEX LMSM SLIDING ANALYSIS RESULTS

The results of nonlinear sliding analyses in terms of maximum total sliding obtained with the validated LMSM are summarized in Table C.1.0-1. These are the results listed in the last lines of Table 5.2.5-1 through Table 5.2.5-6, and obtained by enveloping results from cracked and uncracked sections. This larger sample (15 results for soil profiles and 15 results for rock profiles) is used here to assess the statistics obtained with the smaller samples obtained from FE model analyses. The results in Table C.1.0-1 are grouped by SP in Figure C.1.0-1. For each profile, the five values of maximum sliding obtained using five ATHs are represented by three-bin histograms showing the range of results (blue lines, as well as numbers on the figure) and their grouping. Each range of results (for each SP) is divided into three equal intervals and the numbers of results falling in each interval is shown by the height of the respective bin in the histogram. The mean and sample standard deviations for each profile are also shown in Figure C.1.0-1. The data in Table C.1.0-1 is further grouped into results from soil profiles (270-500, 270-200 and 560-500), and results for rock profiles (900-200, 900-100 and 2032-100) in Figure C.1.0-2.

As seen from comparing the histograms in Figure 5.4.1-1 and Figure C.1.0-2, the two pairs of result samples obtained with the FE model and with the LMSM (for both soil and rock) are relatively close in both ranges and sample statistics. Considering Lognormal distribution for both samples obtained with the LMSM and shown in Figure C.1.0-2, the expected maximum values with a probability of exceedance of 2.5% based on LMSM results are:

Table C.1.0-1 Sliding Analysis Results for the R/B Complex in Terms of Maximum Total Sliding (in inches), Obtained with the Validated LMSM - Envelope of the Results for Cracked and Uncracked Sections

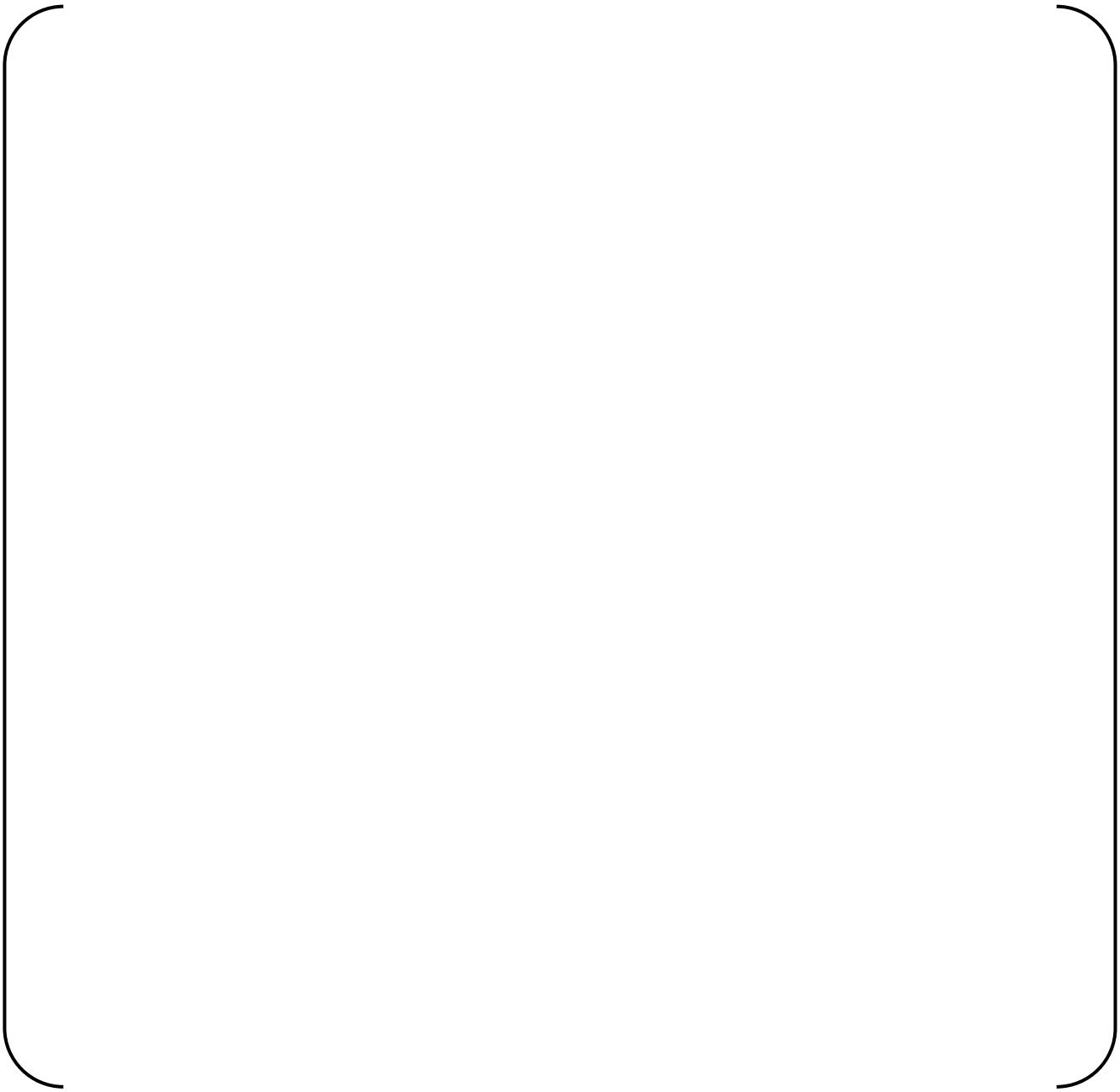

Figure C.1.0-1 R/B Complex: Distribution of Sliding Analysis Results Obtained with the LMSM for Each Subgrade Profile

Figure C.1.0-2 R/B Complex: Grouping of Sliding Analysis Results Obtained with the LMSM by Soil Profiles and Rock Profiles